Mode Identification in δ Scuti Stars

Elizabeth Anne Evers

Thesis prepared under supervision of the South African Astronomical Observatory and the University of the Orange Free State, and submitted in accordance with the requirements for the MSc degree in the Faculty of Science, Department of Physics at the University of the Orange Free State.

October 1998

Supervisor : Dr L.A. Balona
(South African Astronomical Observatory)

Co-supervisor : Dr P.J. Meintjes
(University of the Orange Free State)

To Graeme

My husband, for his continual support and encouragement,

and to my Heavenly Father,

who determines the number of stars and calls them each by name, for His faithfulness and love.

Acknowledgements

I would like to express my gratitude to the South African Astronomical Observatory for giving me the opportunity to do my MSc degree, and for their invaluable support throughout - academically and financially. My special thanks go to Dr Luis Balona, my supervisor, for his guidance, assistance and patience. I am also grateful to Dr Patricia Whitelock, Mrs Ethleen Lastovica, Mrs Cynthia Strydom and Mrs Linda Tobin for their help and friendliness.

I also wish to thank Dr Rafa Garrido (for sending me much of his data), Dr Chris Sterken (for allowing me to use his unpublished data for V853 Cen), Drs W.A. Dziembowski and A.A. Pamyatnykh (for supplying and allowing the use of the stellar evolution and non-adiabatic pulsation codes) and Drs T.T. Moon and M.M. Dworetsky for supplying the computer programs UVBYBETA.FOR and TEFFLOG.FOR. I would also like to thank Prof Don Kurtz for his comments.

I also wish to thank the Physics department of the University of the Orange Free State for allowing me to pursue my studies in their department, and for their financial assistance. I am grateful to Dr Pieter Meintjes, my co-supervisor, especially for his assistance in observing two of the stars. My thanks also to Mrs Adri Kotze, Mrs Elsa Pretorius, Dr Elmarie Viljoen and Dr. Matie Hoffman for their support.

Abstract

This thesis discusses mode-identification from multicolour photometry. First, the need for a better mode identification technique for stars that have significant phase differences between the light curves in different colours is addressed. The necessary equation needed for mode-identification from photometry is then derived and briefly discussed. Then, a new, statistically based algorithm for mode-identification is developed by extending and adapting a method that has been applied to pulsating white dwarfs, to include the information provided by the different phases of the light curves in different wavelengths. This new algorithm allows the best estimate of the spherical harmonic degree ℓ to be determined, as well as a confidence level from which the uniqueness of the mode-identification can be ascertained. The algorithm is then applied to a selection of well-observed δ Scuti stars with the necessary multicolour photometry. It is found that it works well for high amplitude δ Sct stars, but that discrimination between the $\ell = 0$ and $\ell = 1$ modes is sometimes poor for the low amplitude stars.

An algorithm to deduce the effective temperature, luminosity and equatorial velocity from the observed frequencies is also proposed. It is found that some mode-identification is necessary to obtain a unique solution of the stellar parameters. The method is applied to a subset of the δ Sct stars which have a suitable number of frequencies and suitable mode identifications.

Contents

Chapter 1

Introduction

1.1 A brief history

Aristotle's beliefs about the heavens dominated much of Western astronomy until the 16th century. One of these beliefs was the idea that the stars, attached to a moving sphere, were constant in brightness. It is now known that this is not true of any star. As stars evolve, their properties such as size, composition, temperature and luminosity change. In this sense, all stars are variable, although the evolutionary time-scale is very long and the changes that occur in a star due to it ageing are not usually discernible over the relatively short lengths of time measurable by astronomers. Some stars, however, are observed to undergo changes in their properties, either regularly or irregularly, in time scales ranging from a few fractions of a second to a few years. It is these stars which are called the *variable stars*. Cox (1980) defines a variable star as one whose properties change appreciably at a rate fairly easily detectable by astronomers.

Chinese astronomers recorded 'guest stars' (supernovae) even BC. In 134 BC, Hipparchus, a Greek astronomer, observed a nova, which led him to develop the first catalogue of stellar magnitude[1]. The reluctance to give up Aristotle's beliefs, despite much evidence against his ideas, is the most likely reason that the next variable star recorded in Western astronomy was only in 1572, when Tycho Brahe noticed a supernova. A few years later, in 1596, David

[1]Hipparchus divided stars into 6 categories. The brightest he called 1st magnitude stars, and the stars just visible to the naked eye he called 6th magnitude stars. This is a logarithmic scale, so that 6th magnitude stars are about 100 times fainter than 1st magnitude stars. Today the magnitude difference between two stars, or a variable star at two different times, is expressed by Pogson's rule: $m_1 - m_2 = -2.5 \log(l_1/l_2)$ where m_i is the apparent magnitude and l_i is the observed luminosity. The zero point of the magnitude scale is set by certain standard stars.

Fabricius noticed that the star Mira was sometimes visible and sometimes not, and that the cycle of visibility repeated every 11 months. Another supernova was noticed 8 years later, by Kepler, in 1604. Almost two centuries later, in 1784, Goodricke discovered the regular variable δ Cephei, the prototype of the class of Cepheid Variables. These early observations were, of course, made by eye. As the techniques of photography, and later photoelectric photometry were developed and applied to astronomy, an increasing number of variables were detected. By 1865, 113 stars were known to be variable, and by 1915 the number had increased to 1 700. Naturally, as the sensitivity of the instruments increased, variable stars with smaller brightness variations, including the sun, were detected. Today, with the photometer able to measure the brightness of a star to within approximately 0.001 mag, the General Catalogue of Variable Stars (GCVS) lists over 15 000 variable stars.

1.2 Types of variable stars

As suggested above, there are many different types of variable stars. They can be divided into two groups – the extrinsic variables (e.g. binary stars, where the observed changes in apparent brightness are due to partial eclipses, total eclipses, tidal distortions, etc, in a system of two stars) and the intrinsic variables, where the changes in the properties of the stars are due to effects within the stars themselves. Some of the intrinsic variables are plotted on a Hertzprung-Russell (H-R) diagram in Figure 1.1. The ordinate in this diagram is the absolute visual magnitude, M_V, which is related to luminosity[2]. The abscissa is effective temperature, with the spectral type also indicated. The effective temperature of a star is the temperature that a black body would have to be raised to in order to emit the same amount of radiant energy per second per unit area as that of the star. The spectral type describes what lines are most prominent in the spectrum of a star, and is directly related to temperature. An A star, for example, has a temperature between 7500 and 10000 K, and has strong hydrogen lines in its spectrum, lines of ionized metals, where metals in this sense refers to all elements heavier than helium, such as silicon, iron, and calcium, and also weak lines of neutral metals. An F star, which is slightly cooler, has weaker hydrogen lines and stronger neutral metal lines.

The line which stretches from the upper left of the diagram to the lower right is the Main

[2]The absolute magnitude is the magnitude that a star would have if it were at a distance of 10 pc from the observer. It is defined as $M_\lambda = m_\lambda - 5\log(r/10)$, where r is the star's actual distance in pc, and m is the apparent magnitude of the star in wavelength λ.

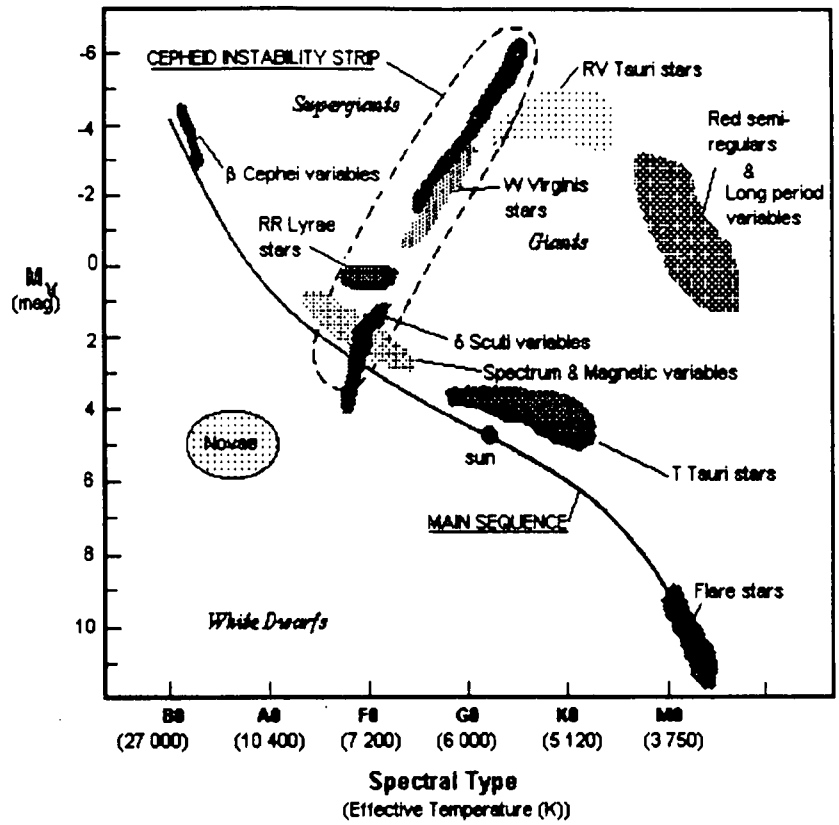

Figure 1.1: The location of the Main Sequence and various types of variable stars on the H-R diagram. Diagram adapted from Cox (1980)

Sequence, where most stars lie. Stars are formed in dense molecular clouds when regions with masses comparable to that of a star decreases in size, and thus increase in density, under the influence of the force of gravity. Eventually, the temperature of the protostars becomes hot enough for them to start burning hydrogen in their cores. At this stage they become stars and, depending on their masses, occupy certain places on the Zero Age Main Sequence (ZAMS) of the H-R diagram. As the hydrogen in the core of a star is converted into helium, the luminosity of the star slowly rises, so that the star moves away from the ZAMS. Eventually, all the hydrogen in the core of the star is converted to helium, so that the core consists of helium, with a shell of hydrogen around it. At this point the star leaves the main sequence. This is known as the end of core hydrogen burning (ECHB). After ECHB, the core contracts under gravity until it becomes hot enough for the star to start burning the hydrogen in the shell around the helium core, and so the evolution of the star continues.

The evolution of a star is due to the finite nature of its energy supply. As it radiates energy

it depletes and eventually exhausts its thermonuclear energy supply. As the star evolves, its temperature, luminosity and chemical composition change, and so the star traces out an evolutionary path on the H-R diagram. At certain times during its evolution, the star may become unstable against pulsations or eruptions, and become a variable star. As can be seen in Figure 1.1, the variable stars are not distributed randomly over the H-R diagram. This suggests that certain combinations of temperature and luminosity favour a state of pulsation as opposed to a state of equilibrium. These different types of variable stars are discussed in many books, such as Motz & Duveen (1977) and Aller (1971).

The intrinsic variables can be subdivided according to the type of variability into irregular stars (e.g novae and supernovae), the semi-regular stars (e.g. the red semi-regular variables), and the periodic stars (e.g. Cepheid and δ Sct variables). They can also be divided according to the cause of the variation e.g. pulsation or eruption. This thesis is concerned with the periodic pulsating stars, which are subdivided further according to Population[3], and length of pulsation period. Table 1.1 lists some of the periodic pulsating variables, including the δ Sct stars, which are the specific subjects of this study.

Table 1.1: Some of the Periodic Pulsating Variables.

Type of star	Characteristic Period (days)	Range of Spectral Types	Absolute Magnitude M_V (mag)
Classical Cepheids	5-10	F6–K2	-0.5 to -6
W Virginis Stars	12-20	F2–G6	0 to -3
RR Lyrae Stars	0.5	A2–F2	0.0 to +1.0
δ Sct Stars	0.08 (2 hours)	A2-F5	+2 to +3
β Cephei Stars	0.2 (5 hours)	B1–B2	-3.5 to -4.5
ZZ Ceti stars	0.006 (500 s)	A5-F5	+10 to +15

Adapted from Cox (1980)

1.3 A brief look at pulsation in the Cepheid Instability Strip

A pulsating variable brightens and fades because of a cyclical expansion and contraction of the star. As the star pulsates, the motion of the stellar surface produces a periodic Doppler shift in the lines of the stellar spectrum. This shift in the lines can be measured, and the velocity of the surface can hence be determined, allowing a velocity curve (radial velocity vs time) to be

[3]Stars are classified according to their spectral characteristics, chemical compositions, radial velocities and ages as either Pop I or Pop II.

plotted. These velocity variations were first observed in the Cepheid δ Cep by A.A. Belopolsky in 1894. The cause of these variations was initially attributed to the orbital motion of an invisible companion, but later (1914) shown to be best explained by pulsation.

In a stable star, the weight of each layer in the star is balanced by the gas and radiation pressure from within. In a pulsating star, the stars contracts until the internal pressure becomes greater than the weight of the outer layers. These layers then start to move outwards, but, because of their inertia, they overshoot the equilibrium position, and the star continues to expand until the pressure has decreased to such an extent that it can no longer support the weight of these layers, and the star then begins to contract under gravity, again overshooting the equilibrium position and so the cycle continues. If a pulsation were to start in any star, it would quickly be damped out through friction. Hence, for a star to continue to pulsate, there must be a driving force which continually feeds mechanical energy into the system. The star must therefore function as a thermodynamic heat engine, absorbing energy when it is most compressed. This heat will then be released as mechanical energy during the expansion phase of the pulsation. When atoms are in a state of partial ionisation, they can become more opaque to radiation under compression, and hence absorb energy. The helium and hydrogen ionisation zones are particularly effective at driving pulsation. In the Helium ionisation zone for example, when the star is most compressed the temperature becomes high enough to strip an electron off the helium nucleus. Any energy that is absorbed above that needed for ionisation is converted into kinetic energy of the free electrons. These free electrons heat the gas through collisions, so that the heat is dammed up in the atmosphere rather than being radiated away. This results in a build up of pressure so that the overlying layers are forced to expand. Once most of the helium is ionized, then radiation can again flow freely through the region, the temperature will drop, and the overlying layers will move inwards under the influence of gravity, thus increasing the pressure. The increase of pressure results in a recombination of the free electrons and the helium nuclei, and the whole process is then ready to start again. Cox (1980), among others, discusses these driving mechanisms in more detail. In the region marked with a dashed line in Figure 1.1, i.e. the Cepheid Instability Strip and its extension, the positions of the helium and hydrogen ionisation zones are close enough to the surface to be able to lift off the overlaying layers, but also deep enough so that the mass of the overlying layers is sufficient to allow them to be pulled back into the star by gravity, and so pulsation can occur here.

Stellar pulsation is similar to the vibration of a column of air inside an organ pipe, closed at

one end and open at the other. A star is a sphere of gas, confined at the centre but free at the surface. In both cases, the gas can vibrate in one or more of several modes. In a star, the simplest of these modes, the fundamental mode, decreases in amplitude towards the centre, where it is zero. There are also overtone modes, which differ from the fundamental in that the periods are shorter and in that there are stationary points or nodes within the gas. The mode in which a star pulsates depends on where the driving mechanism is applied. In an organ pipe, the harmonic frequencies are multiples of the fundamental frequency, but this is not true of a star, since the density and temperature are not constant throughout the star. The modes in a star which behave analogously to sound waves, as described above, are called p-modes (pressure modes). These modes provide information about the structure of the star, but do not allow the core to be probed. There are also g-modes (gravity modes), where, unlike the p-modes where pressure is the restoring force, buoyancy is the restoring force. These g-modes are useful since they tend to have large amplitudes in the centre of the star, and thus allow the structure of the core to be probed. The p-modes usually have higher frequencies than the g-modes. Further information on these two different types of modes can be obtained from Christensen-Dalsgaard (1997) and also from Cox (1980).

The above discussion reveals two reasons for studying pulsating stars: to understand how and why the stars pulsate, and to use the pulsations as a probe of the structure of the stars, which is known as *asteroseismology*. The study of pulsating stars has also yielded other important information. The study of the Classical Cepheids by Henrietta Leavitt yielded the Period-Luminosity law for these stars, which has provided a valuable means of measuring distance in the universe. The study of the 'high amplitude double-mode' stars, for which the physical parameters are easily obtainable from the period ratio (see e.g. Petersen & Christensen-Dalsgaard (1996), and Andreasen (1983)), has led to the revision of the opacity tables used in many branches of astronomy. The δ Scuti stars are of particular interest to astronomers, since, unlike the sun, they have convective cores, and hence have the potential to provide valuable information about stellar structure and evolution.

1.4 Delta Scuti stars

The prototype of the δ Scuti stars was first observed by E.A. Fath in 1935. The DSN (δ Scuti Network)[4] defines δ Sct stars[5] as variable stars of spectral type A or F, with luminosity classes V to III[6], and with pulsation periods between 30 minutes and 8 hours. Most of the δ Sct stars are Pop I, but some have the lower metal content typical of Pop II. The δ Sct stars lie within the Cepheid instability strip and its extension on the H-R diagram. The position of the Pop I δ Sct stars on this diagram implies that they have masses between 1.4 and 2.5 $M_{\odot}$.

The δ Scuti stars can be roughly divided into two groups. Those stars that exhibit an amplitude of variation of the order of 0.3 mag in their light curves are known as high amplitude δ Scuti stars (HADS) and those with lower amplitudes (of the order of 0.03 mag) are known as the low amplitude δ Sct stars (LADS). Many of the δ Sct stars are multiperiodic. Both radial and non-radial pulsations have been observed among them. In radial pulsation, the properties of the star vary radially, while in non-radial pulsation, the spherical symmetry of the star is not preserved. Most of the HADS appear to pulsate radially, while both radial and non-radial pulsations are observed among the LADS. These stars pulsate in p-modes, g-modes, and modes which are not either completely p- or g-modes, but have a mixed character.

One of the problems associated with these stars, which is outside the scope of this thesis, is that of mode selection : models of the δ Sct stars predict many more modes than are actually observed. Possibly these modes are not excited, or have amplitudes below the detection level. Another area in which there is much work to be done is that of asteroseismology. Although asteroseismology has been successful for the sun and PG 1159 stars (pulsating white dwarfs), the use of pulsation frequencies for asteroseismology in other stars such as the δ Sct stars has been very limited. The main obstacle is the correct identification of the mode of pulsation, which is the topic of this thesis.

[4] http://dsn.ast.univie.ac.at/dsn/deltascuti.html

[5] Following Breger (1979), dwarf cepheids and AI Vel stars are also included in this group. The metal-poor objects are called SX Phe stars

[6] This means that they are either main-sequence, sub-giants or giants.

1.5 Mode identification

In linear oscillation theory, the time dependency of the pulsations is assumed to be of the form $e^{i\omega t}$ where ω is the angular frequency of pulsation. The angular dependence of the pulsations is described in terms of spherical harmonics. Then

$$\frac{\delta r}{R_0} = \varepsilon Y_\ell^m(\theta, \phi) e^{i\omega t} \tag{1.1}$$

where ε is the relative amplitude which is assumed to be much less than unity, δr is the radial displacement, and R_0 is the radius of the star in its equilibrium position. If $\ell = 0$, then $Y_\ell^m(\theta, \phi)$ is a constant, and the pulsation is radial. Determination of the spherical harmonic degree ℓ, the azimuthal number m and the number of radial nodes n is known as *mode identification*. Some examples of different modes are shown in Figure 1.2.

In stars with large numbers of modes at very high or very low frequencies, such as the sun and the PG1159 stars, the relative spacings in period (for g-modes) or frequency (for p-modes) for the low degree modes form a pattern predicted by asymptotic theory, which is easily recognised and may be used to identify the modes. Most pulsating stars, however, do not have a large number of excited modes, and their periods do not fall in the asymptotic range, so this method of mode-identification cannot be applied to them. More information on asymptotic theory is available in Unno et al. (1989), chapter 16.

Each mode of pulsation introduces a distinctive velocity field on the surface of the star, which is observed not only by the Doppler shifts in the spectral lines, but also as a periodic variation in the line profiles. These line profile variations can be modelled and compared with observation to identify the mode (See Balona (1987)). The changes in the line profiles are small, which means that high dispersion and high signal-to-noise spectra are required in order to detect them. If the star is multiperiodic, then the star needs to be observed for a length of time sufficient to resolve the individual pulsation frequencies. These requirements mean that a moderately sized telescope is needed for the observations, and that the method is limited to the brightest stars only.

Clearly neither of these methods is suitable for the vast majority of stars, including the δ Sct stars.

Pulsation also affects the light curve of a star. It can be shown that the variation of amplitude and phase with wavelength depends on the spherical harmonic degree ℓ. These small effects can

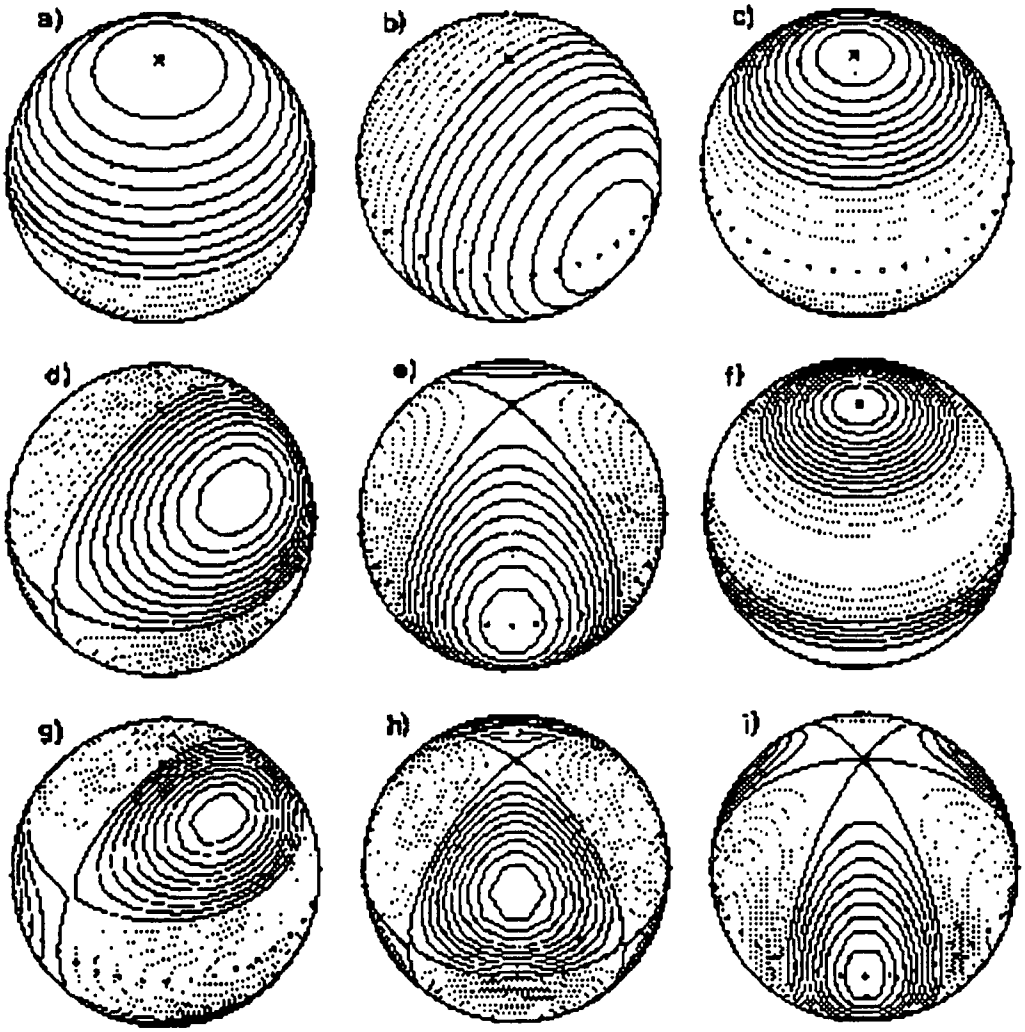

Figure 1.2: Contour plots of the real part of the spherical harmonic Y_ℓ^m, taken from Christensen-Dalsgaard (1997). Positive contours are indicated by continuous lines, and negative contours by dashed lines. The $\theta = 0$ axis is inclined at 45° towards the viewer, and the equator is marked by '+++'. The following cases are illustrated a) $\ell = 1, m = 0$, b) $\ell = 1, m = 1$, c) $\ell = 2, m = 0$, d) $\ell = 2, m = 1$, e) $\ell = 2, m = 2$, f) $\ell = 3, m = 0$, g) $\ell = 3, m = 1$, h) $\ell = 3, m = 2$, i) $\ell = 3, m = 3$.

be detected in accurate multicolour photometry, which is easy to obtain, and already exists for many δ Sct stars. It should be noted here that the azimuthal order m cannot be obtained from photometric means alone.

Many of the methods currently used to identify the modes from photometry do not use all the available information, nor provide a measure of the probability of the identification. The aim of the study presented in this thesis was to develop and apply a method which improves upon the current methods of mode-identification. This was done by using all the available information given in the light curves, and by also assigning a probability to the results.

In photometric observations of pulsating stars, one measures the light integrated over the visible disk of the star. This averaging effect increases with ℓ, so that modes with $\ell > 2$ are not expected to have amplitudes sufficiently large to be detected. Hence, for the δ Sct stars it is usually assumed that $\ell \leq 2$.

Mode identification in δ Sct stars is complicated not only by the presence of the g-modes and modes of mixed character, but also by stellar rotation. Rotation modifies the frequency expected in a non-rotating star, and introduces a fine structure in the modes. At the higher rates of rotation found in the lower amplitude stars ($50 - 100$ km.s^{-1}) the fine structure is not the easily recognisable equidistant pattern observed in the PG1159 stars.

1.6 Outline

The plan for the rest of this thesis is as follows. In the next chapter the equation that describes the change in observed magnitude in terms of the mode and stellar parameters will be derived and discussed. In Chapter 3, some of the methods currently used for mode-identification are outlined. The method used for white dwarfs by Fontaine, Brassard, Bergeron and Wesemael (1996) is adapted and extended for application to the δ Scuti stars.

In Chapter 4, the procedure followed in identifying modes of pulsation for some specific δ Scuti stars is given. The data for the selected stars was obtained largely from published articles for two reasons. Firstly, photometric data for these stars is easily obtainable from the available literature. Secondly, these stars need long periods of observation (at least two weeks) to adequately resolve all the periods present, and there was not enough time available to observe many stars. The results of the mode identification are listed and discussed in Chapter 5.

As already stated, the ultimate aim of mode-identification is asteroseismology. One frequency provides information about the mean density of the star. Two frequencies may allow the mass and temperature to be inferred. The more modes that are obtained in any particular star, the more information can be deduced. The number of detected modes in the δ Sct stars is not sufficient to determine the radial structure of the star, as has been done for the sun which has over 1 million modes, with ℓ between 0 and 1000. It should, however, be possible to determine the physical parameters of mass, luminosity and temperature by comparing the observed frequencies and those predicted from stellar models. Chapter 6 describes an algorithm to deduce

the temperature and luminosity for a subset of the selected stars.

Chapter 7 gives a summary of this work and the conclusions. The work presented in this thesis has also been published as an article in Balona & Evers (1999).

Chapter 2

Light from a Pulsating Star

The light from a pulsating star was first discussed by Dziembowski (1977). By assuming that the surface brightness is correlated with a colour index, Balona & Stobie (1979) were able to show that the mode could be identified from the phasing of the light and colour curves or from colour to light amplitude ratios. Stamford and Watson (1981) placed the method of Balona & Stobie on a sounder theoretical basis. They also discussed how modes could be identified with the help of model atmospheres. Heynderickx, Waelkens & Smeyers (1994) extended the work of Stamford & Watson to include the effects of the limb darkening variation[1]. The derivation given here is based on the more detailed one of Heynderickx, Waelkens & Smeyers (1994) to which the reader is referred.

2.1 The apparent magnitude in terms of the stellar parameters and the pulsation mode.

Consider a non-rotating, non-magnetic, spherically-symmetric star which is pulsating either radially or non-radially in a Cartesian coordinate system x, y, z with the origin at the centre

[1] A star emits a certain light intensity from its surface. Suppose that a photon travels on average a distance d before being reabsorbed by the stellar material. At the centre of the observed stellar disk, the depth of the photosphere in the direction from the stellar surface to the observer is smallest, so that an observer can see to the deep hot levels of the atmosphere. Near the edge (limb) of the observed stellar disk, the light must travel through more of the stellar atmosphere to reach the observer i.e. the light that is observed originates higher up in the atmosphere than at the centre of the disk. Hence the observer sees only the higher, cooler layers of the atmosphere, and so the limb appears darker than the centre. This apparent intensity variation over the stellar disk in known as 'limb darkening' and is usually modelled by a linear or quadratic function in μ where μ is the angle between the point on the stellar surface under consideration and the direction to the observer, as measured from the centre of the star.

of the star and the z-axis coinciding with the direction to the observer. A system of spherical coordinates r, θ, ϕ can be defined, with the polar axis coinciding with the z-axis so that

$$\begin{aligned} x &= r\sin\theta\cos\phi \\ y &= r\sin\theta\sin\phi \\ z &= r\cos\theta. \end{aligned} \tag{2.1}$$

If $\mathrm{P}(r, \theta, \phi)$ is a point on the surface of the star in its equilibrium state then this point P is displaced to a point $\mathrm{Q}(r_p, \theta_p, \phi_p)$ during a pulsation where the subscript p denotes the perturbed surface of the star. The difference in the spherical coordinates between P and Q can, in the linear approximation, be identified with the corresponding components of the Lagrangian displacement of the matter element at point P, i.e. if the spherical coordinates r, θ, ϕ are represented by q^1, q^2, q^3, then

$$\Delta q^i \equiv q_p^i - q^i \simeq \delta q^i.$$

The star's perturbed surface is then determined by the Lagrangian displacements of the motions of the mass elements on the equilibrium surface i.e.

$$\begin{aligned} r_p(r, R_0, \theta, \phi) &= R_0 + \delta r(t, R_0, \theta, \phi) \\ \theta_p(r, R_0, \theta, \phi) &= \theta + \delta\theta(t, R_0, \theta, \phi) \\ \phi_p(r, R_0, \theta, \phi) &= \phi + \delta\phi(t, R_0, \theta, \phi) \end{aligned} \tag{2.2}$$

where R_0 is the equilibrium radius of the star.

Substitution of 2.2 into 2.1 yields equations for x_p, y_p and z_p. If second and higher order terms in the Lagrangian variations are ignored, then the z-component $(d\mathbf{A})_{p,z}$ of the surface normal $(d\mathbf{A})_p$ at point Q on the perturbed surface in the spherical coordinate system is given by:

$$\begin{aligned} (d\mathbf{A})_{p,z} &= \left|\frac{\partial(x_p, y_p)}{\partial(\theta, \phi)}\right| \mathrm{d}\theta\mathrm{d}\phi \\ &\approx R_0^2 \Bigg\{ \sin\theta\cos\theta(1 + 2\frac{\delta r}{R_0}) + (\cos^2\theta - \sin^2\theta)\delta\theta + \sin^2\theta\frac{1}{R_0}\frac{\partial(\delta r)}{\partial\theta} \\ &\quad + \sin\theta\cos\theta\left[\frac{\partial(\delta\theta)}{\partial\theta} + \frac{\partial(\delta\phi)}{\partial\phi}\right]\Bigg\} \mathrm{d}\theta\mathrm{d}\phi. \end{aligned} \tag{2.3}$$

This equation will be useful in the derivation of the observed magnitude of a pulsating star in terms of the stellar parameters and the pulsation mode, which is considered below.

2.1.1 The observed magnitude

The observed magnitude of a star is given by

$$m(\lambda, t) = \text{constant} - 2.5 \log E(\lambda, t) \tag{2.4}$$

where $E(\lambda, t)$ is the energy radiated towards the observer in wavelength λ at time t.

The radiation field of a star can be described by a specific radiation intensity, $I_\lambda(t, r, \theta, \phi, \mathbf{n})$, which is defined as the energy per unit wavelength interval per unit time interval per unit area per unit solid angle passing into the direction $\mathbf{n}$ at the point (r, θ, ϕ). The direction to the observer $\mathbf{n_0}$ is denoted in the Cartesian coordinate system by the vector $\mathbf{n_0} = (0, 0, 1)$. The energy radiated through the perturbed surface element $(dA)_p$ at the point Q on the star's perturbed surface in the direction $\mathbf{n_0}$ to the observer at wavelength λ at time t is given by

$$I_{\lambda,p}(t, r_p, \theta_p, \phi_p, \mathbf{n_0})\mathbf{n_0} \cdot (d\mathbf{A})_p = I_{\lambda,p}(t, r_p, \theta_p, \phi_p, \mathbf{n_0})(d\mathbf{A})_{p,z}. \tag{2.5}$$

The total energy radiated in the direction of the observer at wavelength λ at time t is then

$$E(\lambda, t) = \int_{A_p} I_{\lambda,p}(t, r_p, \theta_p, \phi_p, \mathbf{n_0})(d\mathbf{A})_{p,z} \tag{2.6}$$

where the integral is over the visible part of the star's perturbed surface, A_p. Setting

$$I_{\lambda,p}(t, r_p, \theta_p, \phi_p, \mathbf{n_0}) = I_\lambda(R_0, \mathbf{n_0}) + \delta I_\lambda(t, R_0, \theta, \phi, \mathbf{n_0}) \tag{2.7}$$

where $\delta I_\lambda(t, R_0, \theta, \phi, \mathbf{n_0})$ is the Lagrangian perturbation of the specific radiation intensity at the point (R_0, θ, ϕ) in the direction $\mathbf{n_0}$, then

$$E(\lambda, t) = \int_{A_p} I_\lambda (d\mathbf{A})_{p,z} + \int_{A_p} \delta I_\lambda (d\mathbf{A})_{p,z}. \tag{2.8}$$

The visible perturbed surface is determined by the condition $(d\mathbf{A})_{p,z} \geq 0$ and is covered by the ranges $0 \leq \phi \leq 2\pi$ and $0 \leq \theta \leq \frac{\pi}{2} + \Delta\theta$, where $\Delta\theta$ is determined by setting $(d\mathbf{A})_{p,z} = 0$ and to first order is given by

$$\Delta\theta = \left[\frac{1}{R_0}\frac{\partial(\delta r)}{\partial\theta} - \partial\theta\right]_{\theta=\pi/2}. \tag{2.9}$$

By substituting equation (2.3) into equation (2.8) the integration becomes an integration over the angles θ and ϕ. The integration can be split into two parts : an integration over the interval $0 < \phi < 2\pi$, $0 < \theta < \frac{\pi}{2}$ and then over the interval $0 < \phi < 2\pi$, $\frac{\pi}{2} < \theta < \frac{\pi}{2} + \Delta\theta$. Many terms in

the resulting integrals contain products of Lagrangian variations or tend to 0 as $\Delta\theta \to 0$. The terms which survive are:

$$\begin{aligned} E(\lambda,t) &= R_0^2 \int_0^{2\pi}\int_0^{\pi/2} I_\lambda(R_0,\mathbf{n}_0)\sin\theta\cos\theta \mathrm{d}\theta\mathrm{d}\phi \\ &+R_0^2 \int_0^{2\pi}\int_0^{\pi/2} I_\lambda(R_0,\mathbf{n}_0)\Bigg\{2\sin\theta\cos\theta\frac{\delta r}{R_0}+(\cos^2\theta-\sin^2\theta)\delta\theta+\sin^2\theta\frac{1}{R_0}\frac{\partial(\delta r)}{\partial\theta} \\ &+\sin\theta\cos\theta\left[\frac{\partial(\delta\theta)}{\partial\theta}+\frac{\partial(\delta\phi}{\partial\phi}\right]\Bigg\}\mathrm{d}\theta\mathrm{d}\phi \qquad (2.10) \\ &+R_0^2 \int_0^{2\pi}\int_{\pi/2}^{\pi/2+\Delta\theta} I_\lambda(R_0,\mathbf{n}_0)\sin\theta\cos\theta\mathrm{d}\theta\mathrm{d}\phi \\ &+R_0^2 \int_0^{2\pi}\int_0^{\pi/2} \delta I_\lambda(t,R_0,\theta,\phi,\mathbf{n}_0)\sin\theta\cos\theta\mathrm{d}\theta\mathrm{d}\phi. \end{aligned}$$

The second and third integrals in the above equation account for the changes in the area of the radiating surface element and the changes in the direction of the local surface normal with respect to the observer respectively. The fourth integral accounts for changes in the radiation due to pulsation. The first integral corresponds to the outward normal radiation flux F_λ^+ taken over all directions $\mathbf{n}$ at any point on the equilibrium surface i.e.

$$F_\lambda^+(R_0) = \int_0^{2\pi}\int_0^{\pi/2} I_\lambda(R_0,\mathbf{n})\sin\theta\cos\theta\mathrm{d}\theta\mathrm{d}\phi, \qquad (2.11)$$

The expression for the radiation field $I(R_0,\mathbf{n})$ across the stellar disk at the star's equilibrium surface is assumed to be the product of an angle-independent intensity $I_{\lambda,0}$ and a limb-darkening function $h_\lambda(\mu)$, where $\mu = \cos\theta$ and θ is the angle between the local surface normal and the positive z-axis direction. The limb darkening function is normalised so that

$$\int_0^1 h_\lambda(\mu)\mathrm{d}\mu = 1.$$

Then

$$F_\lambda^+(R_0) = 2\pi I_{\lambda,0} \qquad (2.12)$$

and

$$I_\lambda(R_0,\mathbf{n}) = \frac{1}{2\pi}F_\lambda^+ h_\lambda(\mu). \qquad (2.13)$$

If expression (2.13) is substituted into the third integral of equation (2.10) and integration over the angle θ is performed, then the result is of second order in $\Delta\theta$ and hence (from equation (2.9)) also in δr and $\delta\theta$. This integral can therefore be ignored.

The fourth integral in equation (2.10) can be developed as follows. Assuming that the Lagrangian perturbation $\delta I_\lambda(t, R_0, \theta, \phi, \mathbf{n})$ can be obtained by taking the Lagrangian perturbation of (2.13) then

$$\delta I_\lambda(t, R_0, \theta, \phi, \mathbf{n}_0) = I_\lambda(R_0, \mathbf{n}_0)\left(\frac{\delta F_\lambda^+}{F_\lambda^+} + \frac{\delta h_\lambda}{h_\lambda}\right). \tag{2.14}$$

Assuming that the flux F_λ^+ is a function of the effective temperature T_{eff} and surface gravity g, then

$$\delta F_\lambda^+ = F_\lambda^+\left(\alpha_T \frac{\delta T_{\text{eff}}}{T_{\text{eff}}} + \alpha_g \frac{\delta g}{g}\right) \tag{2.15}$$

where

$$\alpha_T = \left(\frac{\partial \log F_\lambda^+}{\partial \log T_{\text{eff}}}\right)_g \text{ and } \alpha_g = \left(\frac{\partial \log F_\lambda^+}{\partial \log g}\right)_{T_{\text{eff}}}.$$

The Lagrangian perturbation of the limb-darkening function $h(\mu)$ depends on $\delta\mu$ and is also assumed to depend on T_{eff} and g, so that

$$\partial h = \frac{\partial h}{\partial \mu}\delta\mu + h\left[\frac{\partial \log h}{\partial \log T}\frac{\delta T_{\text{eff}}}{T} + \frac{\partial \log h}{\partial \log g}\frac{\delta g}{g}\right].$$

At the star's equilibrium surface, $\mu = \cos\theta$. At the star's perturbed surface,

$$\mu_p = \frac{\mathbf{n}_0 \cdot (d\mathbf{A})_p}{|\,(d\mathbf{A})_p\,|}$$

The Lagrangian perturbation $\delta\mu$ to first order is given by

$$\delta\mu = \sin\theta\left[\frac{1}{R_0}\frac{\partial(\delta r)}{\partial\theta} - \partial\theta\right], \tag{2.16}$$

so that

$$\delta h_\lambda = \sin\theta\frac{\partial h_\lambda}{\partial\mu}\left[\frac{1}{R_0}\frac{\partial(\delta r)}{\partial\theta} - \partial\theta\right] + h_\lambda\left(\beta_T'\frac{\delta T_{\text{eff}}}{T_{\text{eff}}} + \beta_g'\frac{\delta g}{g}\right) \tag{2.17}$$

with

$$\beta_T'(\mu) = \left(\frac{\partial \log h_\lambda(\mu)}{\partial \log T_{\text{eff}}}\right)_g \text{ and } \beta_g'(\mu) = \left(\frac{\partial \log h_\lambda(\mu)}{\partial \log g}\right)_{T_{\text{eff}}}. \tag{2.18}$$

After substitution of the above equations, and some rearrangement of terms, equation (2.10) becomes

$$\begin{aligned} E(\lambda,t) \;=\; & R_0^2 F_\lambda^+ + \frac{1}{2\pi}R_0^2 F_\lambda^+ \int_0^{2\pi}\int_0^1 \left[2\mu h_\lambda \frac{\delta r}{R_0} - (1-\mu^2)\left(h_\lambda + \mu\frac{\partial h}{\partial\mu}\right)\frac{1}{R_0}\frac{\partial(\delta r)}{\partial\mu}\right]\mathrm{d}\mu\mathrm{d}\phi \qquad (2.19)\\ & + \frac{1}{2\pi}R_0^2 F_\lambda^+ \int_0^{2\pi}\int_0^1 \left[\frac{2\mu^2-1}{\sqrt{1-\mu^2}}h_\lambda\delta\theta - \mu\sqrt{1-\mu^2}h_\lambda\frac{\partial(\delta\theta)}{\partial\mu} - \mu\sqrt{1-\mu^2}\frac{\partial h_\lambda}{\partial\mu}\delta\theta + \right.\\ & \left. \mu h_\lambda\frac{\partial(\delta\phi)}{\partial\phi}\right]\mathrm{d}\mu\mathrm{d}\phi + \frac{1}{2\pi}R_0^2 F_\lambda^+ \int_0^{2\pi}\int_0^1 h\left[(\alpha_T+\beta_T')\frac{\delta T_{\text{eff}}}{T_{\text{eff}}} + (\alpha_g+\beta_g')\frac{\delta g}{g}\right]\mu\,\mathrm{d}\mu\mathrm{d}\phi. \end{aligned}$$

Partial integration of the term $\mu\sqrt{1-\mu^2}h_\lambda\frac{\partial(\delta\theta)}{\partial\mu}$ yields

$$\int_0^1 \frac{2\mu^2-1}{\sqrt{1-\mu^2}}\delta\theta h_\lambda \mathrm{d}\mu = \left[-\mu\sqrt{1-\mu^2}\delta\theta h_\lambda\right]_0^1 + \int_0^1 \mu\sqrt{1-\mu^2}h_\lambda\frac{\partial\delta\theta}{\partial\mu}\mathrm{d}\mu + \int_0^1 \mu\sqrt{1-\mu^2}\delta\theta\frac{\partial h_\lambda}{\partial\mu}\mathrm{d}\mu \tag{2.20}$$

so that the terms in equation (2.19) containing $\delta\theta$ vanish. Equation (2.19) can therefore be expressed as

$$\frac{E(\lambda,t)}{R_0^2F_\lambda^+} = 1 + V_1(\lambda,t) + V_2(\lambda,t), \tag{2.21}$$

where

$$V_1 = \frac{1}{2\pi}\int_0^{2\pi}\int_0^1\left[2\mu h_\lambda\frac{\delta r}{R_0} - (1-\mu^2)\left(h_\lambda+\mu\frac{\partial h_\lambda}{\partial\mu}\right)\frac{1}{R_0}\frac{\partial(\delta r)}{\partial\mu} + \mu h_\lambda\frac{\partial(\delta\phi)}{\partial\phi}\right]\mathrm{d}\mu\mathrm{d}\phi, \tag{2.22}$$

$$V_2 = \frac{1}{2\pi}\int_0^{2\pi}\int_0^1 h_\lambda\left[(\alpha_T+\beta_T')\frac{\delta T_{\rm eff}}{T_{\rm eff}} + (\alpha_g+\beta_g')\frac{\delta g}{g}\right]\mu\,\mathrm{d}\mu\mathrm{d}\phi. \tag{2.23}$$

2.1.2 The variations in terms of spherical harmonics

The two integrals V_1 and V_2 can be developed further by expressing the Lagrangian variations in terms of spherical harmonics. Since the star is spherically symmetric, any pulsation modes with time-dependence $e^{i\omega t}$, where ω is the angular frequency of pulsation, can be represented in terms of a spherical harmonic $Y_\ell^m(\Theta,\Phi)$. From the linear theory of stellar oscillations (see for example Cox (1980), Ledoux & Walraven (1958)) it can be shown that the Lagrangian perturbation δr can be written in component form as

$$\begin{aligned}
\delta r(t,R_0,\theta,\phi) &= \frac{u_\ell(R_0)}{R_0^2}Y_\ell^k(\Theta,\Phi)e^{i\omega t}\\
\delta\theta(t,R_0,\theta,\phi) &= \frac{v_\ell(R_0)}{R_0^2}\frac{\partial Y_\ell^k(\Theta,\Phi)}{\partial\theta}e^{i\omega t}\\
\delta\phi(t,R_0,\theta,\phi) &= \frac{v_\ell(R_0)}{R_0^2\sin^2\theta}\frac{\partial Y_\ell^k(\Theta,\Phi)}{\partial\phi}e^{i\omega t}
\end{aligned} \tag{2.24}$$

where $u(r)$ and $v(r)$ are functions depending on r only, and the angles Θ and Φ are the angles in the coordinate system where the Z-axis is inclined at an angle i to the z-axis, which is the direction to the observer. The spherical harmonic $Y_\ell^k(\Theta,\Phi)$ can be expressed as the sum of spherical harmonics in the coordinate system (r,θ,ϕ) as

$$Y_\ell^k(\Theta,\Phi) = \sum_{m=-\ell}^{\ell} A_{\ell km}Y_\ell^m(\theta,\phi)$$

where the $A_{\ell km}$ are constants that are not determined, but can be calculated given ℓ, k and the angle of inclination i.

Defining

$$\varepsilon = \frac{u_\ell(R_0)}{R_0^3} \text{ and } \varepsilon_h = \frac{v_\ell(R_0)}{R_0^3}$$

and using the above relations for the spherical harmonics, the equations (2.24) can be rewritten as:

$$\begin{aligned}
\delta r(t, R_0, \theta, \phi) &= \sum_{m=-\ell}^{\ell} A_{\ell km} \varepsilon R_0 Y_\ell^m(\theta, \phi) e^{i\omega t} \\
\delta\theta(t, R_0, \theta, \phi) &= \sum_{m=-\ell}^{\ell} A_{\ell km} \varepsilon_h R_0 \frac{\partial Y_\ell^m(\theta, \phi)}{\partial \theta} e^{i\omega t} \\
\delta\phi(t, R_0, \theta, \phi) &= \sum_{m=-\ell}^{\ell} A_{\ell km} \frac{\varepsilon_h R_0}{\sin^2\theta} \frac{\partial Y_\ell^m(\theta, \phi)}{\partial \phi} e^{i\omega t}.
\end{aligned} \tag{2.25}$$

Now

$$Y_\ell^m(\theta, \phi) = P_\ell^m(\cos\theta) e^{im\phi}, \tag{2.26}$$

where the P_ℓ^m are the Legendre functions. Upon substitution of these expressions, the integral V_1 (equation (2.22)) becomes separable in θ and ϕ. The integral over ϕ is given by $\int_0^{2\pi} e^{im\phi} \mathrm{d}\phi$ which is only non-zero for $m = 0$. Hence, after integration over ϕ, V_1 becomes

$$V_1 = A_{\ell 0} \varepsilon e^{i\omega t} \int_0^1 \left[2\mu h_\lambda P_\ell(\mu) - (1-\mu^2)\left(h_\lambda + \mu \frac{\partial h_\lambda}{\partial \mu} \right) \frac{\mathrm{d}P_\ell(\mu)}{\mathrm{d}\mu} \right] \mathrm{d}\mu, \tag{2.27}$$

where

$$A_{\ell 0} = P_\ell^m(\cos i). \tag{2.28}$$

Integrating the term $\mu h \frac{\mathrm{d}P_\ell}{\mathrm{d}\mu}$ by parts, and using Legendre's equation

$$\frac{\mathrm{d}(1-x^2)}{\mathrm{d}x} \frac{\mathrm{d}y}{\mathrm{d}x} + \ell(\ell+1) y = 0$$

with $x = \mu$ and $y = \mu h_\lambda \frac{\mathrm{d}P_\ell(\mu)}{\mathrm{d}\mu}$ and discarding the terms in $\frac{\mathrm{d}^2 P_\ell(\mu)}{\mathrm{d}\mu^2}$, the result is

$$V_1 = -A_{\ell 0} \varepsilon (\ell - 1)(\ell + 2) b_{\ell\lambda} e^{i\omega t}, \tag{2.29}$$

where

$$b_{\ell\lambda} = \int_0^1 h_\lambda \mu P_\ell(\mu) \mathrm{d}\mu. \tag{2.30}$$

The integral V_2 (equation (2.23)) can be developed as follows by setting

$$\begin{aligned}
\frac{(\delta T_{\mathrm{eff}})_\ell}{T_{\mathrm{eff}}} &= \frac{(\delta T)_\ell}{T}, \\
\frac{(\delta g)_\ell}{g} &= p^* \frac{(\delta p)_\ell}{p} \text{ where } p^* = \left(\frac{\partial \log g}{\partial \log p_g} \right)_{\tau=1}
\end{aligned} \tag{2.31}$$

where p is the pressure, and τ is the optical depth[2]. The factor p^* is a measure of the variation of the atmospheric gas pressure with surface gravity in the layers that give rise to the observed continuum flux.

From the boundary conditions of pressure, and the gravitational potential and its gradient at the surface, the expression

$$\frac{(\delta p)_\ell}{p} = C\frac{\delta r}{r} = C\varepsilon \text{ where } C = \frac{\ell(\ell+1)}{\omega^2}\frac{GM}{R_0^3} - \omega^2\frac{R_0^3}{GM} - 4 \tag{2.32}$$

is obtained, if the Eulerian perturbation of the gravitational perturbation for non-radial oscillations is neglected. (See, for example, Cox (1980) or Ledoux & Walraven (1958)).

In the adiabatic approximation for a gas, it is can be shown that

$$\frac{(\delta T)_\ell}{T} = \frac{\Gamma_2 - 1}{\Gamma_2}\frac{(\delta p)_\ell}{p} \tag{2.33}$$

where

$$\frac{\Gamma_2 - 1}{\Gamma_2} \equiv \left(\frac{\partial \log T}{\partial \log p}\right)_S, \tag{2.34}$$

and S is the entropy. To describe the non-adiabatic situation, a parameter R is introduced such that $0 < R < 1$ and $R = 1$ describes the adiabatic case. A phase difference ψ between the Lagrangian perturbation of temperature and the radial component of the Lagrangian displacement is also introduced. This phase difference ψ has a value between 0 and π radians. Then, introducing the time and angular dependencies of $T_{\rm eff}$ and g

$$\begin{aligned} \frac{\delta T_{\rm eff}}{T_{\rm eff}} &= R\frac{\Gamma_2 - 1}{\Gamma_2}C\varepsilon \sum_{m=-\ell}^{\ell} A_{\ell km} Y_\ell^m(\theta,\phi)e^{i(\omega t+\psi)}, \\ \frac{\delta g}{g} &= p^* C\varepsilon \sum_{m=-\ell}^{\ell} A_{\ell km} Y_\ell^m(\theta,\phi)e^{i\omega t} \end{aligned} \tag{2.35}$$

and substitution into V_2 yields

$$V_2 = C\varepsilon\frac{e^{i\omega t}}{2\pi}\sum_{m=-\ell}^{\ell} A_{\ell km}\int_0^{2\pi}\int_0^1 h_\lambda\left[R\frac{\Gamma_2-1}{\Gamma_2}(\alpha_T+\beta_T')e^{i\psi}+p^*(\alpha_g+\beta_g')\right]\mu P_\ell(\mu)e^{im\phi}\mathrm{d}\mu\mathrm{d}\phi. \tag{2.36}$$

Once again, the integral can be separated into an integral over θ and an integral over ϕ. The latter integral is, once again, only non-zero if $m = 0$ when it takes the value 2π. After integration

[2]The optical depth of a layer determines the fraction of the intensity from that layer which reaches the surface without absorption by the overlying layers. If a layer within the star has an optical depth τ, then the intensity from that layer that reaches the surface, $I(0)$, is the intensity of the layer $I(\tau)$ multiplied by a factor e^τ. Optical depth increases with distance from the surface. The photosphere of a star is sometimes considered as a single layer at a specific optical depth of $\tau = \frac{2}{3}$ or 1.

over ϕ, V_2 takes the form

$$V_2 = A_{\ell 0} C \varepsilon b_{\ell\lambda} e^{i\omega t} \left\{ R \frac{\Gamma_2 - 1}{\Gamma_2} (\alpha_T + \beta_T) e^{i\psi} + p^* (\alpha_g + \beta_g) \right\}, \tag{2.37}$$

where

$$\beta_T(\mu) = \left(\frac{\partial \log b_{\ell\lambda}}{\partial \log T_{\rm eff}} \right)_g \quad \text{and} \quad \beta_g(\mu) = \left(\frac{\partial \log b_{\ell\lambda}}{\partial \log g} \right)_{T_{\rm eff}}. \tag{2.38}$$

Substituting the expressions for V_1 and V_2 back into equation (2.21) gives

$$\frac{E(\lambda,t)}{R_0^2 F_\lambda^+} = 1 + A_{\ell 0} \varepsilon b_{\ell\lambda} e^{i\omega t} \left\{ -(\ell-1)(\ell+2) + p^* C (\alpha_g + \beta_g) + CR \frac{\Gamma_2 - 1}{\Gamma_2} (\alpha_T + \beta_T) e^{i\psi} \right\}. \tag{2.39}$$

The observed magnitude of the star (equation (2.4)) can be written as

$$m(\lambda,t) = \text{constant} - 2.5 \log(R_0^2 F_\lambda^+) - 2.5 \log \left[\frac{E(\lambda,t)}{R_0^2 F_\lambda^+} \right]. \tag{2.40}$$

The variability of the magnitude is described by the last term, i.e.

$$\Delta m_\lambda = 2.5 \log \left[\frac{E(\lambda,t)}{R_0^2 F_\lambda^+} \right].$$

Defining

$$\begin{aligned} T_1 &= -(\ell-1)(\ell+2) \\ T_2 &= p^* C (\alpha_g + \beta_g) \\ T_3 &= CR \frac{\Gamma_2 - 1}{\Gamma_2} (\alpha_T + \beta_T) e^{i\psi}, \end{aligned} \tag{2.41}$$

then

$$\frac{E(\lambda,t)}{R_0^2 F_\lambda^+} = 1 + A_{\ell 0} \varepsilon b_{\ell\lambda} e^{i\omega t} \{T_1 + T_2 + T_3\}. \tag{2.42}$$

Making use of the fact that $\log(1+x) \approx x \log e$ for x small, and using equation (2.28) then

$$\Delta m(\lambda,t) = A_{\ell\lambda} e^{i(\omega t + \gamma)} = A_0 P_\ell^m(\cos i) b_{\ell\lambda} \{T_1 + T_2 + T_3\} e^{i\omega t}, \tag{2.43}$$

where

$$A_0 = 2.5 \varepsilon \log e = 1.086 \varepsilon \tag{2.44}$$

$$\tan\gamma = \frac{\mathbf{Im}[T_3]}{T_1 + T_2 + \mathbf{Re}[T_3]} \tag{2.45}$$

$$\text{and } A_{\ell\lambda} = A_0 P_\ell^m(\cos i) b_{\ell\lambda} \sqrt{(\mathbf{Im}[T_3])^2 + (T_1 + T_2 + \mathbf{Re}[T_3])^2}. \tag{2.46}$$

Equation (2.43) is the expression that will be used in the mode identification. Note that this expression is written in complex form: the observed quantities result by taking the real part of this expression.

2.2 The terms T_1, T_2 and T_3

2.2.1 Alternative formulation of T_3

The relative flux variation is usually written as follows (see Dziembowski (1977)):

$$\frac{\delta F}{F} = f\frac{\delta r}{R_0}. \tag{2.47}$$

The factor f is thus the ratio of the local flux variation to the local amplitude variation. Since $F \propto T_{\rm eff}^4$,

$$\frac{\delta T_{\rm eff}}{T_{\rm eff}} = \frac{1}{4}\frac{\delta F}{F} = \frac{1}{4}f\frac{\delta r}{R_0}. \tag{2.48}$$

A comparison of equations (2.48) and (2.35) reveals that

$$f = 4R\frac{\Gamma_2 - 1}{\Gamma_2}C. \tag{2.49}$$

The term T_3 can then be written as

$$T_3 = \frac{1}{4}(\alpha_T + \beta_T)fe^{i\psi}. \tag{2.50}$$

The f defined above is not to be confused with the f (denoted f^* here and throughout) of Cugier, Dziembowski & Pamyatnykh (1994). These authors introduce the local luminosity instead of the effective temperature in the following form:

$$\frac{\delta(4\pi r^2 F)}{L} = f^*(r)\frac{\delta r}{R_0} \tag{2.51}$$

where F is the flux, and, in the case of radial pulsation, the eigenfunction $f^*(r)$ describes the radial dependence of the variation of the local luminosity relative to the local radial displacement δr. As above, since $L \propto R^2 T_{\rm eff}^4$

$$\frac{\delta(4\pi r^2 F)}{L} = 4\frac{\delta T}{T}.$$

This can be expanded to reveal that

$$f^* = f + 2.$$

2.2.2 The dependence of the amplitude and phase of the light curve on T_1, T_2 and T_3

Mode identification using the amplitudes and phases is possible as long as the amplitudes and phases (defined by equations (2.45) and (2.46)) in different wavelengths or passbands have different values for different modes i.e. when the amplitudes and phases depend on both wavelength

and spherical harmonic degree ℓ. Under certain conditions, such as very high frequency pulsations, the amplitudes and phases lose their sensitivity to the mode. Under these conditions other information, such as the pattern produced by the spacing of the frequencies, must be used to identify the modes. The amplitudes and phases depend on the three terms T_1, T_2 and T_3. The amplitude also depends on the limb-darkening integral $b_{\ell\lambda}$ and the constant $A_0 P_\ell^m(\cos i)$.

The term T_1 arises from purely geometrical effects (i.e. variations in the surface area and the direction of the surface normal). It depends only on the value of the spherical harmonic degree ℓ, and has values of 2, 0 and -4 for $\ell = 0,1$ and 2 respectively. For $\ell > 2$, T_1 becomes increasingly negative. T_2 is due to changes in the local luminosity and limb darkening as a result of changes in the local surface gravity, and T_3 to changes in the local luminosity and limb darkening as a result of changes in the local temperature. These latter two terms depend on the surface gravity, effective temperature, mass, frequency of pulsation, the spherical harmonic degree ℓ, and the wavelengths in which the star is observed.

The wavelength dependence of the amplitudes and phases comes only from the wavelength dependence of the limb darkening integral $b_{\ell\lambda}$, defined by equation (2.30), and the terms T_2 and T_3. The limb-darkening integral is plotted in Figure 2.1 for different modes. It is most sensitive to wavelength in the far UV wavelengths. Its small magnitude for $\ell > 2$ simply means that these modes, if they exist in the δ Sct stars, have small amplitudes and are more difficult to distinguish above the noise levels of the observations.

The wavelength dependence of T_2 and T_3 comes from the terms α_g, β_g and α_T. The term β_T is much smaller than α_T and can be ignored. β_g is also usually much smaller than α_g for $\ell \leq 2$, but cannot be completely ignored in all wavelengths. All of these terms are largest towards the ultraviolet (UV) wavelengths, and both β_g and β_T are more sensitive to mode in these wavelengths. As a result, both the amplitudes and phases give better discrimination between modes in the UV wavebands. This is shown in Figure 2.2. This figure shows the results from a linear, non-adiabatic model with $M = 1.80 M_\odot$ for some far UV wavelengths and the $uvbyRIJHK$ filters, normalised to the v-filter. The amplitudes are almost independent of ℓ except in the far UV wavebands. The relative phases however are rather sensitive to ℓ. From this diagram it can be seen that the phases give good discrimination in the longer red wavelengths. The amplitudes in these wavelengths are small, however, making observations difficult. Observations in the far UV would be very useful for mode-identification, as both the amplitudes and wavelengths help to

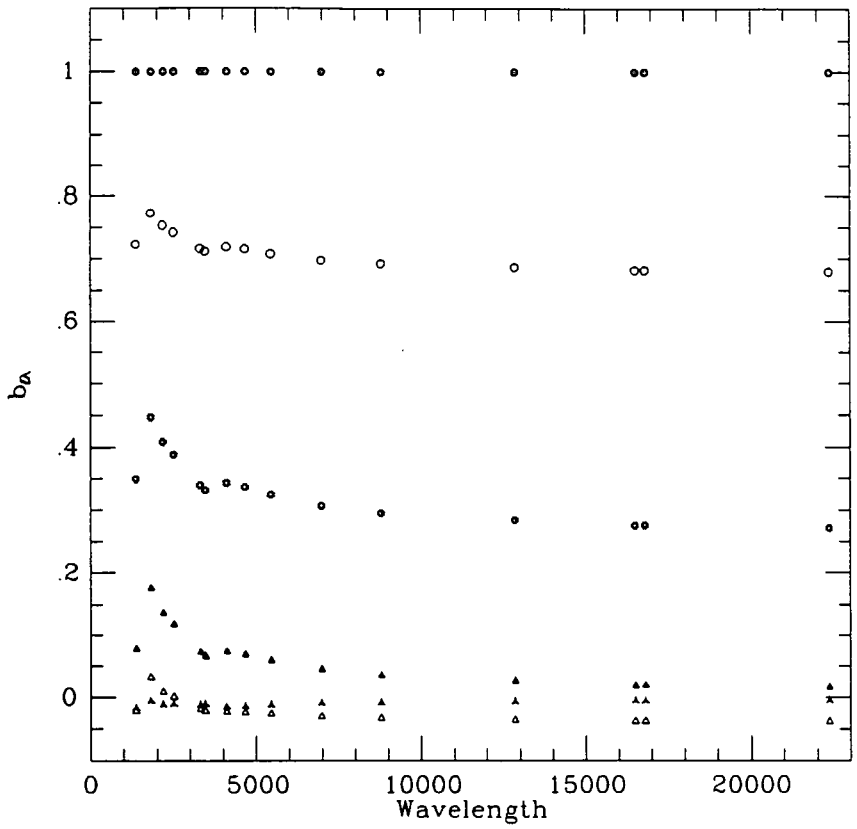

Figure 2.1: The values of $b_{\ell\lambda}$ for different wavelengths (Å) for $\ell = 0$ (filled circles), $\ell = 1$ (open circles), $\ell = 2$ (asterisks), $\ell = 3$ (filled triangles), $\ell = 4$ (open triangles) and $\ell = 5$ (crossed triangles) for a slightly evolved stellar model with mass 1.8 $M_\odot$, $\log T_{\rm eff} = 3.8764$ and $\log g = 4.0347$.

discriminate between modes. Unfortunately, observations in these wavelengths are not available for the δ Sct stars, and so observations of these stars are limited to ground-based photometry. There is much data available for the δ Sct stars in the *uvby* and UBV filters, which cover a wavelength range of approximately 3000 - 6000 Å.

The mode-dependence of the amplitudes and phases comes from the terms T_1, C, β_g and β_T. The terms β_T and β_g are generally small and do not contribute very much to the mode-discrimination. The important terms are T_1 and C. The relative contribution of these terms to the mode discrimination depends on the pulsation frequency. Figure 2.3 shows C plotted against pulsation frequency ν in d^{-1}. For small frequencies, the first term in C, as defined by equation (2.32),

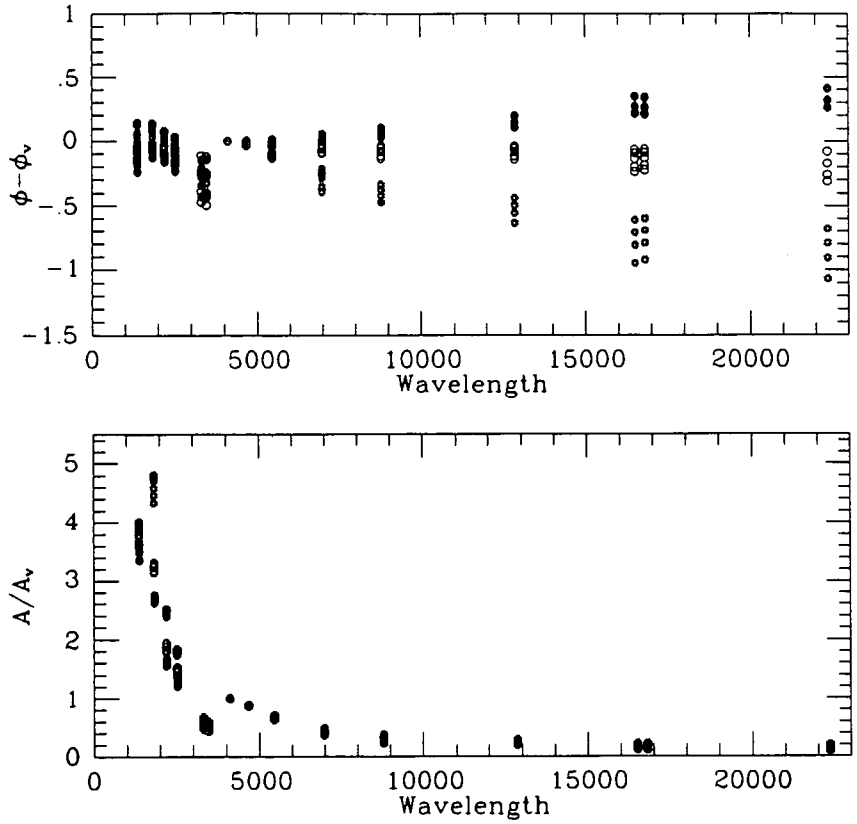

Figure 2.2: The phases (in radians) (top panel) and amplitudes (bottom panel) normalised to the v filter for different wavelengths (Å) for $\ell = 0$ (filled circles), $\ell = 1$ (open circles) and $\ell = 2$ (asterisks) for the same star as in Fig 2.1, for all the frequencies listed in Appendix A.

dominates. Then C is small for radial modes and large for non-radial modes. For very large frequencies, the first term in C becomes insignificant, and C becomes independent of mode.

For the δ Sct stars, T_3 is usually larger than the other two terms in spite of the fact that C is close to a minimum for the frequencies in the region of the fundamental and low-overtone p-modes (≈ 7 d^{-1}), and the factor $R^{\frac{\Gamma_2-1}{\Gamma_2}} \leq 0.4$ for $\Gamma_2 = 5/3$. This is largely because α_T is much larger than α_g, β_g and β_T. (The factor p^* in the expression for T_2 in equation (2.41) is always close to unity. Cugier et al (1994) have argued that it should always be taken as unity, which is the standpoint adopted here). For the δ Sct stars, where $\psi \approx \frac{\pi}{2}$, the imaginary part of T_3 is larger than the other terms. This is shown in Figure 2.4, which is plotted for the same

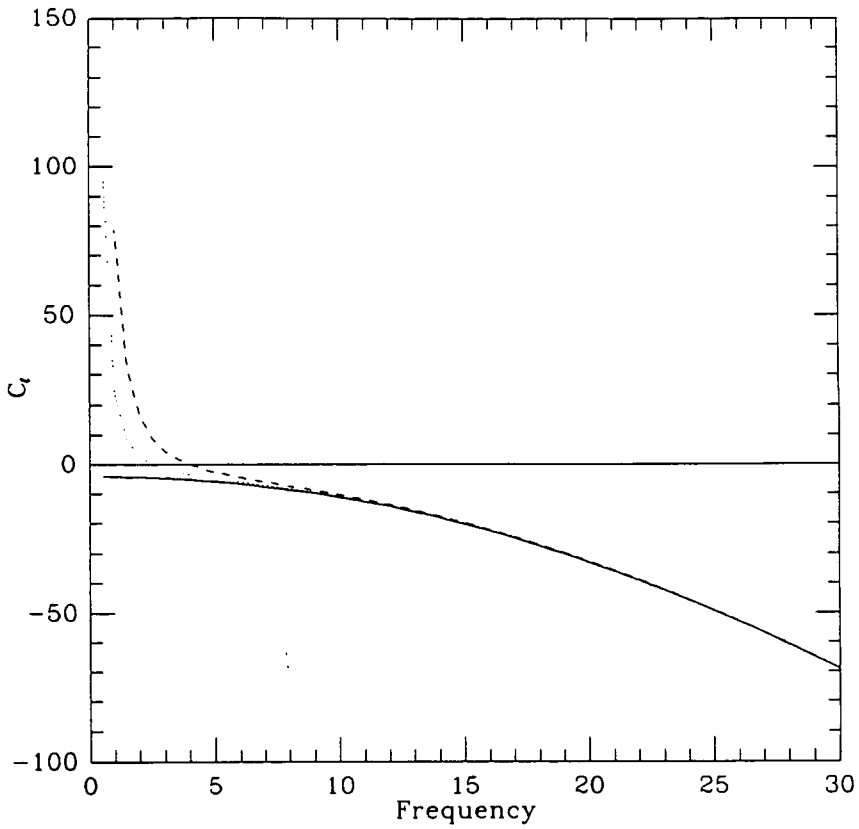

Figure 2.3: The value of C as a function of frequency ν (in d^{-1}) for $\ell = 0$ (solid line), $\ell = 1$ (dotted line) and $\ell = 2$ (dashed line) for a star with mass $M = 1.80 M_{\odot}$, $\log T_{\mathrm{eff}} = 3.8764$ and $\log g = 4.0347$.

star as in Figure 2.1. Hence, the larger the magnitude of C becomes, the less significant the term T_1 becomes, as T_3 then dominates. For very large frequencies, T_1 can be then be ignored. Also, for these large frequencies C becomes independent of mode. As a result, the phases are no longer sensitive to mode, and the mode-dependence of the amplitude comes only from the limb darkening integral $b_{\ell\lambda}$.

For very small frequencies, T_1 is only significant for the radial modes. In this region of the frequency spectrum, the mode-discrimination is dominated by C and $b_{\ell\lambda}$ for the non-radial modes, and by T_1, C and $b_{\ell\lambda}$ for the radial modes. The phases, which do not depend on $b_{\ell\lambda}$ will thus easily discriminate between radial and non-radial modes, but not easily between different non-radial modes. The magnitude of the terms T_1, T_2 and T_3 is plotted against frequency in

Figure 2.5 for a δ Sct model with the same temperature and surface gravity as that of Figure 2.1. The frequency range represented in this figure extends beyond that expected in a δ Sct star. In pulsating white dwarfs, which have small frequencies of pulsation (≈ 0.006 d^{-1}), T_3 is usually so much larger than the other terms that T_1 and T_2 can be neglected completely in calculations of the amplitude. This was done by Brassard, Fontaine & Wesemael (1995). The mode-dependence of the amplitude then comes from the first term in C as mentioned above, and $b_{\ell\lambda}$ only.

Hence mode-identification using amplitudes and phases works best for the intermediate frequencies, which fortunately means the range of frequencies found in the δ Sct stars. The phase differences between light curves in different colours do not always provide much information. In the β Cep stars, $\psi \approx \pi$, and the phase differences that arise between light curves of different colours are small, and do not give much useful information for mode identification. The phase differences for the δ Sct stars are significant and give important information for mode identification. This is because ψ is in the range $90^\circ \leq \psi \leq 140^\circ$ for these stars. This difference allows different approaches to the methods of mode-identification, which are discussed in the next chapter.

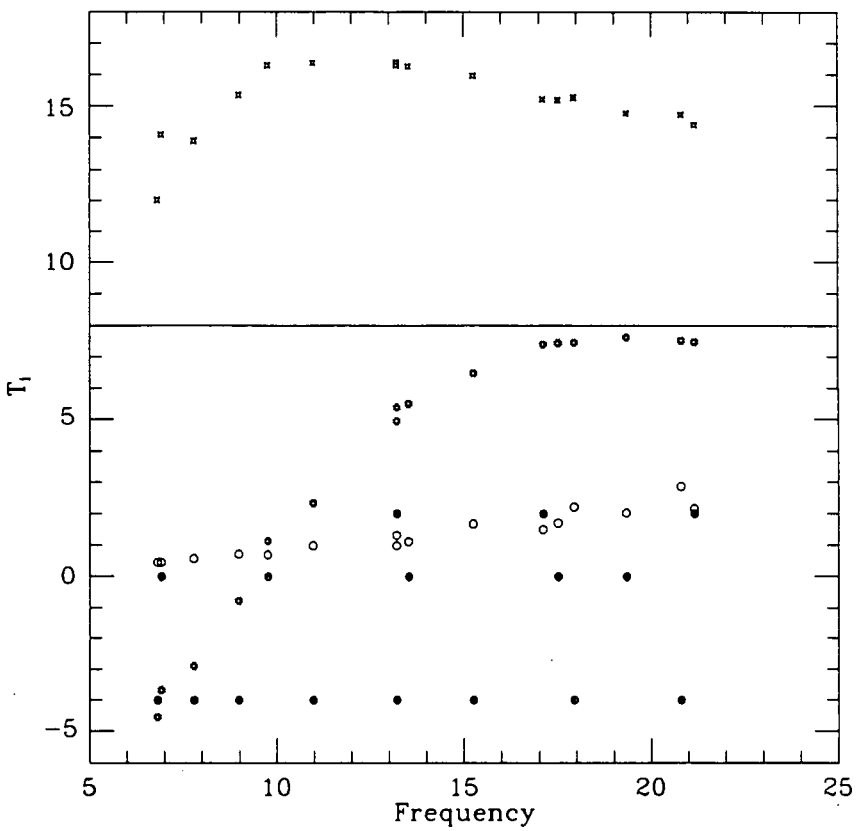

Figure 2.4: The values of the terms T_1 (solid circles),T_2 (empty circles) and the real part of T_3 (asterisks) in the v band as a function of frequency (d^{-1}) for a slightly evolved model with mass 1.8 $M_\odot$, $\log T_{\rm eff} = 3.8764$ and $\log g = 4.0347$ and modes $\ell = 0,1$ and 2. The top panel shows the imaginary part of T_3.

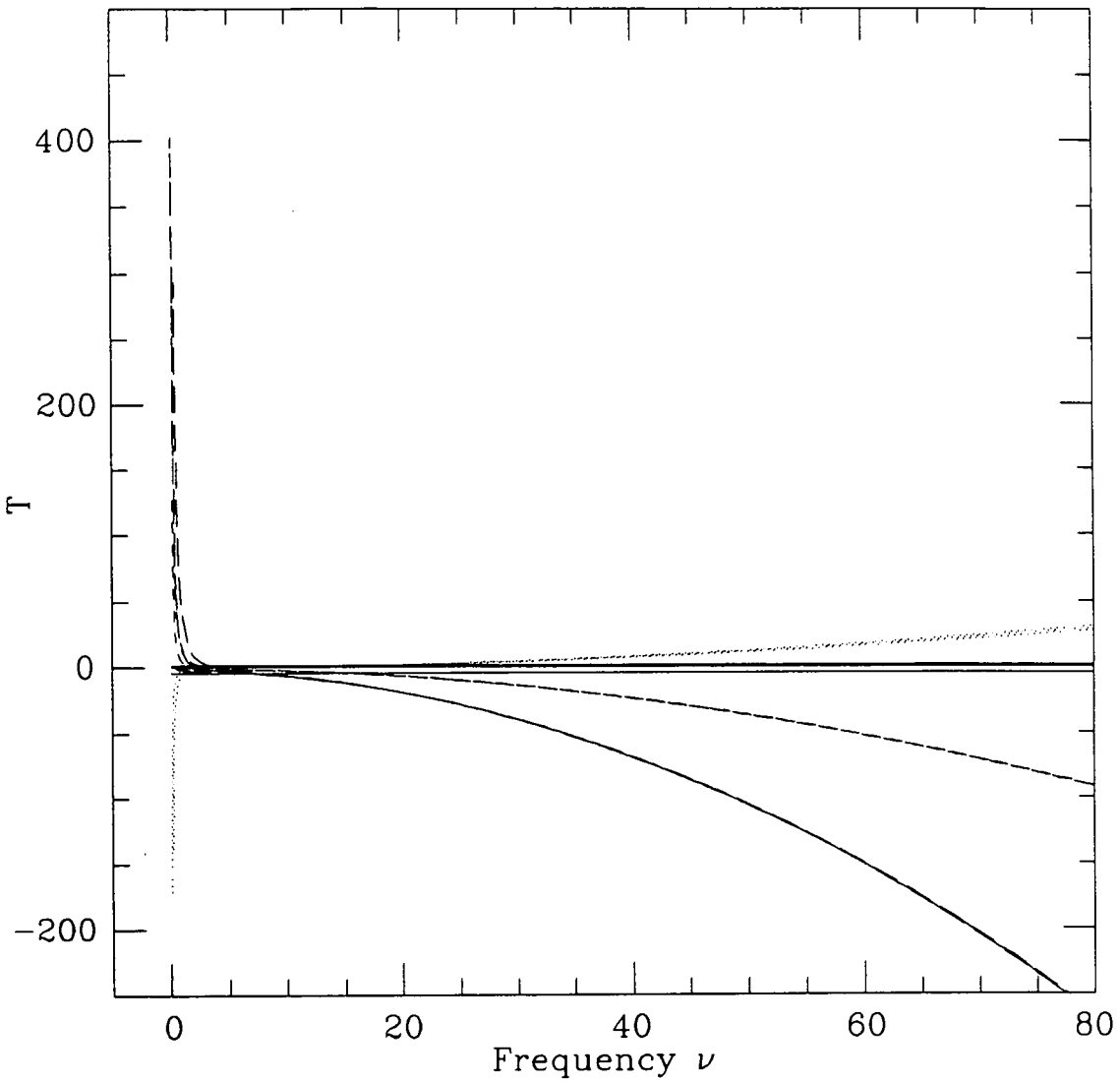

Figure 2.5: The variation of T_1 (solid lines), T_2 (dotted lines), $Re[T_3]$ (short dashed lines) and $Im[T_3]$ (long dashed lines) with frequency (in d^{-1}) in the v filter for the same mass, temperature and surface gravity as in Figure 2.1. The lines are plotted for modes $\ell = 0,1$ and 2 in each case.

Chapter 3

Methods of Mode Identification

In this chapter, some of the methods currently used to identify the spherical harmonic degree ℓ from photometric observations are outlined. As will be discussed at the end of this chapter and in the next chapter, if the spherical harmonic degree, ℓ, frequency of pulsation, ω, effective temperature, $T_{\rm eff}$ and surface gravity, $\log g$, of a star are known, all the terms in equation (2.43) can be determined except for $A_0 P_\ell^m(\cos i)$, f (or R) and ψ. The factor $A_0 P_\ell^m(\cos i)$ is independent of wavelength and can be cancelled out through the use of amplitude ratios rather than actual amplitudes to calculate the mode. R and ψ can be left as free parameters, or determined with the aid of stellar models, as will be discussed here.

There is a fundamental difference in the mode-identification technique for stars inside the Cepheid instability strip and its extension, such as the δ Sct stars, and those outside the strip, such as the β Cep stars. As already mentioned in the previous chapter, for the β Cep stars, all wavelengths vary almost in phase. Hence the phase differences between light curves in different colours do not provide much information. Stars within the Cepheid instability strip and its extension, which includes the δ Sct stars, do have considerable phase variation with wavelength. The phase differences between the light curves in different colours is caused by the hydrogen ionization zone, which introduces a phase shift, ψ, between maximum compression and maximum temperature of approximately 90°. The β Cep stars are too hot to have hydrogen ionization zones and so it is probably safe to assume that $\psi = 180°$. In the β Cep stars therefore, the most useful information for mode-identification is contained in the amplitudes. For stars such as the δ Sct stars, the amplitudes *and* phases provide valuable information that can be used.

3.1 Two-colour diagrams

One of the most popular means of mode-identification is that of 'two-colour diagrams '. These are diagrams in which the amplitude ratio is plotted against the phase difference for any two filter passbands. Watson (1988) showed that different modes ℓ occupy different areas on such a plot, where the size and location of the area is determined by the variation in R and ψ.

If the observations are described by

$$\Delta m_\lambda = B_\lambda \cos(\omega t + \phi_\lambda)$$

where ϕ is the phase in wavelength λ, then, by comparing this with the predicted magnitude variation (equation 2.43) :

$$\left(\frac{B_{\lambda_2}}{B_{\lambda_1}}\right)^2 = \left(\frac{b_{\ell\lambda_2}}{b_{\ell\lambda_1}}\right) \frac{[(\Gamma_2-1)\Gamma_2^{-1}(\alpha_{T\lambda_2}+\beta_{T\lambda_2})CR\sin\psi]^2 + [T_1 + T_{2\lambda_2} + (\Gamma_2-1)\Gamma_2^{-1}(\alpha_{T\lambda_2}+\beta_{T\lambda_2})CR\cos\psi]^2}{[(\Gamma_2-1)\Gamma_2^{-1}(\alpha_{T\lambda_1}+\beta_{T\lambda_1})CR\sin\psi]^2 + [T_1 + T_{2\lambda_1} + (\Gamma_2-1)\Gamma_2^{-1}(\alpha_{T\lambda_1}+\beta_{T\lambda_1})CR\cos\psi]^2}$$

$$\phi_{\lambda_i} = \tan^{-1}\left(\frac{(\Gamma_2-1)\Gamma_2^{-1}(\alpha_{T\lambda_i}+\beta_{T\lambda_i})CR\sin\psi}{T_1 + T_{2\lambda_i} + (\Gamma_2-1)\Gamma_2^{-1}(\alpha_{T\lambda_i}+\beta_{T\lambda_i})CR\cos\psi}\right).$$

For any given ℓ, if ψ and R are fixed, then one can plot the point $(\frac{B_{\lambda_1}}{B_{\lambda_2}}, \phi_{\lambda_1} - \phi_{\lambda_2})$ on a diagram of amplitude vs phase. However, if ψ and R are not fixed, then one can plot the loci of points $(\frac{B_{\lambda_1}}{B_{\lambda_2}}, \phi_{\lambda_1} - \phi_{\lambda_2})$, for a range of R between 0 and 1 and ψ in the range relevant to the type of pulsating variable. This yields a figure such as shown (Figure 3.1) for the β Cep stars, where $\psi = 180 \pm 45°$. A similar diagram is shown in Figure 3.2 for the δ Sct stars. In this figure, ψ is limited to the range of 90° to 140°, which is a range typical of a δ Sct star. The degree ℓ of the observed star is then determined from the area in which the observed point lies.

It can be seen in Fig 3.1 that there is a vertical separation between the areas for the β Cep star. It is the relative amplitudes that are most useful for mode discrimination, as the relative phases are not very sensitive to ℓ. For the δ Sct stars, both amplitudes and phases are useful to distinguish between the modes. The wavelength dependence of the phases is as large or larger than the wavelength dependence of the amplitudes, as seen in the last section of the previous chapter. Examples of the use of this method for the δ Sct stars can be found in Garrido et al. (1990). The disadvantage of using these two-colour diagrams for mode-identification is that only two colours or wavelengths can be used for any one diagram. It is not always easy to decide

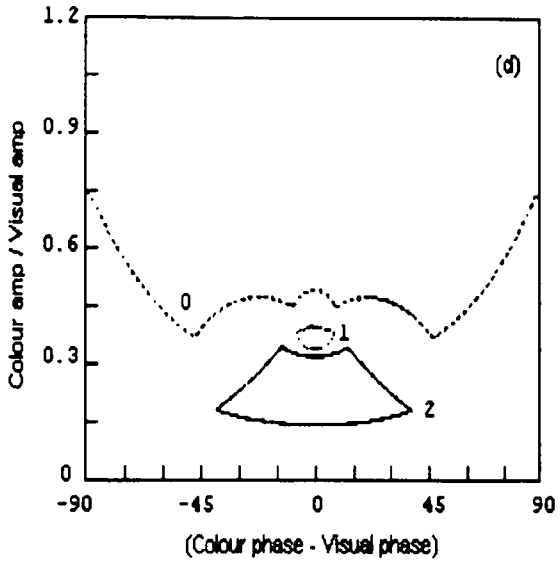

Figure 3.1: A plot of (A_{U-V}/A_V) vs $(\phi_{U-V} - \phi_V)$ (in degrees) for a β Cep star, taken from Watson (1988). The theoretical areas for the (R, ψ) loci were calculated with $0.25 \leq R \leq 1$, and $135^o \leq \psi \leq 225^o$ The modes ℓ are written beside the areas in which observed points of that mode should lie.

which two colours give the best results, nor how to combine the results from many two-colour diagrams. Also, in some cases the areas for different values of ℓ may overlap significantly making it difficult to determine ℓ if an observed point should fall in the region of overlap.

Other methods are also used to identify the modes. The publications discussed below highlight some of the advantages and disadvantages of the current methods.

3.2 Examples of mode identification using amplitudes only.

3.2.1 The β Cep stars

Cugier et al. (1994) improved on the method of the two-colour diagrams described by Watson (1988) by calculating values for f and ψ using a linear non-adiabatic pulsation code. The advantage of doing this is that the areas associated with each mode are smaller, so that discrimination is improved. The authors showed that it is even possible to distinguish between the fundamental and first radial overtones if the phases are used as well.

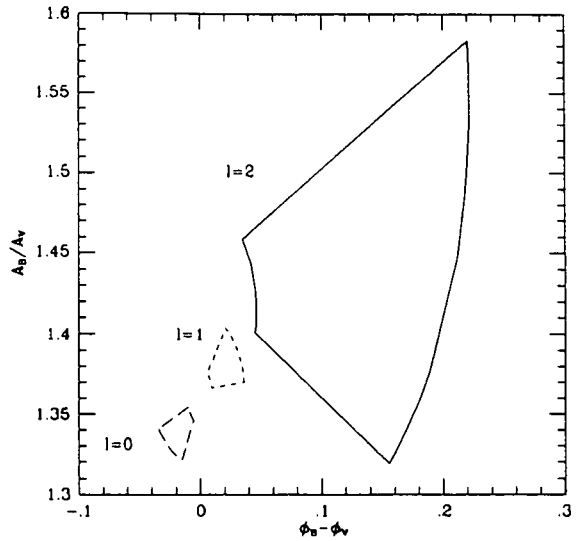

Figure 3.2: A plot of (A_B/A_V) vs $(\phi_B - \phi_V)$ (in radians) for a δ Sct star. The theoretical areas for the (R, ψ) loci were calculated with $0.25 \leq R \leq 1$, and $90° \leq \psi \leq 140°$ The modes ℓ are written beside the areas in which observed points of that mode should lie.

Mode identification for the β Cep stars has also been discussed by Heynderickx et al. (1994). The authors set $\psi = \pi$ and left R as a free parameter. They determined ratios of the oscillation amplitudes at pairs of wavelengths for a given ℓ using model atmospheres. A plot of these normalised amplitudes as a function of wavelength was compared to the corresponding observed ratios to determine the mode. The authors determined R by changing it to get the best agreement between the observed and calculated amplitude ratios. Two of the diagrams from Heynderickx et al. (1994) are shown in Figures 3.3 and 3.4. The value of ℓ chosen was the one that gave the closest agreement with all the colour ratios in each case. As can be seen from fig 3.4, it is not always easy to deduce the mode from the plot. The advantage of this method over that of the two-colour diagrams is that the information from many, rather than just two, wavebands can be used.

Similar to Heynderickx et al. (1994), Balona, Dziembowski & Pamyatnykh (1997) also compared the relative amplitudes in different wavebands to the calculated values to determine ℓ, but, following Cugier et al. (1994), they fixed f and ψ by using stellar models. Furthermore, they chose the value of ℓ as the one which gave the smallest rms difference between the calculated

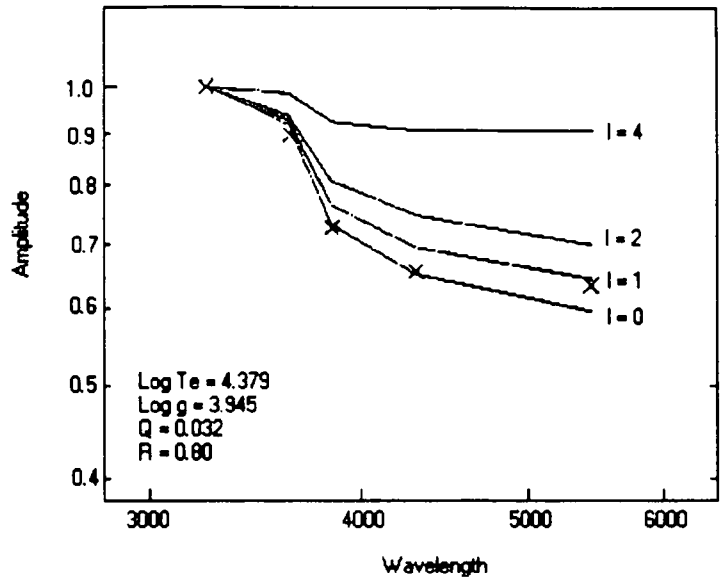

Figure 3.3: Amplitude ratios as a function of wavelength (Å) for the fundamental frequency of the β Cep star V348 Nor. The lines indicate calculated values, and the $\times's$ the observed points. From Heynderickx et al. (1994).

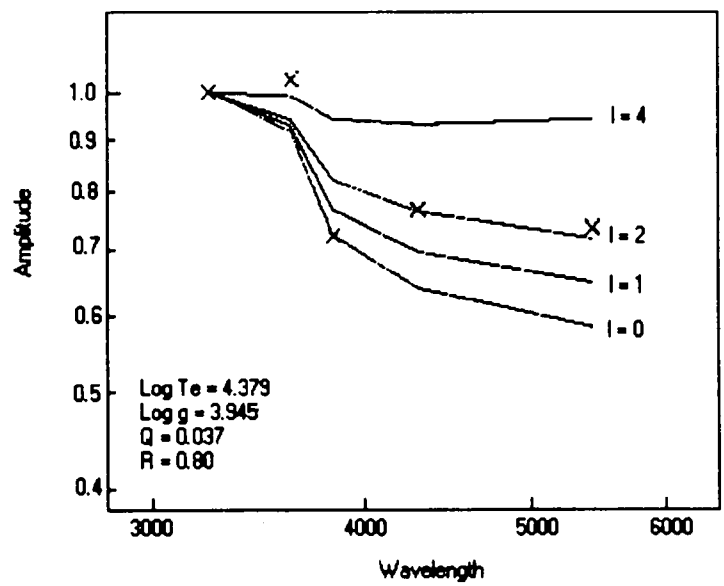

Figure 3.4: Amplitude ratios as a function of wavelength (Å) for the second harmonic of the β Cep star V348 Nor. Also from Heynderickx et al. (1994).

and observed normalised amplitudes. This improves on the method of Heynderickx as it allows the comparison between observed and calculated amplitudes to be quantified, and allows more reliable values of f and ψ to be used.

3.2.2 White dwarfs

Fontaine, Brassard, Bergeron & Wesemael (1996) studied the pulsating white dwarf G117-B15A. They calculated amplitudes of pulsation for the star, and compared this to observed amplitudes. They quantified the comparison by calculating χ^2 defined by

$$\chi^2(\ell) = \Sigma\left(\frac{qa_{\ell j} - b_j}{\sigma_j}\right)^2 \tag{3.1}$$

where the sum is over the wavebands j. Here $a_{\ell j}$ is the calculated amplitude for degree ℓ in waveband j,and b_j is the observed amplitude with corresponding uncertainty σ_j. The factor q is a scale factor which acts as a normalization constant.

The authors calculated $\chi^2(\ell)$ for $\ell = 1$ and 2 at each point on three 91 x 91 $(T_{\rm eff}, \log g)$ grids, where each grid allowed a different treatment of convection. At each point they chose the value of q which minimised χ^2. The place on each grid where $\chi^2(\ell)$ was lowest gave the point at which the observed and predicted amplitudes were in best agreement. For all three grids, values of $\chi^2(1)$ were lower than $\chi^2(2)$ and so the authors concluded that the star was most probably pulsating in an $\ell = 1$ mode.

The advantage of this method over the ones discussed for the β Cep stars is that the comparison between predicted and observed amplitudes is quantified, and a probability can be assigned to the comparison. As the authors note, another advantage is that the method does not rely on the arbitrary choice of a specific waveband for normalization. They do, however, conclude that the results are sensitive to the treatment of convection.

3.3 Mode identification using amplitudes and phases.

The best approach to mode-identification is to use all the available information. For stars such as the δ Sct stars this means that the amplitudes *and* phases for all the wavebands in which a star is observed should be used. There is no obvious way of extending the two-colour diagrams to do this, so a different approach is necessary.

For a star observed in N passbands, there are 2N-1 pieces of information : each passband provides an amplitude and a phase, but one of the phases is fixed by the choice of the time epoch. Hence, given ℓ and the information from two passbands, an algebraic solution is possible using equation 2.43 since there are only three unknowns, *viz* R (or f), ψ and $A_0 P_\ell^m(\cos i)$. Hence, given ℓ, values for R and ψ can be determined. The mode could be identified as that value of ℓ for which the resulting values of R and ψ are in the acceptable range for the type of variable star under investigation, in this case the δ Sct stars. It is possible that more than one value of ℓ will yield acceptable results. In such a case, there is no way to decide between the values of ℓ. If, however, the star is observed in three or more passbands, then a statistical solution becomes possible i.e. one solves for the best values of R and ψ. As for the two-passband case, values of ℓ which do not yield acceptable values for R and ψ can be discarded. If more than one value of ℓ remains, the one that gives the smallest rms value between observed and calculated values of the amplitudes and phases should be selected.

For the δ Sct stars, one of the purposes of identifying the mode is to determine the stellar parameters. In other words, the effective temperature and surface gravity of a δ Scuti star are usually known with some uncertainty. Hence a procedure similar to that of Fontaine et al. (1996) could also be followed, *viz* calculating on a grid of $(T_{\rm eff}, \log g)$ the values of the $\chi^2(\ell)$ for various value of ℓ, and selecting the mode using this information in a way similar to that used by the authors. Instead of leaving f and ψ as free parameters, theoretical values of f and ψ can be calculated using stellar models. The advantage of doing this is that the number of free parameters is reduced. For these reasons, the approach of Fontaine et al. is extended and adapted to include the information provided by the phases of each light curve, but the values of f and ψ are calculated from stellar models. This method is sensitive to the treatment of convection, which is therefore discussed briefly below before the new procedure for mode-identification is outlined.

3.3.1 Stellar convection

In stars, the heat that is generated in the core by the nuclear reactions is transported outwards through the star to the surface. The energy can be transported outwards by radiation, convection, and in a few cases, conduction. Conduction is limited to those stars which consist of degenerate matter, which is outside the scope of this thesis. Radiative transport occurs as photons are continually absorbed and re-emitted by the stellar material until they reach the

surface. As the photons can be re-emitted in any direction, this is not a very efficient means of energy transport. Convection is far more efficient means of energy transport than radiation, but only occurs in certain parts of certain stars. In the sun for example, the granulation of the surface reveals that there is a convective zone close to the surface. In other stars, such as some of the M stars, convection currents may travel completely through the stars from the centre to the surface.

Convective transport of energy occurs when macroscopic elements (called convective cells) move upwards (and downwards) through their surroundings, setting up currents of gas that transport energy outwards. Energy transport by convection is poorly understood. The standard approach is the *mixing length theory.*

Suppose that a local density fluctuation causes a macroscopic element of gas to be buoyed upwards. If the element returns immediately to its original position, then convection cannot occur. If, however, the density of the displaced element is less than that of its surroundings, then it will continue to move upwards and allow convection currents to be set up. Since the element will always take on the same pressure as the surrounding areas, and temperature decreases outwards in a star, this means that convection will occur as long as the temperature within the cell decreases at a slower rate than that of its surroundings. In other words, the rising convective cell is warmer than its surroundings, and thus the atoms in the cell have a higher kinetic energy that the atoms of the surroundings. After moving, on average, one mixing length l, this convective cell will have delivered all of its excess kinetic energy to the surrounding material, and blend in smoothly with its surroundings. There are also descending convective cells to compensate for the rising ones, which descend until they have absorbed the deficiency in kinetic energy that they had. In both cases, the results is a net outward flow of heat.

The mixing length l after which a moving convective cell blends in with its surroundings is usually measured in terms of the isothermal pressure scale height H, which is the distance over which the pressure (or density) varies by a factor of e. The ratio l/H, denoted by α is called the mixing length parameter. It is not well determined, and is usually taken in the range $0.5 \leq \alpha \leq 2.0$.

More details on the transport of energy by convection are available in Kippenhahn & Wiegert (1990) or Mihalas (1978). Novotny (1973) discussed mixing length theory in the context of stellar models.

The δ Sct stars at the upper end of the temperature scale are almost purely radiative in the outer layers, but convection becomes important for the cooler stars. Values of f and ψ can be calculated reliably for the purely radiative models, but where convection becomes important, the precise value of α can change the calculated value of f and ψ determined from stellar models quite significantly. The effect of the mixing length parameter α on the calculated values of f and ψ for the models stars is shown in Figure 3.5. It can be seen from this figure that convection becomes important for $\log T_{\rm eff} < 3.93$. Since α is not well determined, three sets of stellar models were calculated, with values of α covering the whole range of $0.5 \leq \alpha \leq 2.0$. It was hoped that this would allow the effect of the uncertainty in the treatment of convection on the mode-identification procedure to be explored.

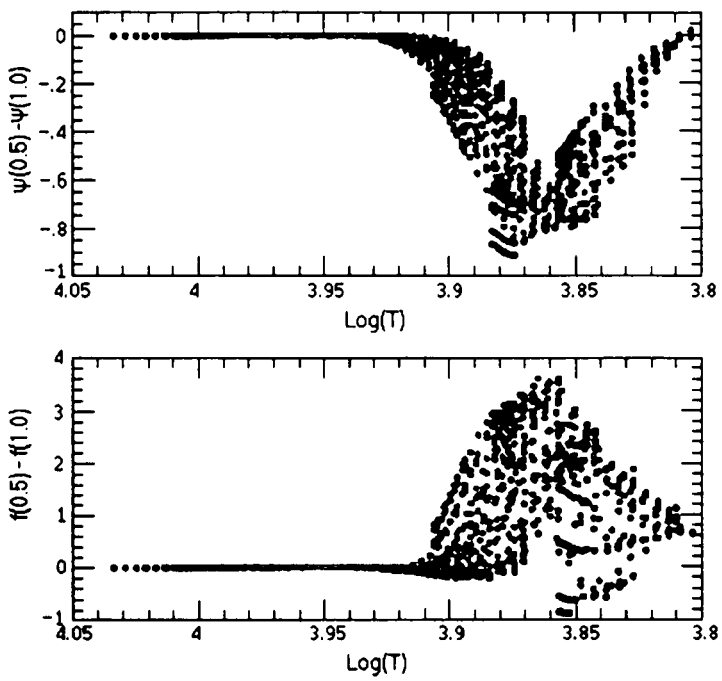

Figure 3.5: Bottom panel: the difference in the non-adiabatic parameter f, for models with mixing length parameters $\alpha = 0.5$ and $\alpha = 1.0$ as a function of the effective temperature. The top panel shows the phase difference ψ (in radians) as a function of effective temperature. From Balona & Evers (1999).

3.3.2 A new mode identification algorithm

The linear non-adiabatic pulsation code NADROT written by W. Dziembowski was used to calculate values for f and ψ, for three different sets of evolutionary models corresponding to three different choices of the mixing length, α = 0.5, 1.0 and 2.0. In terms of the two colour diagrams, fixing the values of f and ψ reduces the calculated areas to points. The uncertainty in the mixing length extends the points to areas again, although these are much smaller than the areas with the full range of variation in f and ψ. The comparison between the observed and calculated amplitudes and phases was quantified through the calculation of a χ^2 expression, which then also allowed a probability to be associated with each mode identification.

A χ^2 expression which includes the phases

If χ^2 is defined by

$$\sigma^2\chi^2 = \sum_j (M_j - qm_j)^2$$

where $M_j = a_{1j}\cos\omega t$ describes the observed light curve, and $m_j = b_{1j}\cos\omega t$ is the calculated variation with time with time for filter j , then, assuming that the light curve is continuous in time, integration over a period and minimization of χ^2 gives

$$q = \frac{< ab >}{< b^2 >}$$
$$\frac{2\sigma^2\chi^2}{N} = < a^2 > - \frac{< ab >^2}{< b^2 >}. \qquad (3.2)$$

We can extend this equation to include the phases by defining

$$M_j = A_{j,obs}\cos(\omega t + \phi_{j,obs}) = a_{1j}\cos\omega t + a_{2j}\sin\omega t$$

and

$$qm_j = qB_{j,cal}\cos(\omega t + \phi_{j,cal} + \gamma) = (q_1 b_1 - q_2 b_2)\cos\omega t + (q_1 b_2 + q_2 b_1)\sin\omega t,$$

where $b_1 = B_{j,cal}\cos\phi_{j,cal}$, $b_2 = -B_{j,cal}\sin\phi_{j,cal}$, $q_1 = q\cos\gamma$, and $q_2 = -q\sin\gamma$, and γ is an unknown phase shift required to bring the calculated light curve into phase with the observed curve. It is easy to show, by following the same method as above, that

$$q_1 = \frac{< a_1 b_1 > + < a_2 b_2 >}{< b_1^2 > + < b_2^2 >}$$

$$q_2 = \frac{< a_2 b_1 > - < a_1 b_2 >}{< b_1^2 > + < b_2^2 >}$$

$$\frac{2\sigma^2\chi^2}{N} = < a_1^2 > + < a_2^2 > - \frac{(< a_1 b_1 > + < a_2 b_2 >)^2}{< b_1^2 > + < b_2^2 >} - \frac{(< a_2 b_1 > - < a_1 b_2 >)^2}{< b_1^2 > + < b_2^2 >}. \quad (3.3)$$

This equation reduces to equation (3.2) if $b_2 = q_2 = a_2 = 0$. Equation (3.3) is the equation that was used to calculate $\chi^2(\ell)$ for the δ Sct stars in the next chapter.

As already discussed, each waveband provides two items of information - an amplitude and a phase. One of the observed phases is fixed by the choice of time epoch, and one of the observed amplitudes is used to fix the constant $A_0 P_\ell^m(\cos i)$ of equation (2.43). The number of degrees of freedom, which is needed to calculate the probability, is then 2(N-2), provided that f and ψ are known. Hence, for two passbands, an algebraic solution is possible, but a minimum of three passbands in needed for a statistical solution.

From the goodness of fit criterion, χ^2, the significance of the result can be calculated provided that the number of degrees of freedom is known. The probability P of a mode identification can be calculated using printed tables of the χ^2 function or various subroutines available for this purpose.

A brief overview of the method used to identify the mode in δ Sct stars

For any particular star, the observed frequencies of pulsation and the associated amplitudes and phases in each passband need to be identified from the photometric observations. These observations can also be used to determine a range of possible values for each of the stellar parameters $T_{\rm eff}$, $\log g$ and mass M.

In this study, the Warsaw-New Jersey evolutionary code was used to construct models with solar composition for a range of masses typical of the δ Sct stars between the zero-age main sequence (ZAMS) and the end of core-hydrogen burning (ECHB) for three different values of the mixing length α = 0.5, 1 and 2. Use of Dziembowski's linear non-adiabatic pulsation code (NADROT) gave, for each model, modes ℓmn, with $m = 0$, and the associated pulsation frequencies, and values of f and ψ, as well as values describing the stability and nature of the modes. (For the δ Sct stars, non-radial modes have mixed p- and g-mode characteristics, except close to the ZAMS.) A typical output file is given and explained in Appendix A.

Models with stellar parameters within the allowed ranges were then selected and for each fre-

quency in these models close to the observed frequency, the associated values of ℓ, f and ψ were used to calculate amplitudes and phases through each filter in which the star was observed. The observed and theoretical frequencies do not match exactly, but it was hoped that the values of f and ψ used here would be in approximate agreement with the observed frequency, so that ℓ could be determined.

The calculated amplitudes and phases were then compared to the observed values through the evaluation of the χ^2 expression derived above. The set of calculated amplitudes and phases (and associated values of f, ψ and ℓ) that gave the lowest χ^2 value thus also yielded the most probable mode.

At first, only model frequencies associated with excited p-modes were selected. If this yielded no results, then excited g-modes were also selected. If still no results were obtained, then stable modes were allowed as well. This was done in order to obtain a unique identification across the spectrum of mixing lengths. In this context, a g-mode was considered to be any mode that was not a p- or almost pure p-mode. This algorithm is discussed in more detail in the next chapter, where it is applied to some δ Sct stars.

The model that gives the best fit to the observed data also gives stellar parameters which could describe the observed star. To obtain accurate stellar parameters there should be the best possible match between observed and theoretical frequencies, and so the stellar parameters which result from the mode-identification procedure are not reliable since the theoretical and observed frequencies do not match exactly. The models are used only to give appropriate values of f and ψ for each model frequency and ℓ value which is in approximate agreement with the observed frequency. A suggestion of how to obtain more reliable stellar parameters is given in Chapter 6.

Chapter 4

Procedure

In this chapter the method outlined in Chapter 3 is applied to some δ Sct stars. The selection of these δ Sct stars is discussed first, as well as the determination of the period(s) of pulsation $P = 1/\nu_0 = 2\pi/\omega$, $T_{\rm eff}$, $\log g$ and the mass M for each star. Thereafter, the models used to determine f and ψ are briefly discussed, with some notes on rotation. After that the calculation of the terms T_1, T_2, T_3 and $b_{\ell\lambda}$ in equation (2.43) are explained. At this point there is enough information to predict the amplitudes and phases for each passband, and so the last section deals with how all the information is assembled and used to determine the mode.

4.1 The observations

4.1.1 Selecting appropriate δ Sct stars

The more periods present in a δ Sct star or the closer the frequencies are spaced, the longer the period of observation needed to resolve the individual periods. Many of these stars are multiperiodic and should be observed for two weeks or more to obtain accurate estimates of the periods. Fortunately, many δ Sct stars have already been observed and the data published. Hence, due to constraints on time available to observe these stars, and the time available to complete this study, most of the data used here was taken from the literature. Only two stars, CC Oct and EW Aqr, were actually observed. The observations for these two stars were taken through the Strömgren *uvby* filters using the 0.5-m telescope and the Modular Photometer at the SAAO site near Sutherland, in August 1997. The conditions during the two weeks for which these stars were observed were not very photometric, but some data were nevertheless obtained,

as can be seen in Appendix C.

In searching for data for about a dozen stars in the literature, only δ Sct stars that were not clearly Pop II and had been observed in at least three colours were selected. Most of the data found was in the Strömgren (*uvby*) system. Both high and low amplitude stars were chosen, including three double mode high amplitude stars. The high amplitude stars are known to pulsate radially, and were chosen to see whether the modes would be identified as such using the algorithm outlined in the previous chapter. Any data series which was not of a sufficient length, or gave different frequencies in the different wavebands when Fourier-analysed was also rejected. In searching for the data, extensive use was made of the NASA Astrophysics Data Service (ADS) abstract service[1], as well as the over 800 references of the 'δ Sct Table' published by Rodriguez et al. (1994). Where the data were not specifically published, they were obtained directly from the authors, or from the IAU Commission 27 archives of unpublished data. A list of the stars for which satisfactory data was found is given in Table 4.1.

4.1.2 Determining the period(s) of pulsation

In most cases, the articles on each of the selected δ Sct stars provided the frequencies of pulsation found by the authors. In spite of this, a periodogram analysis[2] was performed on each star to determine the periods of pulsation present. In some cases more periods were found than discussed in the literature. In other cases, different authors quoted different results for the same star, and the periodogram analysis was used to decide which frequencies and data to use. It should be noted here that many of the high-amplitude δ Sct stars do not have sinusoidal variations, which is the assumption of equation (2.43). In all cases the light curves in the different wavebands were analysed into the fundamental Fourier component and its harmonics by least squares. Only the amplitude and phase of the fundamental component was used. The standard error of the sine and cosine amplitude is approximately independent of wavelength. The average value was used as an estimate for σ in the χ^2 expression equation (3.3). Tests showed that when sigma was allowed to vary with wavelength, the results for the mode identification were the same as when an average value was used, except that the resulting calculated probabilities of the identification differed slightly (by approximately 1 percent).

Once the frequencies of pulsation had been determined, they were refitted to the data, and the

[1] http://adsabs.harvard.edu/abstract_service.html
[2] See Appendix B.

Table 4.1: Table with selected stars and the pulsation frequencies ν (d^{-1}), amplitudes A (mag), phases ϕ (radians) and the uncertainty in the amplitudes σ (mag) extracted from the light curves using Fourier analysis.

Star	Ref	ν	A_u ϕ_u σ_u	A_v ϕ_v σ_v	A_b ϕ_b σ_b	A_y ϕ_y σ_y
AE UMa	2	11.6253	0.2362	0.3002	0.2622	0.2151
			-1.1140	-1.0001	-1.0053	-0.9898
			0.0089	0.0115	0.0101	0.0085
		15.0326	0.0370	0.0439	0.0369	0.0301
			-0.9979	-0.9659	-0.9854	-1.0058
			0.0089	0.0115	0.0101	0.0085
BP Peg	2	9.1263	0.2343	0.2899	0.2433	0.2022
			-1.0632	-1.0291	-1.0111	-0.9913
			0.0075	0.0047	0.0046	0.0045
		11.8242	0.0557	0.0527	0.0450	0.0396
			0.4617	0.5355	0.5364	0.7056
			0.0072	0.0045	0.0044	0.0043
RV Ari	2	10.7360	0.2466	0.3188	0.2754	0.2293
			0.7354	0.8184	0.8268	0.8407
			0.0131	0.0172	0.0146	0.0127
		13.8964	0.0988	0.1211	0.1059	0.0831
			1.1172	1.1924	1.1968	1.1617
			0.0127	0.0166	0.0140	0.0122
AD CMi	1	8.1318	0.1740	0.2221	0.1885	0.1517
			0.8193	0.9152	0.9162	0.9294
			0.0044	0.0042	0.0037	0.0033
BE Lyn	4	10.4309	0.1828	0.2446	0.2140	0.1744
			-0.9519	-0.8539	-0.8519	-0.8315
			0.0058	0.0077	0.0068	0.0057
EH Lib	11	11.3110	0.2517	0.3184	0.2756	0.2231
			0.4001	0.4970	0.5043	0.5347
			0.0170	0.0185	0.0158	0.0130
DY Her	10	6.7282	0.2396	0.3007	0.2514	0.2010
			-1.2911	-1.2387	-1.2236	-1.2045
			0.0108	0.0133	0.0113	0.0091
RS Gru	14	6.8000	0.2352	0.3176	0.2725	0.2217
			-0.0863	-0.0063	0.0003	0.0207
			0.0094	0.0126	0.0109	0.0090
V567 Oph	15	6.7000	0.1948	0.2425	0.2010	0.1600
			-0.3810	-0.3113	-0.3117	-0.2969
			0.0085	0.0104	0.0082	0.0071
V1719 Cyg	19	3.7400	0.0807	0.1030	0.0829	0.0685
			1.1717	1.2384	1.2368	1.2402
			0.0093	0.0114	0.0090	0.0073
β Cas	3	9.9100	0.0210	0.0249	0.0209	0.0167
			0.3785	0.6077	0.5888	0.5696
			0.0007	0.0006	0.0004	0.0004

Table 4.1: Continued...

Star	Ref	ν	A_u	A_v	A_b	A_y
			ϕ_u	ϕ_v	ϕ_b	ϕ_y
			σ_u	σ_v	σ_b	σ_y
BF Phe	5	16.0100	0.0084	0.0106	0.0094	0.0072
			-1.1022	-0.9608	-1.0001	-0.9626
			0.0008	0.0007	0.0007	0.0006
	6	16.0166	0.0059	0.0091	0.0079	0.0062
			0.8355	0.8855	0.8443	0.8537
			0.0006	0.0004	0.0004	0.0005
DL Eri	9	6.4018	0.0151	0.0202	0.0175	0.0153
			-0.6203	-0.6033	-0.5671	-0.5717
			0.0010	0.0011	0.0011	0.0009
		10.8587	0.0110	0.0144	0.0126	0.0103
			0.2740	0.5895	0.5173	0.5043
			0.0010	0.0011	0.0011	0.0009
EW Aqr	12	10.2500	0.0291	0.0267	0.0223	0.0137
			-1.2581	-0.9550	-1.1706	-1.0433
			0.0089	0.0091	0.0074	0.0065
	8	10.3400	0.0211	0.0269	0.0221	0.0206
			0.7978	0.8839	0.9124	0.8828
			0.0024	0.0029	0.0026	0.0031
		10.0180	0.0103	0.0130	0.0093	0.0073
			-0.1153	0.1698	0.1818	0.2017
			0.0024	0.0028	0.0025	0.0030
		4.7400	0.0089	0.0115	0.0096	0.0092
			0.1548	0.0961	0.1254	0.2475
			0.0024	0.0029	0.0026	0.0031
GN And	13	14.4292	0.0344	0.0356	0.0317	0.0273
			1.4948	-1.4995	-1.5215	1.5696
			0.0030	0.0030	0.0030	0.0030
o^1 Eri	9	13.2600	0.0147	0.0199	0.0134	0.0117
			1.3998	1.4642	1.5375	1.4499
			0.0010	0.0042	0.0010	0.0016
		6.7400	0.0089	0.0131	0.0096	0.0088
			0.0353	-0.2141	0.0713	0.1697
			0.0010	0.0042	0.0010	0.0016
V853 Cen	16	18.9186	0.0098	0.0103	0.0093	0.0076
			1.0064	1.1113	1.0507	1.0999
			0.0007	0.0006	0.0006	0.0005
		16.7520	0.0011	0.0018	0.0021	0.0011
			0.1121	0.0253	-0.2258	-0.0992
			0.0007	0.0006	0.0006	0.0005
		18.9186	0.0040	0.0055	0.0044	0.0035
			1.2666	1.4823	-1.5516	1.5286
			0.0017	0.0012	0.0022	0.0018
		16.7520	0.0013	0.0013	0.0011	0.0002
			0.9170	1.4489	0.8501	0.5693
			0.0017	0.0012	0.0022	0.0018
		18.9200	0.0036	0.0050	0.0041	0.0035
			-0.5799	-0.3955	-0.2263	-0.3208
			0.0016	0.0011	0.0021	0.0017
		16.5820	0.0014	0.0016	0.0019	0.0011
			-1.1578	-0.6726	-1.1905	-1.3868
			0.0016	0.0011	0.0021	0.0017

Table 4.1: Continued...

Star	Ref	ν	A_u	A_v	A_b	A_y
			ϕ_u	ϕ_v	ϕ_b	ϕ_y
			σ_u	σ_v	σ_b	σ_y
CC Oct	7	8.0062	0.0262	0.0361	0.0258	0.0214
			0.4741	0.5854	0.6746	0.7026
			0.0031	0.0020	0.0011	0.0010
		12.5763	0.0262	0.0361	0.0258	0.0214
			0.4741	0.5854	0.6746	0.7026
			0.0031	0.0020	0.0011	0.0010
		8.1100	0.0051	0.0084	0.0067	0.0066
			1.2695	1.4532	1.3786	1.4081
			0.0031	0.0020	0.0011	0.0010
	8	8.0000	0.0189	0.0275	0.0202	0.0127
			0.7753	0.6918	0.9168	0.8747
			0.0029	0.0029	0.0022	0.0018
		8.1120	0.0067	0.0106	0.0085	0.0049
			1.5542	1.1723	1.3707	1.3975
			0.0027	0.0027	0.0020	0.0017
		12.6200	0.0048	0.0063	0.0042	0.0023
			-1.3679	1.4994	-1.3640	-1.5689
			0.0023	0.0023	0.0018	0.0015
AN Lyn	17	10.1756	0.0733	0.0946	0.0814	0.0681
			0.0900	6.1790	6.1790	6.1750
			0.0010	0.0005	0.0006	0.0007
		18.1309	0.0047	0.0050	0.0044	0.0040
			2.1550	1.6530	1.7170	1.6940
			0.0010	0.0005	0.0006	0.0007
		9.5598	0.0043	0.0044	0.0046	0.0043
			0.7180	0.6230	0.6300	0.7040
			0.0010	0.0005	0.0006	0.0007
V393 Car	18	7.0770	0.0859	0.1131	0.0949	0.0771
			-1.2840	-1.2075	-1.1900	-1.1719
			0.0034	0.0045	0.0038	0.0031
		12.5780	0.0046	0.0058	0.0045	0.0038
			-0.0645	0.4711	0.3626	0.2409
			0.0034	0.0045	0.0038	0.0031
	18	7.0770	0.0861	0.1132	0.0950	0.0772
			-1.2823	-1.2059	-1.1885	-1.1704
			0.0034	0.0044	0.0037	0.0031
		13.5780	0.0064	0.0077	0.0065	0.0052
			-0.1886	0.2519	0.1396	0.0644
			0.0034	0.0045	0.0037	0.0031

Table 4.1: Continued...

Star	Ref	ν	A_V	A_B	A_U	A_{B1}	A_{B2}	A_{V1}	A_G
			ϕ_V	ϕ_B	ϕ_U	ϕ_{B1}	ϕ_{B2}	ϕ_{V1}	ϕ_G
			σ_V	σ_B	σ_U	σ_{B1}	σ_{B2}	σ_{V1}	σ_G
HD 105513	20	6.8559	0.0124	0.0170	0.0151	0.0179	0.0153	0.0122	0.0101
			1.4585	1.4255	1.3409	1.4052	1.3182	1.4097	1.3092
			0.0012	0.0015	0.0022	0.0017	0.0017	0.0015	0.0014
		6.6388	0.0122	0.0164	0.0130	0.0167	0.0165	0.0124	0.0111
			-0.6961	-0.7652	-0.8734	-0.7379	-0.7610	-0.7763	-0.6978
			0.0012	0.0015	0.0022	0.0016	0.0017	0.0015	0.0014
		6.8902	0.0067	0.0105	0.0098	0.0113	0.0107	0.0073	0.0053
			0.0697	0.1187	-0.0349	0.0531	0.0431	0.0651	-0.1232
			0.0011	0.0015	0.0021	0.0016	0.0017	0.0015	0.0014
		6.4586	0.0053	0.0071	0.0053	0.0070	0.0063	0.0050	0.0042
			-0.4162	-0.5722	-0.7777	-0.6702	-0.5391	-0.8711	-0.5420
			0.0011	0.0015	0.0021	0.0016	0.0017	0.0014	0.0014

1 - Rodriguez et al. (1988a); 2 - Rodriguez et al. (1992a); 3 - Rodriguez et al. (1992b); 4 - Rodriguez et al. (1990); 5 - Rodriguez et al. (1988b); 6 - Poretti et al. (1996); 7 - Kurtz (1980); 8 - Evers & Meintjes (unpublished); 9 - Jørgensen & Nørgaard-Nielsen (1975); 10 - Breger et al. (1978); 11 - Joner (1986); 12 - Kilambi et al. (1978); 13 - Rodriguez et al. (1993); 14 - Rodriguez et al. (1994); 15 - Powell et al. (1990); 16 - Vander Linden & Sterken (1986); 17 - Rodriguez et al. (1997); 18 - Helt (1984); 19 - Joner & Johnson (1985); 20 - Heynderickx (1994)

amplitude and phase determined for each filter using least squares. These results are also listed in Table 4.1.

AE Uma, BP Peg and RV Ari are all high amplitude double mode stars, i.e. both frequencies listed for each star are associated with radial pulsation. The other HADS are AD CMi, BE Lyn, EH Lib, DY Her, RS Gru, V567 Oph and V1719 Cyg. All the other stars are low or medium amplitude pulsators.

The frequency analysis of some of the stars needs to be discussed as the frequencies found differ between authors and sets of data. There are two sets of data for BF Phe (HD 223480), taken a few years apart by different authors. The single frequency found by Rodriguez et al. (1988b) differs only slightly from that of Poretti et al. (1996). Both sets of data were used independently to determine the pulsation mode.

Gupta (1980) observed DL Eri (HR 1225) and found two frequencies of 6.415 d^{-1} and 8.418 d^{-1}. Poretti (1989) found frequencies of 6.41, 10.26 and 8.98 d^{-1}. Using the data of Jørgensen & Nørgaard-Nielsen (1975) two frequencies, 6.4018 and 10.8587 d^{-1}, close to two of the frequencies found by Poretti, were found in the periodogram analysis and used for the mode identification.

Kilambi, DuPuy & Koegler (1978) observed EW Aqr (HR 8102) and found only a single period of 0.097 d. This star was also observed on the 0.5-m telescope at the SAAO site near Sutherland in August 1997 (see Appendix C) to obtain better data through the Strömgren filters. Three frequencies of 10.340, 10.018 and 4.74 d^{-1} were found. These frequencies are similar to those of Hobart, Pena & Peniche (1989): 10.34750, 9.19588 and 4.7195 d^{-1}, except that the alias of their 9.19588 d^{-1} frequency, namely 10.018 d^{-1}, was found in the Sutherland data, and used to determine the mode ℓ.

Although Jørgensen & Nørgaard-Nielsen (1975) quote only one period for o^1 Eri (12.26 d^{-1}), a second frequency 6.74 d^{-1} was found when searching for frequencies in their data. Poretti (1989) found three frequencies, 13.38 d^{-1}, 6.94 d^{-1} and 6.03 d^{-1} when he observed this star. As this data set is much longer than that of Jørgensen & Nørgaard-Nielsen, the alias of 12.26, i.e. 13.26 d^{-1}, and the second frequency of 6.74 d^{-1} were fitted to their data and used to identify the mode.

Vander Linden & Sterken (1986) observed V853 Cen (HR 126859) in 1982 and 1984. The frequencies identified in the 1982 set were 18.9186 and 16.7520 d^{-1}. In the 1984 set the two frequencies of 18.2 and 16.5820 d^{-1} were identified. The authors considered the 1982 set to be more reliable, and so the frequencies identified in 1982 were also fitted to the 1984 set of data. Hence three sets of data were available for mode identification.

Kurtz (1980) observed CC Oct (HD 188136) in the B and V filters as well as the Strömgren filters. Using the more numerous B and V data, three frequencies of 8.0062, 8.1100 and 12.5763 d^{-1} were identified. As the data in the Strömgren filters were not of sufficient number to resolve the frequencies well, the star was observed again in August 1997, and three frequencies close to those of Kurtz were found: 8.000, 8.1120 and 12.6200 d^{-1}(See Appendix C).

In the frequency analysis of V393 Car, it was difficult to decide between the two aliases 12.578 and 13.578 d^{-1}, hence both were fitted to the data and used for the mode identification.

4.2 Determining ranges in the stellar parameters

In order to determine the mode of pulsation, it was necessary to estimate ranges in the temperature, mass and surface gravity for each star. This was done as described below.

4.2.1 Geneva photometry

Künzli, North, Kurucz & Nicolet (1997) provide a calibration (based on Kurucz (1979) models and standard stars) for B to G stars observed in seven colour Geneva photometry. Their calibration, together with a value for the reddening[3] E(B2-V1) = 0.044 from Heynderickx (1994) was used to obtain values of $T_{\rm eff} = 6961 \pm 59K$ and $\log g = 3.95 \pm 0.11$ for the star HD 105513. The colour indices for this star, U = 1.491, V = 0.539, B1 = 0.958, B2 = 1.412, V2 = 1.261 and G = 1.635, were obtained from the *General Catalogue of Photometric Data.*[4]

4.2.2 Strömgren photometry

The data for all the stars besides HD105513 was in the *uvby* system, for which there are a few calibrations. Since so many of the selected stars were observed in through these filters, it was decided to use three of the available calibrations in order to get a better estimate of the uncertainty in the stellar parameters.

Crawford (1975, 1979) provides empirical calibrations for A and F stars. His calibrations allow the reddening $E_{(b-y)}$, the dereddened indices (denoted by subscript 0) and the absolute visual magnitude, M_V, to be determined from the observed indices, defined by:

$$\begin{aligned} (b-y) &= b-y \\ m_1 &= v-2b+y \\ c_1 &= u-2v+b \\ \beta &= H_{\beta(narrow)} - H_{\beta(intermediate)} \end{aligned}$$

where the H_β filters are narrow filters centred at approximately 4850 Å. These indices and their sources are listed for all the selected stars in Table 4.2.

Balona (1994) gives interpolation formulae for $T_{\rm eff}$, the bolometric correction[5] BC, surface gravity $\log g$, and mass in terms of the dereddened Strömgren indices. His calibration is based on synthetic *uvby* colours, and the zero points of the relations are fixed using stars for which the physical parameters are well known.

[3]Interstellar grains absorb and scatter starlight. The blue light is more efficiently scattered than the red light, and so the light is said to be 'reddened'.

[4]http://obswww.unige.ch/gcpd

[5]The bolometric magnitude of a star, m_{bol} is the magnitude of the star calculated over all wavelengths. The bolometric correction is the difference between the visual magnitude and the bolometric magnitude, i.e. $m_{bol} = m_V + BC$.

Table 4.2: The colour indices of δ Sct stars for which a time series of multicolour photometry was available. The values in brackets are derived and not observed.

Star	$b-y$	m_1	c_1	β	Reference
AD CMi	0.182	0.179	0.853	2.760	1,2
AE UMa	0.176	0.155	0.841	2.770	3
β Cas	0.216	0.177	0.785	2.721	4
BE Lyn	0.160	0.159	0.841	2.780	5
BF Phe	0.167	0.186	0.769	(2.776)	2
BP Peg	0.228	0.161	0.857	2.775	3
CC Oct	0.272	0.360	0.429	2.733	2
DL Eri	0.163	0.183	0.877	2.762	2
DY Her	0.217	0.181	0.821	2.783	2
EH Lib	0.179	0.156	0.859	2.787	2
EW Aqr	0.179	0.180	0.905	2.758	2
GN And	0.169	0.165	0.869	2.755	6
RS Gru	0.176	0.150	0.922	2.774	2
RV Ari	0.280	0.147	0.812	2.756	3
o^1 Eri	0.198	0.194	0.792	2.730	2
V567 Oph	0.451	0.079	0.927	2.764	2
V853 Cen	0.130	0.187	1.007	2.837	7
AN Lyn	0.202	0.191	0.796	2.762	2
V393 Car	0.181	0.181	0.844	2.761	2
V1719 Cyg	0.249	0.174	0.833	2.710	2

1 - Rodriguez et al. (1988a); 2 - Rodriguez et al. (1994); 3 - Rodriguez et al. (1992a); 4 - Rodriguez et al. (1992b); 5 - Rodriguez et al. (1990); 6 - Rodriguez et al. (1993); 7 - Vander Linden & Sterken (1986)

Moon & Dworetsky (1985) give calibrations for the effective temperature and surface gravity of B, A and F stars using Strömgren photometry in terms of grids. Their calibrations are also based on synthetic colour indices, which are empirically corrected to be in agreement with observed values. The calibration for the surface gravity was found to be incorrect for Am stars[6] by the authors, and subsequently corrected in Dworetsky & Moon (1986). Two FORTRAN programs were obtained through correspondence with M.M. Dworetsky. The one program, TEFFLOG.F, implements the grids of Moon & Dworetsky (1985). The other program, UVBYBETA.F assembles various empirical calibrations between the stellar parameters and the Strömgren colour indices. This program gives the dereddened indices, the reddening $E_{(b-y)}$, M_V, the radius R and the metallicity indicator δm_1.

[6]These stars have a higher metal content that usual.

Finally, Ribas, Jordi, Torra & Giménez (1997) give calibrations of mass, radius and surface gravity in terms of u,v,b,y and β for main sequence stars, based on the data obtained from binary stars.

These calibrations were used as to determine the ranges in the stellar parameters as follows:

1. The colour indices listed in Table 4.2 were dereddened using the calibrations of Crawford (1975, 1979). No published value was available for β for the star BF Phe, so it was estimated using Moon & Dworetsky's program UVBYBETA.F which gives an estimate of β from c_1 and $(b-y)$. M_V was also calculated using Crawford's calibrations. The bolometric correction BC, and effective temperature were calculated using the formulae of Balona (1994). The luminosity of each star was calculated using

$$\log L = -0.4(M_V + BC - M_{bol\odot}) \text{ where } M_{bol\odot} = 4.76 \text{ mag}$$

and this was then used to determine the mass of each star, again using Balona's formulae. Here, both the mass and luminosity are given in terms of the solar mass and luminosity. Balona also gives formulae for $\log g$ but does not recommend their use. Hence the surface gravity was calculated using the relation:

$$\log g = \log M - \log L + 4\log(\frac{T_{\text{eff}}}{T_{\text{eff}\odot}}) + \log g_{\odot}.$$

Using these calibrations, the uncertainties in $\log T$, $\log g$ and M are 0.009 dex[7], 0.3 dex and 0.076 $M_{\odot}$ respectively.

2. The two FORTRAN programs obtained from M.M. Dworetsky were used to determine the dereddened colour indices, the metallicity indicator[8] δm_1, and values for effective temperature and surface gravity. The $\log g$ values were corrected for the Am stars using the formula given in Dworetsky & Moon (1986). The values of BC were calculated using the results of UBVYBETA.F and Balona's formula, and the luminosity and mass were calculated as above. The uncertainties in $\log T$, $\log g$ and M are 0.015 dex, 0.10 dex and 0.076 $M_{\odot}$ respectively.

3. The calibrations of Ribas et al. (1997) were applied to all the stars for which the calibrations were valid i.e. those with $\beta > 2.720$. The dereddened colour indices obtained above

[7]The word 'dex' means 'difference in the logarithm'.

[8]The metallicity indicator $\delta m_1 = m_1(\textit{standard}) - m_1(\textit{observed})$ for a given β. The standard values are tabulated in Crawford (1975, 1979).

were used. The uncertainties in the mass and surface gravity are 0.10 $M_{\odot}$ and 0.08 dex respectively.

Where possible, M_V was calculated from the parallax π and visual magnitude m_V measured by the HIPPARCOS Satellite, using

$$M_V = m_V + 5\log(10\pi).$$

where π is measured in arcsec. In the above calculations of the stellar parameters, if the uncertainty in this HIPPARCOS magnitude was found to be less than 0.4 mag, then it was used instead of the M_V calculated using the other calibrations.

The results obtained from all these calibrations are summarised in Table 4.3. According to the program documentation for UVBYBETA.F, the metallicity indicator δm_1 given in the table allows the stars to be classified as follows: $\delta m_1 < -0.10$ – metallic line (Am) or peculiar stars; $0.0015 < \delta m_1 < 0.025$ – normal Pop I stars; $0.025 < \delta m_1 < 0.045$ – older Pop I stars; $\delta m_1 > 0.045$ – Pop II stars. o^1 Eri and CC Oct fall into the first category, and AE UMa, BE Lyn, EH Lib and RS Gru all fall into the third category. However, Rodriguez, Rolland, & Lopez de Coca (1988a) argue that AE UMa is a normal Population I star (based on its period ratio) and Joner (1986) argues that EH Lib is a normal Population I dwarf Cepheid based on his photometric and spectroscopic investigation of the star. Rodriguez et al (1990) classify BE Lyn as a main sequence or close post main sequence star, and Rodriguez et al (1995) also consider RS Gru as either a post main sequence or main sequence star. McNamara (1997) examines eight of the stars selected in the literature survey, and lists AE UMa, BE Lyn, EH Lib and RS Gru as having [Fe/H]≈ -0.5 (Z $\approx$ 0.005) which means that these stars have a low metal content. Clearly, there is much uncertainty as to the evolutionary state of these high-amplitude δ Sct stars (HADS).

Powell, Joner, & McNamara (1990) suggest that V567 Oph is in the hydrogen shell burning phase of evolution, and Breger, Campos & Roby (1978) suggest that DY Her is immediate post main sequence based on its metallicity and space motion. Petersen & Christensen-Dalsgaard (1996) propose that it is necessary for a star to be in the post-main-sequence stage of evolution for it to appear as a HADS.

In this study, all stars are assumed to be less evolved than the end of core hydrogen burning, and to have normal metallicity (Z = 0.02). This assumption is required because models outside

Table 4.3: The unreddened colour indices and stellar parameters for the selected stars. Top line -Balona (1994); middle line - Moon & Dworetsky (1985); bottom line - Ribas et al. (1997). The values with an asterisk were calculated from the HIPPARCOS parallaxes. The metallicity indicator, δm, is shown under the name of the star.

Star/δm	$(b-y)_0$	m_0	c_0	M_V	BC	$\log T_{\rm eff}$	$\log L/L_\odot$	$M/M_\odot$	$\log g$
AD CMi	0.166	0.184	0.850	1.544	0.051	3.871	1.266	1.959	3.904
0.007	0.171	0.183	0.851	1.52	0.054	3.865	1.274	1.959	3.67
								1.963	3.849
AE UMa	0.157	0.161	0.837	1.826	0.046	3.877	1.155	1.824	4.008
0.034	0.164	0.159	0.839	1.78	0.051	3.870	1.171	1.892	3.90
								1.774	4.098
β Cas	0.202	0.181	0.782	1.167*	0.057	3.847	1.414	2.089	3.688
0.000	0.212	0.178	0.784		0.055	3.842	1.415	2.089	3.48
								-	-
BE Lyn	0.148	0.162	0.839	1.963	0.040	3.883	1.103	1.799	4.078
0.036	0.156	0.160	0.840	1.92	0.047	3.876	1.117	1.799	3.87
								1.742	4.161
BF Phe	0.162	0.188	0.768	2.494*	0.036	3.887	0.892	1.706	4.282
0.009	0.166	0.186	0.769		0.049	3.874	0.887	1.667	4.12
								1.690	4.194
BP Peg	0.155	0.183	0.842	1.860	0.043	3.880	1.143	1.820	4.031
0.011	0.159	0.184	0.844	1.81	0.049	3.873	1.160	1.824	3.85
								1.875	3.985
CC Oct	0.220	0.376	0.419	1.627*	0.043	3.880	1.236	1.945	3.967
-0.189	0.230	0.374	0.421		0.055	3.862	1.231	1.923	4.81
								1.837	3.786
DL Eri	0.162	0.183	0.877	1.048*	0.050	3.872	1.465	2.138	3.747
0.025	0.163	0.183	0.877		0.054	3.865	1.463	2.128	3.59
								-	-
DY Her	0.154	0.200	0.808	2.286	0.037	3.886	0.975	1.738	4.203
-0.004	0.157	0.201	0.810	2.24	0.045	3.878	0.990	1.726	3.99
								1.828	4.045
EH Lib	0.141	0.167	0.851	1.957	0.035	3.887	1.107	1.807	4.092
0.032	0.149	0.166	0.853	1.91	0.043	3.880	1.123	1.807	3.99
								1.770	4.142
EW Aqr	0.163	0.185	0.902	0.825*	0.052	3.868	1.553	2.203	3.656
0.005	0.167	0.184	0.903		0.055	3.863	1.552	2.203	3.49
								1.974	3.850
GN And	0.168	0.165	0.869	1.430*	0.053	3.867	1.311	1.991	3.850
0.023	0.169	0.165	0.869		0.055	3.862	1.310	1.986	3.62
								1.950	3.859
RS Gru	0.146	0.159	0.916	1.179	0.045	3.878	1.414	2.104	3.815
0.037	0.153	0.158	0.918	1.13	0.050	3.872	1.432	2.113	3.70
								1.963	3.902
RV Ari	0.175	0.179	0.791	2.005	0.051	3.870	1.082	1.766	4.039
0.008	0.180	0.180	0.793	1.98	0.055	3.863	1.090	1.758	3.84
								1.801	4.014
o^1 Eri	0.194	0.195	0.791	1.113*	0.057	3.853	1.436	2.104	3.693
-0.017	0.198	0.194	0.792		0.057	3.848	1.436	2.104	3.49
								2.018	3.696
V567 Oph	0.160	0.166	0.869	1.440	0.049	3.873	1.308	1.991	3.877
0.018	0.165	0.173	0.873	1.39	0.052	3.835	1.327	1.995	3.26
								1.932	3.900
V853 Cen	0.089	0.199	0.999	1.004*	0.006	3.906	1.500	2.195	3.860
0.005	0.093	0.199	1.000		0.008	3.905	1.500	2.193	3.84
								2.173	3.841
AN Lyn	0.172	0.200	0.790	2.118	0.049	3.874	1.037	1.742	4.093
-0.009	0.177	0.199	0.791	2.09	0.049	3.866	1.048	1.734	3.85
								1.863	3.950
V393 Car	0.166	0.185	0.841	1.642	0.050	3.872	1.227	1.932	3.940
0.006	0.171	0.184	0.842	1.62	0.050	3.865	1.236	1.932	3.71
								1.937	3.877
V1719 Cyg	0.205	0.187	0.824	1.147*	0.053	3.838	1.424	2.094	3.642
-0.009	0.221	0.183	0.828		0.053	3.835	1.424	2.094	3.20
								-	-

Table 4.4: The ranges in mass, effective temperature and surface gravity used in searching for mode identification. The projected rotational velocity from the literature (in km s^{-1}) is given in the last column.

Star	Mass	$\log T_{\rm eff}$	$\log g$	$v \sin i$
AE UMa	1.7 – 2.0	3.85 – 3.89	3.70 – 4.32	
BP Peg	1.8 – 2.0	3.85 – 3.89	3.72 – 4.34	< 18
RV Ari	1.7 – 1.9	3.84 – 3.88	3.73 – 4.35	18
AD CMi	1.9 – 2.1	3.85 – 3.88	3.57 – 4.21	20
β Cas	2.0 – 2.2	3.82 – 3.90	3.38 – 3.80	70
BE Lyn	1.7 – 1.8	3.86 – 3.90	3.77 – 4.39	
BF Phe	1.6 – 1.8	3.86 – 3.90	4.00 – 4.47	80
CC Oct	1.8 – 2.0	3.83 – 3.89	3.60 – 4.90	< 10
DL Eri	1.8 – 2.2	3.84 – 3.88	3.49 – 3.96	140
DY Her	1.7 – 1.9	3.84 – 3.90	3.86 – 4.51	20
EH Lib	1.7 – 1.9	3.86 – 3.90	3.78 – 4.40	16
EW Aqr	2.1 – 2.6	3.84 – 3.90	3.37 – 3.94	150
GN And	1.9 – 2.1	3.84 – 3.89	3.52 – 3.98	30
RS Gru	1.9 – 2.2	3.84 – 3.89	3.50 – 4.13	40
o^1 Eri	2.0 – 2.2	3.83 – 3.88	3.39 – 3.90	105
V567 Oph	1.8 – 2.1	3.82 – 3.89	3.16 – 4.19	< 18
V853 Cen	1.4 – 2.3	3.88 – 3.92	3.59 – 4.13	
AN Lyn	1.7 – 2.0	3.85 – 3.89	3.75 – 4.40	
V393 Car	1.7 – 2.0	3.85 – 3.88	3.61 – 4.25	
V1719 Cyg	1.8 – 2.2	3.82 – 3.88	3.10 – 3.95	
HD 105513	1.4 – 2.5	3.83 – 3.85	3.84 – 4.06	

this range were not calculated.

The results in Table 4.3 and their uncertainties were used to calculate the ranges in Table 4.4. Where necessary, the ranges were extended to include some of the published results. The range in mass for V583 Cen, for example, is very large because the published estimate of 1.4 $M_\odot$ (Vander Linden & Sterken (1986)) is very different to the value listed in Table 4.3. Also given in this table are the rotational velocities $v \sin i$.

4.3 Some comments on the stellar models and rotation

The models, whose primary purpose was to provide values of f and ψ, were constructed for solar masses 1.4 – 2.5 in steps of 0.1 $M_\odot$, for discrete stages between the Zero-Age Main Sequence (ZAMS) and the end of core-hydrogen burning (ECHB). Dziembowski's non-adiabatic pulsation

code NADROT was used to calculate for each model the pulsation frequencies for values of ℓ = 0, 1 and 2. The frequencies were constrained to be in the expected range for δ Sct stars by constraining the dimensionless frequency, σ to be in the range 1 to 3. The dimensionless frequency σ is defined by

$$\sigma = \frac{\omega'}{\sqrt{4\pi G\rho}}.$$

Since the models are calculated at discrete values of mass and stages of evolution, an exact match between an observed frequency and calculated frequency is unlikely. If the frequencies calculated using the code are listed in numerical order, then the maximum difference between any two successive frequencies is approximately 0.6 d^{-1}. Hence, when comparing the observed and calculated frequencies, any calculated frequency within 0.6 d^{-1} of the observed frequency was accepted, so that at least one model would be selected.

The model stars were calculated assuming no rotation. Rotation would, however, affect the calculated frequencies of the models. In a rotating star, the frequencies for non-axisymmetric ($m \neq 0$) modes will be shifted significantly. This is discussed in a little more detail in Chapter 6. To take this into account, m was allowed to take the full range of values $(-\ell, -\ell+1....\ell-1, \ell)$ for each ℓ, and the observed frequency was modified by $m\Omega$ where Ω is the frequency of rotation. The angle of inclination i of each star is not known. If the axes are randomly oriented in space, then the most likely angle of inclination is one where the star is viewed equator on. The frequency of rotation was therefore calculated from the projected rotational velocity assuming the star to be viewed equator-on. Hence, any frequency ν such that

$$\nu = \nu_0 - m\Omega$$

(where ν_0 is the model frequency) that was in the acceptable frequency range was also permitted. This has no effect on the mode-identification, since the method is essentially independent of m, but was used to include modes that would otherwise not have been considered.

4.4 Calculating the terms T_1, T_2, T_3 and $b_{\ell\lambda}$

T_1 depends only on ℓ and so is easily calculated. T_2 and T_3 need a little more discussion. The factor $\Gamma_2 = \frac{5}{3}$. The factor p^* is taken as unity as mentioned in Chapter 2. Defining

$$\alpha_H \equiv \frac{GM}{r^3\omega^2} = \frac{g}{\omega^2 r} = 74.41Q^2,$$

where Q is the pulsation constant in days defined by

$$Q = P\sqrt{\frac{\rho}{\rho_\odot}}, \tag{4.1}$$

then the factor C, defined by equation (2.32), and appearing in the expression for T_2 can be rewritten as

$$C = \ell(\ell+1)\alpha_H - \frac{1}{\alpha_H} - 4.$$

Equation (4.1) and the definition of density can be used to write

$$\log Q = -\log \nu_o + 0.75 \log g - 0.25 \log M - 3.328.$$

Hence, α_H can be found given the surface gravity and stellar mass, and hence C can be found for any mode ℓ.

The only other terms that need to be calculated are the terms α_T, α_g, β_T, β_g and $b_{\ell\lambda}$. These terms were calculated using the latest version of the Kurucz (1979) model atmospheres. They are the wavelength dependent terms of equation (2.43). Equation (2.43) defines the observed magnitude variation in a single wavelength. This is not a realistic approach as the stars are observed through filters which are not monochromatic. This is easily corrected by calculating the terms α_T, α_g, β_T, β_g and $b_{\ell\lambda}$ for various wavebands using the transmission functions of the Geneva and Strömgren filters. The *uvby* functions given in Crawford & Barnes (1970) were used. All the transmission functions were obtained in electronic form from the General Catalogue of Photometric Data. [9]. It should also be noted here that in using the Kurucz model atmospheres to calculate these quantities, it is assumed that at any instant the atmosphere of the pulsating star has the same structure as that of a static star of the same temperature and gravity.

Calculating α_T and α_g

The filter transmission functions $T_i(\lambda)$ are defined at discrete wavelengths over the width of the filter i. The transmission curves were interpolated to be defined at regular intervals of 10 Å, and then normalised so that

$$\int_{\lambda_1}^{\lambda_2} T_i(\lambda) d\lambda = 1.$$

It was necessary for the curves to be defined at regular intervals for Simpson integration to be used in the calculations. Here λ_1 and λ_2 are the minimum and maximum wavelengths transmitted through filter i.

[9] http://obswww.unige.ch/gcpd/filters

The fluxes from the Kurucz (1979) model atmospheres for solar composition in the relevant wavelength ranges define a flux curve for each filter. Here the flux is the flux normal to the stellar surface. These flux curves were also interpolated to be defined at the same regular intervals as the filter transmission curves, and then Simpson integration was used to calculate the flux through the filter given by

$$\log F_i = \log\Big(\int_{\lambda_1}^{\lambda_2} T_i(\lambda) F_i(\lambda) d\lambda\Big).$$

These fluxes, $\log F_i$, were calculated for each filter for each Kurucz model in the range $6000K \leq T_{\text{eff}} \leq 8500K$ and $2.5 \leq \log g \leq 4.0$ cm s^{-2} which adequately covers the range of temperature and surface gravity for those δ Sct stars selected in the literature survey. Hence, a $(T_{\text{eff}}, \log g)$ grid was formed giving values of $\log F_i$ for each filter at each grid point for which the Kurucz models provided information.

The values of α_T and α_g were then calculated by fitting a surface to this grid. Given any value of $(T_{\text{eff}}, \log g)$ within the range of the grid, the value of the corresponding $\log F_i$ could be found by interpolating between the grid points. By fitting a parabola

$$\log F_i = a_0 + a_1(T)^2 + a_2 T$$

through three points $(T_{\text{eff}}, \log g)$, $(T_{\text{eff}} + dT, \log g)$ and $(T_{\text{eff}} - dT, \log g)$, the derivative

$$\left(\frac{\partial \log F_i}{\partial T_{\text{eff}}}\right)_g = 2a_1 T_{\text{eff}} + a_2$$

could be found. Then

$$\alpha_{T\lambda} = \frac{T_{\text{eff}}}{\log_e 10}\left(\frac{\partial \log F_i}{\partial T_{\text{eff}}}\right)_g = \frac{T_{\text{eff}}}{\log_e 10}(2a_1 T_{\text{eff}} + a_2).$$

The value of $\alpha_{g\lambda}$ was found by fitting a similar parabola $\log F_i = b_0 + b_1(T)^2 + b_2 T$ through the three points $(T_{\text{eff}}, \log g)$, $(T_{\text{eff}}, \log g + dg)$ and $(T_{\text{eff}}, \log g - dg)$, giving

$$\alpha_{g\lambda} = \left(\frac{\partial \log F_i}{\partial \log g}\right)_g = 2b_1 \log g + b_2.$$

Calculating β_T, β_g and $b_{\ell\lambda}$

The Kurucz model atmospheres for solar composition give the intensities for wavelengths within the range of each filter at 17 values of μ, where $\mu = \cos\theta$ and θ is the polar angle in the spherical

coordinate system where the z-axis is the line-of-sight to the observer. These intensities were used to define an intensity curve $I_i(\lambda, \mu)$ for each filter for each μ, The intensity curves $I_i(\lambda, \mu)$ were also interpolated to be defined at regular intervals, and then Simpson integration was used to calculate

$$I_i(\mu) = \frac{\int_{\lambda_1}^{\lambda_2} T_i(\lambda) I_i(\lambda, \mu) d\lambda}{\int_{\lambda_1}^{\lambda_2} T_i(\lambda) I_i(\lambda, 1) d\lambda}$$

so that $I_i(\mu)$ is normalised to be unity at $\mu = 1$. This normalised intensity curve was then interpolated in order to calculate $I_i(0.1)$. Simpson integration was again used to calculate the angle averaged flux

$$F_i = 2 \int_0^1 I_i(\mu) \mu d\mu. \tag{4.2}$$

The limb darkening function

$$h_i(\mu) = 1 - a_i(1 - \mu) - b_i(1 - \mu^2) \tag{4.3}$$

was used to approximate the limb darkening. Following Wade & Rucinski (1985), the quadratic limb darkening coefficients a and b were calculated from the equations:

$$a_i = [-486F_i + 386I_i(1) + 100I_i(0.1)]/72;$$

$$b_i = [540F_i + 340I_i(1) - 200I_i(0.1)]/72.$$

These equations follow from $I_i(\mu) = I_i(1)h_i(\mu)$, equation (4.2) and the requirement that $I_i(0.1) = I_i(1)h_i(0.1)$.

Rewriting the limb darkening function as $h(\mu) = \chi_0 + \chi_1\mu + \chi_2\mu^2$, then

$$\begin{aligned} \chi_1 &= \frac{2(a + 2b)}{1 - a/3 - b/6} \\ \chi_2 &= \frac{-2b}{1 - a/3 - b/6} \\ \chi_0 &= 2 - 2/3\chi_1 - \chi_2 \end{aligned}$$

where the last equation follows from the normalization of the limb darkening function.

The values of χ_1 and χ_2 could then be calculated for each of the Kurucz models for which data is available, thus forming a grid of values of χ_1 and χ_2 at points $(T_{\text{eff}}, \log g)$. By a fitting a surface of χ_1 and χ_2 to the grid, as before, through interpolation and the use of parabolas, the derivatives of χ_1 and χ_2 with respect to $\log T_{\text{eff}}$, and $\log g$ could be calculated for any T_{eff} and $\log g$ within the range of the grid.

Table 4.5: The coefficients c_i for the first few values of the mode ℓ.

ℓ	c_0	c_1	c_2
0	1	0	0
1	2/3	1/36	1/30
2	1/4	1/20	1/16

Using the equation for the limb-darkening function above, $b_{\ell\lambda}$ can be rewritten as:

$$b_{\ell\lambda} = \int_0^1 h_\lambda \mu P_\ell(\mu) d\mu = c_0 + \chi_1 c_1 + \chi_2 c_2,$$

where the coefficients c_j are given in Watson (1988) and listed for $\ell = 0$, 1, and 2 in Table 4.5. They are easily calculated from the above equation using the definition of $P_\ell(\mu)$.

If ℓ is known, then $b_{\ell\lambda}$ and its derivatives with respect to $\log T$ and $\log g$ are easily calculated from the values of χ_1 and χ_2 and their derivatives with respect to $\log T_{\rm eff}$, and $\log g$, and hence β_g and β_T can be determined using the equations

$$\begin{aligned} \beta_T &= \frac{c_1}{log_e 10} \frac{\partial \chi_1}{\partial \log T_{\rm eff}} + \frac{c_2}{log_e 10} \frac{\partial \chi_2}{\partial \log T_{\rm eff}} \\ \beta_g &= \frac{c_1}{log_e 10} \frac{\partial \chi_1}{\partial \log g} + \frac{c_2}{log_e 10} \frac{\partial \chi_2}{\partial \log g}. \end{aligned}$$

4.5 Identifying the mode

The amplitude and phases were all calculated using the concepts outlined above by a FORTRAN program, which also allowed the mode to be identified. The program essentially did the following:

1. Calculated the parameters necessary to fit surfaces of $\log F$, χ_1 and χ_2 to the grids of $(T_{\rm eff}, \log g)$ using a subroutine obtained from a library of subroutines.

2. Requested the ranges in mass, effective temperature, surface gravity, and frequency for the star being processed, and information about the stability and type of modes being searched for. The rotational velocity was also requested.

3. Requested, for each filter, the observed amplitudes A and their uncertainties σ, and the phases ϕ and calculated a_1, a_2 and σ^2, where $a_1 = A\cos\phi$, and $a_2 = A\sin\phi$.

4. For each file with temperature T_f and surface gravity $\log g_f$ resulting from the non-adiabatic pulsation code within the given ranges of mass, temperature and surface gravity for the star, the following was done:

   (a) The surfaces of $\log F$, χ_1 and χ_2 were fitted to the grids of $(T_{\rm eff}, \log g)$ using another subroutine obtained from a library of subroutines. At the point $(T_f, \log g_f)$ the derivatives of $\log F$, χ_1 and χ_2 with respect to temperature and surface gravity were calculated.

   (b) For each frequency within the acceptable range the theoretical amplitude and phase were calculated using the associated values of ℓ, f and ψ. Hence the amplitude and phase could be predicted for each filter i. The models, as can be seen in Appendix A actually provide the real and imaginary parts of f^* rather than f and ψ. The values of f and ψ are easily obtained using

$$f^* = f + 2 \quad \text{and} \quad \psi = \tan^{-1} \frac{Im[f^* - 2]}{Re[f^*]}$$

   (c) Finally, the theoretical and calculated amplitudes and phases were compared through the evaluation of the χ^2 expression equation (3.3), and the corresponding probability (calculated from the χ^2 value and the number of degrees of freedom) and the mode ℓ, n were recorded.

The results for each observed frequency for a star was therefore a list of modes ℓ, n and the associated probability of the identification.

The process was repeated three times - once for each set of models corresponding to the different mixing length parameters $\alpha = 0.5$, 1, and 2, measured in pressure scale heights.

Chapter 5

Mode Identification Results

The results of the mode-identification are listed in Table 5.1 . The second column gives the reference to the data used. The frequencies listed beside each star are those identified in the Fourier analysis described in Chapter 4. P is the highest probability of the mode identification for mode ℓ for the mixing length α. Those frequencies which could not be identified with a p-mode are labelled 'g'. If, in addition, the mode is not excited, it is labelled '$g-$'. The first 10 stars listed in the table are all high amplitude δ Scuti stars. The others are all medium or low-amplitude pulsators.

The high amplitude double-mode stars, AE UMa, BP Peg and RV Ari, are useful as a check on the method of mode identification, since both modes are known to be radial on the basis of the period ratio[1]. The table shows that the most likely identification for both periods is, indeed, a radial mode. However, discrimination between $\ell = 0$ and $\ell = 1$ is sometimes poor. AE UMa is known to have a much lower metallicity than the other two stars, but even so, the mode identification is not affected. The fit for the first frequency in BP Peg is very poor. Upon closer examination of the results, it was found that the predicted and observed amplitudes in the u filter differed much more than in the other filters. (See figure 5.1.)

In the HADS stars AD CMi and BE Lyn radial modes were expected in both cases. Although this is achieved for BE Lyn, the fit is very poor. AD CMi is not identified as a radial mode, and the fit, once again, is very poor. The reason for the poor fits is once again traced to a discrepant

[1]From equation (6.2) it can be seen that, for any particular star, the period ratio $P_i/P_j = Q_i/Q_j$.The pulsation constants Q have different values for different modes. For the fundamental radial mode and the first harmonic, Q has approximate values 0.033 and 0.025 respectively, and hence a period ratio $P_1/P_0 \approx 0.76$ means that the pulsation is radial.

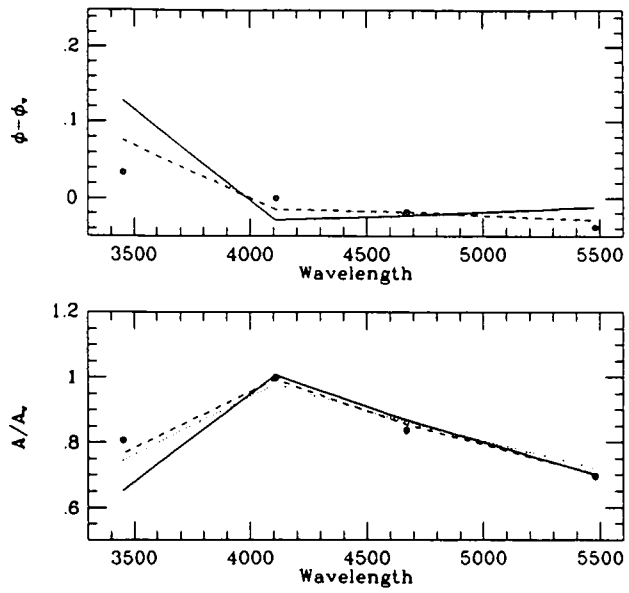

Figure 5.1: Observed (solid circles) and calculated amplitudes and phases relative to the v band for the best-fitting mode in BP Peg. The solid line is for models with $\alpha = 0.5$, the dotted line for $\alpha = 1.0$, and the dashed line for $\alpha = 2.0$.

u-amplitude. (See Figures 5.2 and 5.3.)

EH Lib is also a HADS and the mode appears to be radial, as expected. The evolutionary status of this star is not clear and the models may not be appropriate.

DY Her, RS Gru and V567 Oph are also all HADS, but the single frequency in each case is identified with an $\ell = 1$ g mode. As far as could be ascertained, the mode identification has not previously been discussed for DY Her or V567 Oph, although the HADS are usually assumed to have radial pulsation. All three of these stars have approximately the same frequency of pulsation (≈ 6.7 d^{-1}). Between the ZAMS and the end of core hydrogen burning, the radial mode has a frequency larger than 7.3 d^{-1} for stars in the δ Sct instability strip, according to the models used. The most likely explanation is that these are evolved radially-pulsating stars outside the range of the models used in the identification. The models show that there are some unstable g modes in this frequency range for main sequence stars, but these are unlikely to attain the high amplitudes which are observed.

Joner & Johnson (1985) were able to determine only the main period for V1719 Cyg, though

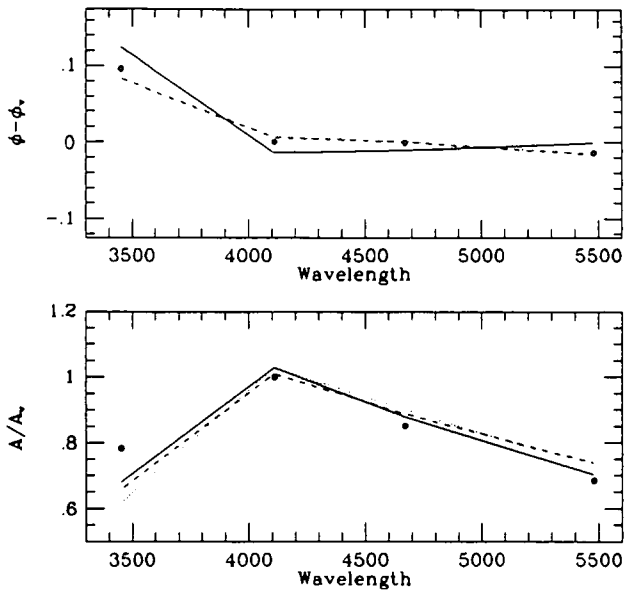

Figure 5.2: Observed (solid circles) and calculated amplitudes and phases relative to the v band for the best-fitting mode in AD CMi. The solid line is for models with $\alpha = 0.5$, the dotted line for $\alpha = 1.0$, and the dashed line for $\alpha = 2.0$.

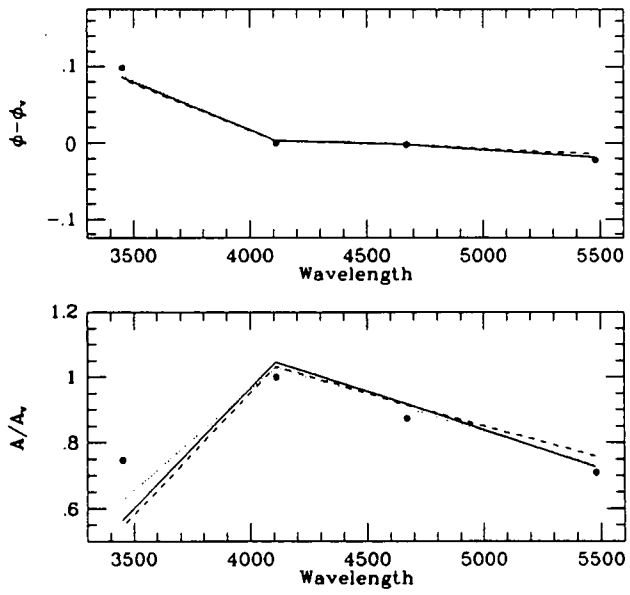

Figure 5.3: Observed (solid circles) and calculated amplitudes and phases relative to the v band for the best-fitting mode in BE Lyn. The solid line is for models with $\alpha = 0.5$, the dotted line for $\alpha = 1.0$, and the dashed line for $\alpha = 2.0$.

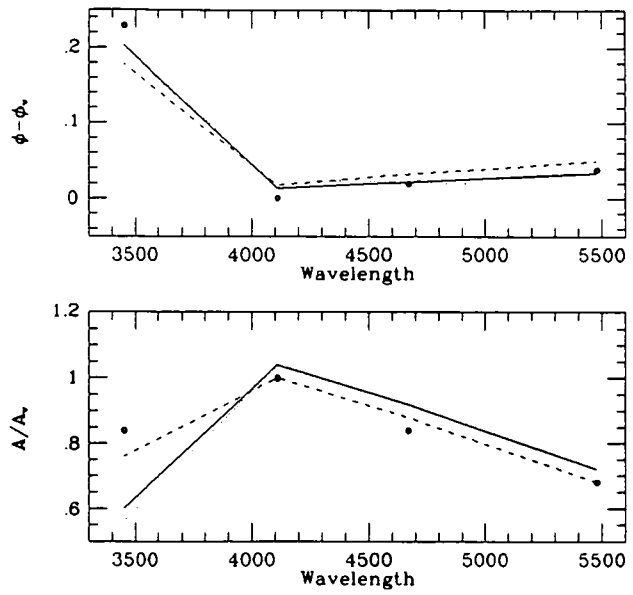

Figure 5.4: Observed (solid circles) and calculated amplitudes and phases relative to the v band for the best-fitting mode in β Cas. The solid line is for models with $\alpha = 0.5$, the dotted line for $\alpha = 1.0$, and the dashed line for $\alpha = 2.0$.

more frequencies were suspected owing to the apparently variable amplitude. The star has a peculiar light curve which was analysed in more detail by Rodriguez et al. (1997). The frequency of pulsation is far too small for a δ Sct star. The star is probably evolved, but further data is required to establish the nature of this object.

The low amplitude δ Scuti stars can now be discussed. It should be noted throughout the discussion that these stars generally have higher rotational velocities than the HADS. This results in a shift in the frequencies which the non-rotating models have not taken into account. The shift is small for $m = 0$, but, since the rotation period for these stars is about 2 days, the frequency shift may reach values higher than 1 cycle.d^{-1} for $\ell = |m| = 2$. This has been taken into account in the mode identification procedure, as discussed in section 4.3.

Rodriguez et al. (1992a) discuss the possibility of $\ell = 0$ and $\ell = 1$ for β Cas, and settle on the non-radial mode. The results show very poor agreement between observed and calculated amplitudes for any choice of mode. This could be due to a discrepant u-filter. (See figure 5.4.)

As far as could be ascertained, the mode identification for BF Phe has not been discussed. The

results show that the mode is probably radial or $\ell = 1$.

Gupta (1980) identified the two frequencies he observed in DL Eri (6.415 d^{-1} and 8.418 d^{-1}) with radial pulsation from the period ratio of 0.76. Poretti (1989), who also observed the star, identified his frequencies of 6.41 and 10.26 d^{-1} with non-radial pulsation, and the third frequency 8.98 d^{-1} with radial pulsation. The two frequencies found in the data of Jørgensen and Nørgaard-Nielsen (1975), 6.4018 and 10.8587d^{-1}, were identified as non-radial, probably $\ell = 1$, in agreement with Poretti (1989).

Using the data of Kilambi, DuPuy and Koegler (1978), the single frequency found in their data (10.25 d^{-1}) is identified as a non-radial mode, probably $\ell = 1$. Hobart, Pena and Peniche (1989) identified all three frequencies they found with non-radial modes based on the period ratios. The results obtained using the data obtained in Sutherland in August 1997 (10.340, 10.018 and 4.74 d^{-1}) agree with this, although the frequency at 10.34 d^{-1} may be radial. No stable p-mode could be found with a frequency near 4.74 d^{-1}. If real, it is probably a g-mode.

Rodriguez et al. (1993) identify the pulsation mode for GN And (28 And) as $\ell = 2$. Here, on the contrary, it has been identified as probably a radial or an $\ell = 1$ mode.

Poretti (1989) identified all three frequencies that he found in the star o^1 Eri as non-radial. The two frequencies identified in the data of Jørgensen & Nørgaard-Nielsen (1975) agree with Poretti as in that they are also identified as non-radial.

Vander Linden & Sterken (1986) observed V853 Cen (HR 126859) in 1982 and 1984. The 1982 frequencies are listed first in Table 4. Here the higher frequency appears to be radial, but the fit is poor. The frequencies found in the 1982 data were fitted to the 1984 data. After this, the actual frequencies found in the 1984 set were fitted to the data. Vander Linden & Sterken suggest that the mode at 18.9186 d^{-1} be identified with high overtone radial, or non-radial pulsation. Here the mode at 16.752 d^{-1} is identified as either radial or $\ell = 1$ in all cases, the discrimination being very poor.

Kurtz (1980) observed CC Oct, determining the three frequencies listed first for this star. He identified the frequency 8.0062 d^{-1} with radial pulsation, in agreement with the results listed. However, the fit is very poor. The frequency at 8.11 d^{-1} is identified as a radial mode using Kurtz's data or the data obtained in Sutherland in August 1997. This star has a high metallicity, and, according to Wegner (1981) is quite evolved.

Rodriguez et al. (1997) suggest that the 10.1756 d^{-1} frequency in AN Lyn is probably radial on the basis of the phase shift. There is no clear discrimination between the radial and $\ell = 1$ modes for the other two frequencies.

V393 Car (HD 66260) is a medium amplitude δ Scuti. Helt (1984) identifies the frequency 7.077 d^{-1} with the fundamental radial frequency, but the results listed in Table 5.1 show it as non-radial. Once again, it should be noted that in the models this frequency can only be identified with a stable radial mode or with an unstable non-radial mode. The second frequency is identified as an $\ell = 0$ or 1 mode.

HD 105513 (Heynderickx 1994) is the only star in the list which was observed in the Geneva photometric system. The four frequencies are all less than expected for the fundamental radial mode in main sequence and giant δ Sct stars. Unless the star is evolved, they are all non-radial g modes.

Table 5.1: The results of mode identification for three different mixing lengths (α). The confidence probability, P (percent), as determined from χ^2, is given for each identification. The identification was confined to excited p-modes in the models. Those modes for which no p-mode could be found are label g; if, in addition, such a mode is not excited then the label $g-$ is given.

			$\alpha = 0.5$		$\alpha = 1.0$		$\alpha = 2.0$	
Star	Ref	Freq	ℓ	P	ℓ	P	ℓ	P
AE UMa	2	11.6253	1	42.09	0	99.45	0	96.41
			0	3.09	1	74.02	1	64.05
		15.0326	0	99.92	0	99.87	0	98.61
			1	99.57	1	99.76	1	96.96
BP Peg	2	9.1263	-	-	-	-	0	39.38
			-	-	-	-	1	5.77
		11.8242	0	6.51	0	37.25	0	33.13
			1	3.43	1	21.51	1	22.86
RV Ari	2	10.7360	0	99.78	0	85.03	0	33.11
			1	99.41	1	79.46	1	3.64
		13.8964	1	99.11	1	94.80	0	80.58
			0	98.25	0	94.59	1	75.56
AD CMi	1	8.1318	1	0.02 g	-	-	-	-
BE Lyn	4	10.4309	-	-	0	1.38	-	-
EH Lib	11	11.3110	0	0.28	0	91.97	0	22.47
			1	0.13	1	4.89	-	-
DY Her	10	6.7282	1	95.61 g	1	89.79 g	1	0.24 g
			2	16.38 g	-	-	-	-
RS Gru	14	6.8000	1	99.31 g	1	96.17 g	1	98.47 g
			2	16.06 g	2	0.03 g	2	25.90 g
V567 Oph	15	6.7000	1	99.13 g	1	81.89 g	1	1.34 g
			2	21.22 g	-	-	-	0.01 g
V1719 Cyg	19	3.7400	2	80.37 g-	1	99.13 g-	1	53.22 g-
			1	73.00 g-	2	85.46 g-	2	48.30 g-
β Cas	3	9.9100	-	-	-	-	1	0.77
BF Phe	5	16.0100	1	60.23	1	98.08	0	92.93
			0	23.61	0	5.72	1	92.11
	6	16.0166	1	83.89	1	70.42	1	89.99
			0	61.98	0	23.98	0	86.45
DL Eri	9	6.4018	1	92.05 g	1	93.85 g	1	62.99 g
			2	39.88 g	2	11.61 g	2	2.72 g
		10.8587	1	92.59	1	83.49	0	47.02
			0	77.78	0	75.35	1	43.03
EW Aqr	12	10.2500	1	81.88	1	87.45	1	93.15
			0	81.83	0	78.45	0	91.97
	8	10.3400	0	83.37	1	95.10	0	99.01
			1	81.81	0	73.38	1	98.20
		10.0180	1	92.00	1	95.38	1	98.10
			0	89.48	0	85.09	0	97.63
		4.7400	1	99.64 g-	1	99.64 g-	1	95.59 g-
			2	99.56 g-	2	99.50 g-	2	99.16 g-

Table 5.1: Continued.

Star	Ref	Freq	$\alpha = 0.5$ ℓ	P	$\alpha = 1.0$ ℓ	P	$\alpha = 2.0$ ℓ	P
GN And	13	14.4292	0	96.67	0	92.13	0	41.06
			1	93.78	1	88.59	1	27.66
o^1 Eri	9	13.2600	1	76.77	1	67.63	1	20.93
			0	56.94	0	38.29	0	7.53
		6.7400	1	61.30 g	1	63.40 g	1	73.71 g
			2	49.33 g	2	50.89 g	2	42.29 g
V853 Cen	16	18.9186	0	50.65	0	29.56	0	39.86
			1	33.86	1	6.72	1	27.60
		16.7520	1	91.47	1	92.00	0	93.67
			0	89.13	0	91.88	1	93.48
		18.9186	0	99.95	1	99.94	0	99.95
			1	99.93	0	99.93	1	99.94
		16.7520	1	99.83	1	99.82	1	99.81
			0	99.81	0	99.81	0	99.80
		18.2000	0	99.92	0	99.93	0	99.90
			1	99.89	1	99.92	1	99.89
		16.5820	1	99.77	1	99.78	1	99.77
			0	99.75	0	99.76	0	99.75
CC Oct	7	8.0062	0	26.07	0	10.20	0	2.69
		12.5763	1	94.48	1	96.16	1	93.18
			0	93.94	0	96.03	0	93.12
		8.1100	0	99.10	0	99.02	0	99.62
	8	8.0000	0	37.90	0	28.82	0	18.89
		8.1120	0	88.26	0	88.37	0	86.98
		12.6200	1	93.95	0	94.46	0	93.26
			0	93.63	1	94.44	1	93.18
AN Lyn	17	10.1756	1	0.01 g	1	-	1	0.02 g
		18.1309	1	79.56	0	66.27	0	31.95
			0	68.91	1	58.86	1	24.17
		9.5598	0	75.94	1	80.75	0	88.78
			1	69.05	0	66.37	1	84.90
V393 Car	18	7.0770	1	94.30 g	1	9.71 g	1	-
			2	3.99 g	-	-	-	-
		12.5780	1	99.93	1	99.91	1	99.76
			0	99.87	0	99.87	0	99.75
	18	7.0770	1	93.95 g	1	8.77 g	1	-
			2	3.50 g	-	-	-	-
		13.5780	1	99.93	1	99.65	0	98.44
			0	99.83	0	99.54	1	97.16
HD 105513	20	6.8559	1	99.99 g	1	99.89 g	1	96.01 g
			2	98.47 g	2	0.05 g	2	37.76 g
		6.6388	1	99.98 g	1	99.99 g	1	99.96 g
			2	61.04 g	-	-	2	46.05 g
		6.8902	1	99.94 g	1	99.78 g	1	98.80 g
			2	99.85 g	2	23.91 g	2	71.98 g
		6.4586	1	99.99 g	1	99.99 g	1	99.99 g
			2	99.55 g	2	56.62 g	2	98.64 g

1 - Rodriguez et al. (1988a); 2 - Rodriguez et al. (1992a); 3 - Rodriguez et al. (1992b); 4 - Rodriguez et al. (1990); 5 - Rodriguez et al. (1988b); 6 - Poretti et al. (1996); 7 - Kurtz (1980); 8 - Evers & Meintjes (unpublished); 9 - Jørgensen & Nørgaard-Nielsen (1975); 10 - Breger et al. (1978); 11 - Joner (1986); 12 - Kilambi et al. (1978); 13 - Rodriguez et al. (1993); 14 - Rodriguez et al. (1994); 15 - Powell et al. (1990); 16 - Vander Linden & Sterken (1986); 17 - Rodriguez et al. (1997); 18 - Helt (1984); 19 - Joner & Johnson (1985); 20 - Heynderickx (1994)

Chapter 6

Asteroseismology

In this chapter an algorithm to determine the stellar parameters of luminosity, and temperature will be discussed. In the algorithm used to identify the degree of pulsation ℓ , the most likely mode identified was associated with a particular model, and hence a set of stellar parameters $T_{\rm eff}$, $\log g$ and $\log L$. These stellar parameters are not reliable since the observed frequencies do not match the model frequencies exactly and rotation has not been taken into account in the calculation of the model frequencies.

In the presence of rotation, the degeneracy of the modes is lifted i.e. a frequency ν_0 of mode ℓ of a non-rotating star is split into $2\ell + 1$ frequencies, corresponding to the values of m = -ℓ, -(ℓ-1), ..., ℓ-1, ℓ. To first order in the angular rotation velocity Ω, the frequencies can be written as

$$\omega_0 = \omega_{\ell m} + m\Omega(1 - C_{\ell n}) \tag{6.1}$$

where $\omega_0 = 2\pi\nu_0$ is the angular frequency of the non-rotating star, and $C_{\ell n}$ is a constant that depends on the structure of the star, and is usually small for p-modes. This equation is discussed in Cox (1980) Chapter 19, and also in Unno et al. (1989). Hence, to first order, the splitting is symmetrical about the frequency of the non-rotating star, which also coincides with the frequency for $m = 0$.

It should be noted here that the first order approximation is only valid for slow rotation. If second order terms in Ω are included then the splitting is not symmetrical, and the frequency with m = 0 no longer coincides with the frequency for zero rotation. Although these second order effects do become important for rotational speeds as low as 50 km.s^{-1}, which are present in the low amplitude δ Sct stars, they have not been included in this study.

The axisymmetric modes ($m = 0$) are least affected by rotation, and are thus the easiest to deal with. They will be discussed first.

6.1 Axisymmetric modes

In order to determine the stellar parameters from the observed frequencies and mode identifications, an interpolation formula is needed. Eddington's period-density relation

$$P\sqrt{\frac{\overline{\rho}}{\overline{\rho}_\odot}} = Q \tag{6.2}$$

implies a relationship between the observed frequency of pulsation and the stellar parameters. Here P is the period of pulsation in days, $\overline{\rho}$ is the average density of the star and Q is a constant dependent on the mode and the type of variable star. For a δ Sct star, Q $\approx$ 0.03 for the fundamental radial mode. Since the density $\overline{\rho} \propto M/R^3$ and the luminosity $L \propto T^4R^2$, the frequency ν_0 for a given non-axisymmetric mode $(\ell, 0, n)$ can be written as

$$\log \nu_o = a_{0\ell n} + a_{1\ell n} \log T_{\rm eff} + a_{2\ell n} \log L + a_{3\ell n} \log M \tag{6.3}$$

where the $a_{i\ell n}$'s are constants dependent on the mode.

Evolutionary models show that a simple power law is a good approximation to the mass, given the luminosity. Hence mass can be discarded as a variable. Then

$$\log \nu_o = a_{0\ell n} + a_{1\ell n} \log T_{\rm eff} + a_{2\ell n} \log L. \tag{6.4}$$

The coefficients are shown in Table 6.1. These were obtained by doing a multivariate least squares fit (with frequency as the independent variable) on the data for pure or almost pure p-modes in the models that had not evolved beyond ECHB. Equation (6.4) is not valid for non-radial g-modes, or modes of mixed character where the g-mode component is significant. The interpolation coefficients a_i are sensitive to mixing length and probably also to composition, although the latter is beyond the scope of this study.

Given a frequency of radial pulsation and its mode (ℓ, n), the star can be placed on a $\log L - \log T$ line in the H-R diagram. If two or more radial frequencies are present in the star, then the intersection of the lines provides a point in the HR diagram. The formulae are most useful for the radial modes, since these are known to be axisymmetric.

Table 6.1: The coefficients of the frequency – luminosity – temperature relationship for axisymmetric p-modes in δ Sct models for two values of the mixing length parameter, α. The rms error in the fitted frequency is given by σ; N is the number of models used in the least squares solution.

α	(ℓ, n)	a_0	a_1	a_2	σ	N
0.5	(0, 1)	-10.2984	3.1336	-0.65208	0.00087	313
1.0	(0, 1)	-10.3101	3.1367	-0.65228	0.00095	298
0.5	(0, 2)	-10.1789	3.1321	-0.65345	0.00064	313
1.0	(0, 2)	-10.1930	3.1358	-0.65365	0.00071	298
0.5	(0, 3)	-9.6714	3.0202	-0.63758	0.00078	313
1.0	(0, 3)	-9.6829	3.0232	-0.63765	0.00094	298
0.5	(1, 1)	-10.2864	3.1340	-0.65272	0.00058	32
1.0	(1, 1)	-10.2959	3.1366	-0.65309	0.00055	32
0.5	(1, 2)	-10.6291	3.2565	-0.67186	0.00076	92
1.0	(1, 2)	-10.6408	3.2596	-0.67211	0.00071	92
0.5	(1, 3)	-10.3789	3.2150	-0.66608	0.00063	135
1.0	(1, 3)	-10.3898	3.2178	-0.66620	0.00061	136
0.5	(2, 1)	-8.2123	2.6076	-0.57441	0.00026	42
1.0	(2, 1)	-8.2123	2.6076	-0.57441	0.00026	42
0.5	(2, 2)	-8.9570	2.8228	-0.60642	0.00090	120
1.0	(2, 2)	-8.9582	2.8251	-0.60574	0.00098	121

6.2 Non-axisymmetric modes

For non-axisymmetric modes, the effect of rotation must also be considered. As already stated, $C_{\ell n}$ is small. Also, the ratio of $\Omega/2\pi\nu$ is small as the frequency of rotation is usually much smaller than the frequency of pulsation. Using these facts, equations (6.4) and (6.1), and the fact that $\ln(1+x) \approx x$ if $x << 1$, then

$$\log \nu = a_{0\ell n} + a_{1\ell n} \log T_{\rm eff} + a_{2\ell n} \log L + a_{3\ell n} m \tag{6.5}$$

where $a_{3\ell n} = -(\log e)(1 - C_{\ell n})\Omega/\nu$. This relation is once again only valid for p-modes, or almost-pure p-modes. Since another unknown, $(1 - C_{\ell n})\Omega$ has been introduced, a minimum of three frequencies is required for a unique determination of $\log T_{\rm eff}$, and $\log L$.

Suppose there is a star with a number of frequencies, N. If the modes (ℓ, m, n) are known, then the interpolation constants are known. The sum of squares $\sum \epsilon_i^2$ where ϵ_i is given by

$$\log \nu_i + \epsilon_i = a_{0\ell n} + a_{1\ell n} \log T_{\rm eff} + a_{2\ell n} \log L + a_{3\ell n} m \tag{6.6}$$

can be minimised to obtain the most probable values of $\log T_{\rm eff}$, $\log L$ and $(1 - C_{\ell n})\Omega$.

The pulsation modes, as well as the stellar parameters, might be identified using the observed frequencies and the above equations. For example, in a star with four observed frequencies, each frequency ν_i could be allowed to take on an identification $(\ell, m, n)_i$, and the sum of squares minimised. A solution set would then be one for which the particular set of modes give stellar parameters which are reasonable i.e. fall within the expected ranges for these stars. However, in the range $0 \leq \ell \leq 2$, $-\ell \leq m \leq \ell$ and $1 \leq n \leq 3$ there are over 530 000 possible combinations of modes for four frequencies, and a unique solution for the stellar parameters is not obtained. It is therefore useful to use the mode-identification as a constraint when using the equations discussed above to obtain the stellar parameters.

6.3 Application to specific stars

The stars discussed in Chapters 4 and 5 are, unfortunately, not ideally suited for asteroseismology as most of them have only one or two observed frequencies associated with p-modes. For those stars which are likely to be pulsating in the fundamental and first overtone radial modes, $\log T_{\rm eff}$ and $\log L$ were calculated using the equations for the axisymmetric modes for $\alpha = 1$. Although not always valid, the stars were assumed to have the same abundance, $Z = 0.02$, used in the models, and to be less evolved than the end of core hydrogen burning. The results are shown in Table 6.2 and in Figure 6.1. Those stars with only one frequency of pulsation were assumed to be pulsating in the fundamental radial mode, and the $\log L - \log T_{\rm eff}$ locus plotted.

The results do not depend much on the adopted mixing length: a maximum difference of 0.002 dex in $\log T_{\rm eff}$ and 0.08 dex in $\log L$ was found for $\alpha = 0.5$ relative to $\alpha = 1.0$. In other words, the effect of changing α is mostly a small change in luminosity; the temperature is more or less unaffected.

Table 6.2: The effective temperatures and luminosities as determined from the pulsation frequencies and mode identifications. For stars with only one frequency, the values of c_0 and c_1 in $\log L = c_0 + c_1 \log T_{\rm eff}$ are given.

Star	ν	(ℓmn)	c_0 or $\log T_{\rm eff}$	c_1 or $\log L$
AE UMa	11.6253	(0 0 1)	3.926	1.441
	15.0326	(0 0 2)		
BP Peg	9.1263	(0 0 1)	3.779	0.892
	11.8242	(0 0 2)		
RV Ari	10.7360	(0 0 1)	3.854	1.147
	13.8964	(0 0 2)		
AD CMi	8.1318	(0 0 1)	-17.202	4.8088
BE Lyn	10.4309	(0 0 1)	-17.367	4.8088
EH Lib	11.3110	(0 0 1)	-17.421	4.8088
β Cas	9.9100	(0 0 1)	-17.333	4.8088
BF Phe	16.0100	(0 0 1)	-17.653	4.8088
GN And	14.4292	(0 0 1)	-17.584	4.8088

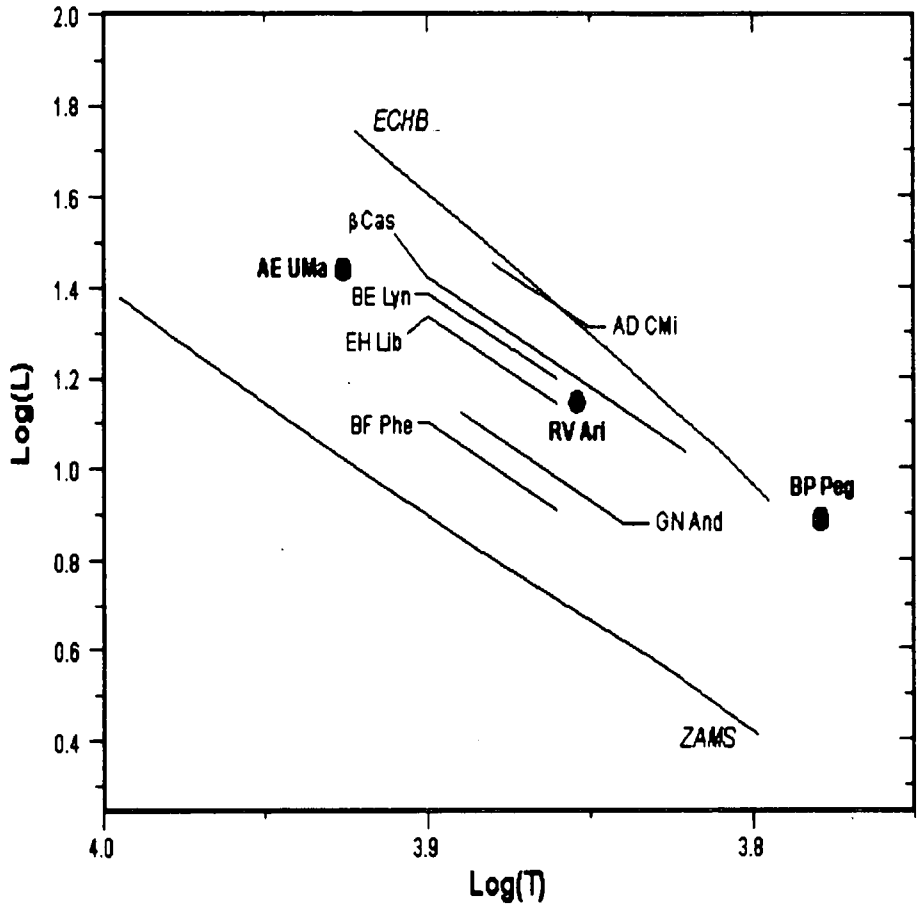

Figure 6.1: Location of the δ Sct stars on the H–R diagram as determined from the pulsation parameters. For stars with only one mode, the locus is given within the most probable temperature range.

Chapter 7

Summary and Conclusions

7.1 The mode-identification

A new algorithm for mode-identification using multicolour photometry has been developed. This new method, which allows both the phases and amplitudes to be used for mode identification, differs from the currently used two-colour diagrams in that it allows the information from *all* the filter passbands in which the star is observed to be used simultaneously. It also allows a probability to be assigned to each mode identification, provided that the amplitudes and phases from at least three filter passbands are available.

Although it would have been possible to leave f and ψ as free parameters in the mode identification procedure, they have been calculated using linear non-adiabatic models that could describe the δ Sct stars. This was done to reduce the number of free parameters in the mode identification procedure. There was some uncertainty in the values of f and ψ used, due to the uncertainty in the treatment of convection for $\log T_{\rm eff} < 3.93$, and also due to the fact that the observed and calculated frequencies do not match exactly. In order to explore the uncertainty in f and ψ due to convection, the mode identification procedure was applied using three sets of models corresponding to the mixing lengths, $\alpha = 0.5, 1.0$ and 2.

The method was applied to some δ Sct stars for which the required photometric observations were available. The data for two of the stars, CC Oct and EW Aqr were obtained by observing the two stars in August 1997. The δ Sct stars are particularly interesting, as, unlike the β Cep stars, there are significant phase differences between light curves in different colours, which can

be used in the mode-identification procedure. For stars where the phase differences between light curves in different colours are small, other methods are available which use the amplitudes only for mode-identification. Some of these methods were discussed in Chapter 3.

The expected radial mode was identified in all the HADS to which the method was applied, except in five cases. In three of the cases where the identification was not correct, i.e. DY Her, RS Gru and V567 Oph, it is probable that the stars are evolved beyond the ECHB, and thus beyond the scope of the models used. This is indicated by the fact that the frequency of pulsation, which is similar in all three the stars, cannot be identified with radial modes in the models. In the other two cases, AD CMi and BE Lyn, the fit was extremely poor. The reason for the poor fit was traced to a discrepant u-amplitude.

For the other stars, there was frequently little discrimination between the $\ell = 0$ and $\ell = 1$ modes. The $\ell = 2$ mode was more easily discriminated, but there was very little evidence for this mode in the selected sample of stars. For the selection of stars in this study, the algorithm developed was useful for some of the LADS, but worked best for the HADS.

A larger sample of stars may have been more indicative of the success of the method. However, published observations of Pop I stars in three or more colours were not easy to find, especially for low-amplitude pulsators. The sample would, therefore, need to be increased through observations, but time constraints did not allow this.

Although the models were assumed to be non-rotating, frequencies that would have been present in a rotating star were allowed in the mode-identification procedure. This did not affect the mode identification, since the method is independent of m. The algorithm does not seem to be very sensitive to the different metallicities found in the selected stars, although only stars that were not clearly Pop II were selected. The results are, however, not independent of the mixing length. The same modes were identified for each star, regardless of the mixing length used, although the significance of the modes varies with mixing length. There is no single value of α that seems to give the best results - it varies from star to star.

Discrimination between modes would be improved if observations of these stars are supplemented with data in longer or shorter wavelengths. As discussed in Chapter 2, in the longer wavelengths, the phases provide better discrimination between modes, while in the shorter wavelengths the amplitudes also become more sensitive to mode. Observations in either case would help to pin down the mode identification more securely, although they are difficult to obtain for the

δ Sct stars. Unfortunately, the algorithm does not allow the number of radial nodes n, or the azimuthal number m to be determined.

7.2 Asteroseismology

The main aim of mode identification is to enable the stellar parameters to be determined from the pulsation parameters. This is called *asteroseismology*. Although the mode-identification algorithm discussed above also selected the stellar parameters of the 'best fit' model, these stellar parameters are not reliable because the models were calculated assuming zero rotation, and also because the model frequencies do not exactly match the observed frequencies.

An algorithm to deduce the temperature and luminosity from the pulsation frequencies was formulated. This consisted of relationships between frequency and the stellar parameters obtained from linear non-adiabatic models. The resulting equations are mode dependent and also depend on the choice of mixing length. The equations are only valid for p-modes or almost pure p-modes, and are thus not really useful for many of the non-radial modes found in δ Sct stars since these modes have a mixed p- and g-mode character. Slow rotation is also assumed, and so the equations are not useful for stars with rotational velocities greater than 50 km.s^{-1}, i.e. most of the LADS. Second order effects must be included if the equations are to be applied to these stars. Using these equations, a solution for the temperature and luminosity is in principle possible if two axisymmetric frequencies or if three or more frequencies are available.

The method was applied to a small selection of δ Sct stars, assuming radial pulsation in axisymmetric modes. Those with only one frequency were assumed to be pulsating in the fundamental mode, and those with two frequencies were assumed to be pulsating in the fundamental and first harmonic modes. These stars were also assumed to be in a stage of evolution before ECHB, which may not be valid for all of them. It was found that the resulting luminosity is sensitive to the choice of mixing length, while the temperature seems to be less sensitive.

If the algorithm is used without the mode-identification, and all modes are allowed for each of the frequencies present in a star, then a unique solution for the stellar parameters is not obtained. Mode identification is therefore useful for constraining the number of valid solutions and essential if a unique solution is desired, especially as the number of frequencies increases.

The amount of information that can be determined from the pulsation parameters is propor-

tional to the number of pulsation frequencies present. In the sun, where millions of modes have been identified, the radial structure can be determined. In the δ Sct stars, where only a few frequencies of pulsation are present, much less information can be obtained. The temperatures and luminosities of the HADS stars which are pulsating radially in the fundamental and first harmonic can be determined using the equations in the previous chapter (which are sensitive to mixing length). The temperatures and masses can also be obtained from 'Petersen' diagrams. (See for example Petersen & Christensen-Dalsgaard (1996) or Andreasen (1983).) These diagrams are, however, sensitive to metallicity. Obtaining the stellar parameters for the low amplitude δ Sct stars is more difficult, because of the effects of rotation. Rotation, which alters the frequencies expected in a non-rotating star, is higher for these stars, and the resulting splitting of the frequencies is no longer a simple symmetrical pattern. Asteroseismology for these lower amplitude stars seems to be less hopeful. Clearly there is still much work to be done on asteroseismology in δ Sct stars.

Appendix A

Example of Output of Dziembowski's Pulsation Code NADROT

Table A.1: An example of an output file from W. Dziembowski's linear non-adiabatic pulsation code NADROT.

Mass	Log(Te)	Log(L)	Log(g)	Vrot					
1.80	3.8764	1.1155	4.0347	0.0					
ℓ	n	sig	P[min]	fa[c/d]	Re(fn)	ekg/ek	fr	fi	eta
0	1	2.061	109.05	13.205	13.205	0.000	5.576	10.863	0.061
0	2	2.670	84.20	17.103	17.103	0.000	6.929	10.137	0.077
0	3	3.302	68.08	21.151	21.151	0.000	6.983	9.592	0.084
1	3	1.078	208.45	6.908	6.908	0.947	-0.427	9.334	-0.187
1	1	1.524	147.54	9.760	9.760	0.937	2.750	10.803	0.014
1	3	2.110	106.51	13.519	13.519	0.021	5.633	10.770	0.063
1	4	2.732	82.27	17.503	17.503	0.029	6.929	10.059	0.078
1	3	3.017	74.49	19.331	19.331	0.346	7.050	9.777	0.081
2	6	1.062	211.59	6.805	6.805	0.971	-0.963	7.845	-0.348
2	5	1.214	185.09	7.780	7.780	0.958	0.110	9.080	-0.174
2	4	1.402	160.34	8.981	8.981	0.939	1.486	10.028	-0.050
2	3	1.713	131.20	10.976	10.976	0.843	3.525	10.700	0.038
2	4	2.061	109.05	13.205	13.205	0.396	5.221	10.716	0.062
2	3	2.381	94.41	15.253	15.253	0.504	6.229	10.434	0.072
2	4	2.800	80.29	17.934	17.934	0.340	6.874	9.976	0.079
2	3	3.247	69.23	20.799	20.799	0.285	6.914	9.621	0.084

The first two lines in the above table give the star's mass in solar masses, effective temperature, surface gravity and rotational velocity, which was set to zero for all the model stars. The first column gives the spherical harmonic degree ℓ, and takes integer values in the range 0 to 2. The

second column gives the harmonic n. The fundamental radial mode is thus $(\ell, n) = (0,1)$. The third column 'sig' is the dimensionless frequency σ defined by

$$\sigma = \frac{Re[\omega]}{\sqrt{4\pi G < \rho >}}$$

where G is the Gravitational constant, and $< \rho >$ is the average density of the star.

The fourth column gives the period P of pulsation in minutes. The fifth column, fa, gives the adiabatic frequency, and the sixth column gives the real part of the non-adiabatic frequency. The seventh column 'ekg/ek' indicates the type of mode, and has values varying between 0 and 1. A p-mode has a value close to zero, and a g-mode has a value close to 1. In this thesis, all modes with a value higher than 0.2 have been denoted g-modes. As seen in this file, different frequencies are in some cases assigned the same (ℓ, n). This is possible because the modes are of different types i.e. p-modes, g-modes or mixed p- and g-modes.

The eighth and ninth column give the real and imaginary parts of f^* as defined in Chapter 2. The values of f and ψ are easily extracted as described in Section 4.5 of Chapter 4.

The last column gives the growth rate of the pulsations. Thus those modes with a negative growth rate are damped, or stable modes, and those with a positive growth rate are the excited modes.

Appendix B

Periodogram Analysis

B.1 Determining the period

Suppose that the true magnitude Y_i of a star at any time t_i can be described by a series of cosine functions with different angular frequencies ω and amplitudes A i.e.

$$Y_i = A_0 + \sum_k A_k \cos(\omega_k t_i + \phi_k) \qquad \text{for } k = 1,2,3 \ldots \tag{B.1}$$

The observed magnitude y_i, which has a certain error ε_i associated with it, can then be written as

$$\begin{aligned} y_i + \varepsilon_i &= A_0 + \sum_k A_k \cos(\omega_k t_i + \phi_k) \qquad \text{for } k = 1,2,3 \ldots \\ &= A_0 + \sum_k \Big(a_{1k} \cos\omega_k t_i + a_{2k} \sin\omega_k t_i \Big). \end{aligned} \tag{B.2}$$

If both sides of the equation are multiplied by $\cos\omega_j t_i$ then

$$y_i \cos\omega_j t_i + \varepsilon_i \cos\omega_j t_i = A_0 \cos\omega_j t_i + \sum_k \Big(a_{1k} \cos\omega_k t_i \cos\omega_j t_i + a_{2k} \sin\omega_k t_i \cos\omega_j t_i \Big). \tag{B.3}$$

If the star is observed N times, then there are N such equations (i.e. $i = 1,2,3, \ldots \text{N.}$) The average of these N equations, obtained by adding them and dividing by N, gives :

$$\begin{aligned} < y_i \cos\omega_j t_i > + < \varepsilon_i \cos\omega_j t_i > \;=\; & A_0 < \cos\omega_j t_i > + \sum_k \Big(a_{1k} < \cos\omega_k t_i \cos\omega_j t_i > \\ & + a_{2k} < \sin\omega_k t_i \cos\omega_j t_i > \Big) \end{aligned} \tag{B.4}$$

where the angle brackets denote the averages.

The observational error ε_i is random. Hence, if N is sufficiently large, $< \varepsilon_i \cos\omega_j t_i >= 0$. Also, all terms on the right hand side of equation (B.4) are zero except the term $a_{1k} < \cos\omega_k t_i \cos\omega_j t_i >$ when $k = j$. Then

$$< y_i \cos\omega_j t_i > \approx \frac{1}{2\pi}\int_0^{2\pi} \cos\omega t \, d(\omega t) = \frac{1}{2}a_{1j}. \tag{B.5}$$

The larger the number of data points N, or the more even the phase coverage is, the closer this approximation becomes. Similarly,

$$< y_i \sin\omega_j t_i >= \frac{1}{2}a_{2j} \tag{B.6}$$

The amplitude then becomes

$$A_j^2 = 4(< y_i \cos\omega_j t_i > + < y_i \sin\omega_j t_i >) \tag{B.7}$$

The constant A_0 is simply given by $A_0 =< y_i >$.

The aim of periodogram analysis is to determine the frequencies present in a set of data from an observed star. A plot of the amplitude A_j as a function of ω_j is called the periodogram. In order to determine what frequencies are present in the data, a particular frequency ω_j is chosen, and the corresponding amplitude A_j is calculated. This is repeated for many frequencies over the range in which the pulsation frequencies are expected to lie. How well any particular frequency describes the data set is given by the variance $< \varepsilon_i^2 >$. The minimum value of the variance coincides with the largest amplitude, which hence coincides with the most likely value ω or $\nu = \frac{\omega}{2\pi}$. This is easily seen by considering the simple case of a single oscillation i.e.

$$y_i + \varepsilon_i = A_0 + A_k \cos(\omega_k t_i + \phi_k).$$

Then

$$\varepsilon_i^2 = y_i^2 + A_0^2 + 2A_0A_k\cos(\omega_k t_i + \phi_k) + A_k^2\cos^2(\omega_k t_i + \phi_k) - 2y_iA_0 - 2y_iA_k\cos(\omega_k t_i + \phi_k).$$

Taking averages and using the expression for A_0, then

$$< \varepsilon_i^2 >=< y_i^2 > - < y_i >^2 + \frac{A_k^2}{2} - 2A_k < y_i \cos(\omega_k t_i + \phi_k) > .$$

Now $< y_i \cos(\omega_k t_i + \phi_k) >= \frac{A_k}{2}$ so that

$$< \varepsilon_i^2 >=< y_i^2 > - < y_i >^2 - \frac{A_k^2}{2}.$$

From the above equation, it can be seen that the magnitude of $< \varepsilon_i^2 >$ depends only on A_k, since the terms in y_i are constant for any set of data, and that $< \varepsilon_i^2 >$ is a minimum when A_k is a maximum.

Once the most likely frequency, say ω_a has been found, a new data set can be formed by subtracting this frequency from the data set. This is known as *prewhitening* the data. This new data set can then be used to determine the next most likely frequency ω_b, and so on.

It should be noted that this works best for a large number of data points, and assumes sinusoidal variations, which is not always true of the high amplitude δ Sct stars.

B.2 Some further notes

A periodogram has some further properties due to the nature of the observations of stars. For simplicity, consider the light curve to be described by a single cosine function

$$Y(t) = A\cos(\omega_0 t - \phi)$$

If the star were observed for all time, then the periodogram would be a single spike at frequency ω_0, and have zero amplitude elsewhere. Because stars are observed for a finite amount of time, say $t = 0$ to $t = T$ this single spike broadens out into a line with a width $\delta\omega$ which is inversely proportional to the length of observation T. If a star has two closely spaced frequencies, then the resolution of these two peaks becomes easier as T increases.

Other features are present in the periodogram because a star's magnitude or luminosity is sampled at discrete times. If a star, which is pulsating at a frequency ν (measured in d^{-1}) is sampled every 5 minutes, i.e. at a frequency of 0.0035 d^{-1} then there will be peaks in the periodogram at frequencies of $\nu \pm n0.0035$ d^{-1} where n is an integer. Furthermore, stars are usually observed in blocks, with gaps between the blocks where no data are taken (e.g daytime). These gaps result in the appearance of *sidebands* or *aliases* in the periodogram around the pulsation frequency. For example, aliases at intervals of n d^{-1} are present in the periodogram if the star is observed at a single site due to the gap in the data because of daytime. These aliases can have amplitudes in the periodogram which are comparable to that of the pulsation frequencies, making discernment of the pulsation frequencies difficult. These aliases can only be eliminated in multi-site campaigns, in which a star is sampled at different observatories situated at different places on the globe, so that the gaps in the data due to daytime are eliminated. Some examples of periodograms are given in the next appendix, for the two δ stars CC Oct and EW Aqr.

Appendix C

Observations of CC Oct and EW Aqr

The δ Scuti stars CC Oct (HD188136) and EW Aqr were observed in August 1997, at the SAAO site near Sutherland, on the 0.5-m telescope using the SAAO Modular Photometer. The stars and their comparison stars are listed in Table C.1.

Table C.1: The two variable stars and the comparison stars used to obtain the differerantial photometry.

star	Spectral type
CC Oct	A3
HR 7698	A2
HD 188230	A0
EW Aqr	F0
HR 8018	A7
HR 8212	F5

CC Oct was visible all night, but EW Aqr was only up for 6.5 hours. When both stars were up, the observing sequence was HR7698, CC Oct, HD 188230, HR 8018, EW Aqr, HR 8212. When only CC Oct was visible, the observing sequence was HR7698, CC Oct, HD 188230, CC Oct.

Conditions were not very photometric during the two weeks of observations, but some useful data were nevertheless obtained. A journal of the observations is given in Table C.2. Differential photometry was obtained for these stars through the *uvbyI* filters. The integration time through the *u*-filter was 40 s, and 20 s through all the other filters. Sky observations were taken every 10 minutes during the first hour while the sky was not completely dark, and thereafter

Table C.2: A journal of the observations. The number of data points obtained per filter is indicated by n.

Date	HJD 2450000.+	n (CC Oct)	n (EW Aqr)
12/8-13/8	0674	23	10
13/8-14/8	0675	18	12
14/8-15/8	0676	3	4
15/8-16/8	0677	15	11
19/8-20/8	0681	17	11
20/8-21/8	0682	20	13
21/8-22/8	0683	14	13
22/8-23/8	0684	13	6
23/8-24/8	0685	7	6
	TOTAL	130	86

approximately every 30 minutes.

After reduction of the data, the frequencies present in the data of the two variable stars were determined using the principles of periodogram analysis described in Appendix B. The periodograms are shown in Figures C.1 and C.2. In these figures, each successive panel is the result of prewhitening the previous panel with that panel's most probable frequency. The results of the periodogram analysis are listed in Table 4.1 of Chapter 4.

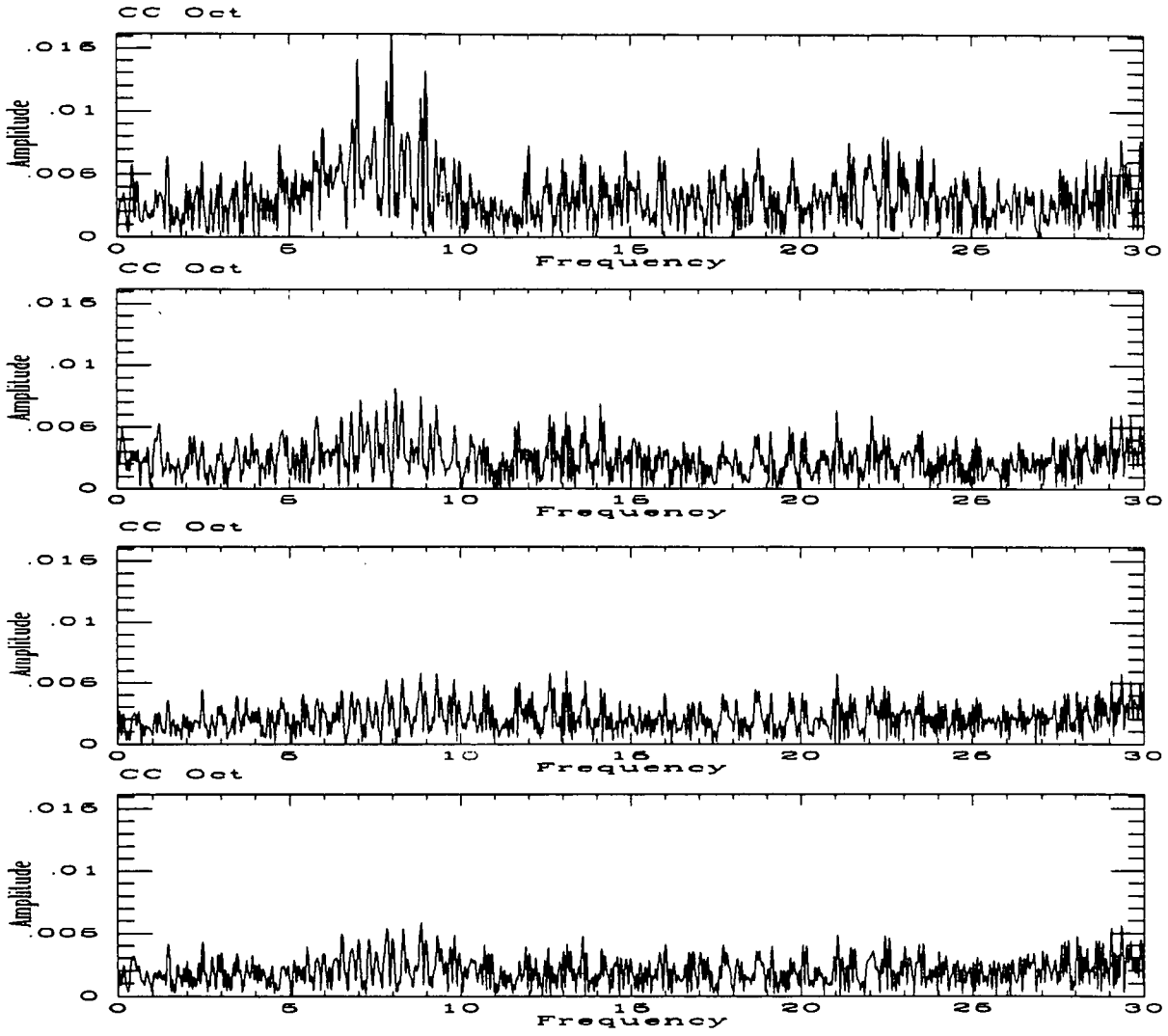

Figure C.1: Periodograms for CC Oct. The top panel shows the periodogram for (with the amplitude in mag) with the frequency of 8.000 d^{-1} being predominant. The next panel is has been prewhitened with the frequency of 8.000 d^{-1}, and shows the second frequency of 8.112 d^{-1}. The third panel has been prewhitened again to reveal the frequency of 12.62 d^{-1} This frequency is not really visible above the noise, but was accepted as it agrees with that of Kurtz (1980). The last panel has been prewhitened with the frequency of 12.62 d^{-1}. There is no clear frequency that can be extracted from this last periodogram.

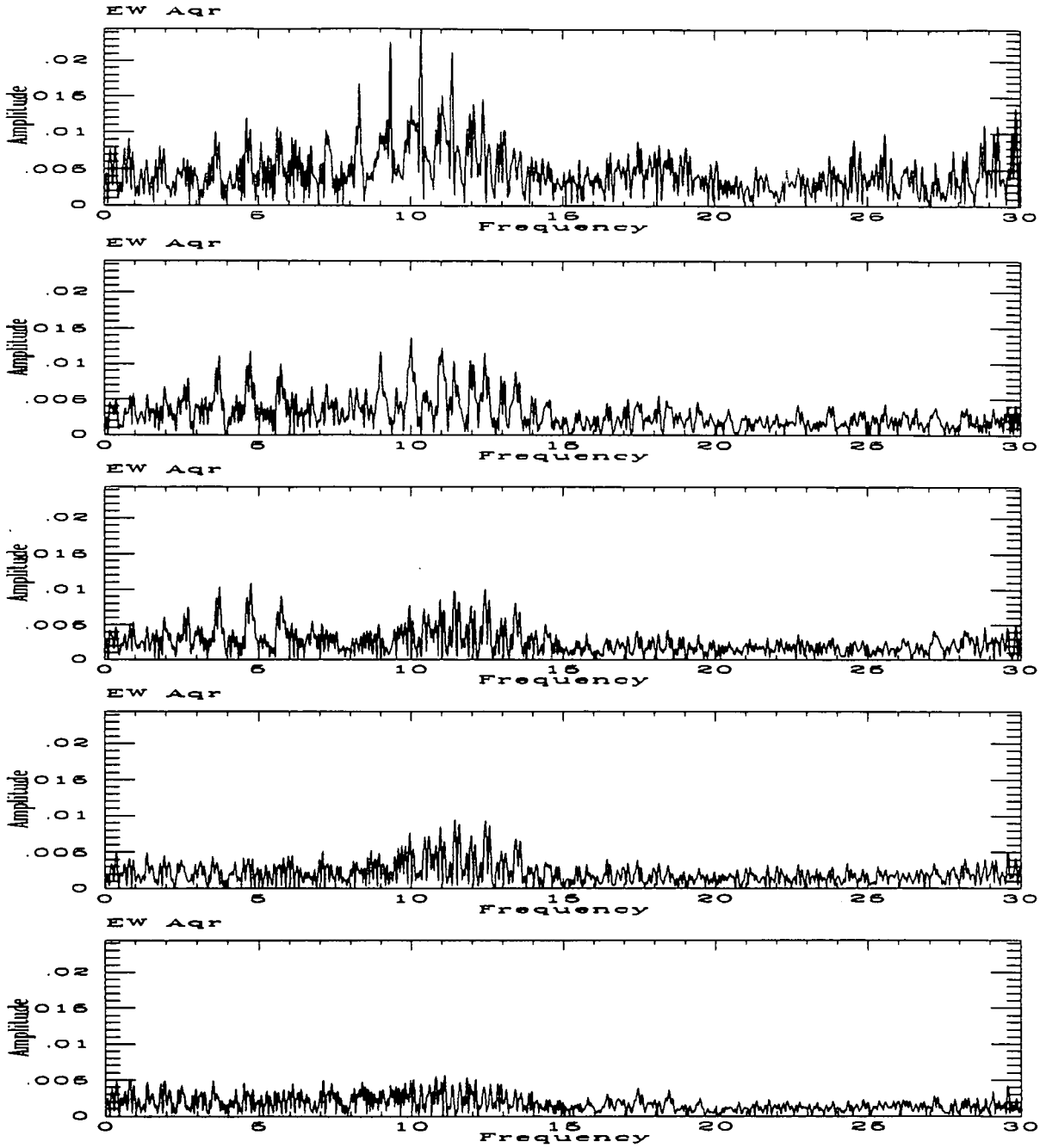

Figure C.2: The top panel shows the periodogram (with the amplitude in mag) with the dominant frequency of 10.340 d^{-1} for EW Aqr. The next panel is has been prewhitened with the frequency of 10.340 d^{-1}, and shows the second frequency of 10.018 d^{-1}. The third panel has been prewhitened again to reveal the frequency of 4.74 d^{-1}. The next panel has been pre-whitened again, and reveals a frequency of approximately 11 d^{-1}. No record of this frequency was found in any other published literature. Furthermore the software package used to perform the periodogram analysis indicated that this frequency was probably not real, and so this frequency was ignored. The last panel has been prewhitened with the frequency of approximately 11 d^{-1}, and shows only noise.

References

Aller L.H., 1971, Atoms, Stars & Nebulae, Revised Edition, Harvard University Press

Andreasen, G.K., 1983, A&A 121, 250

Balona L.A., 1994, MNRAS 268, 119

Balona L.A., 1987, MNRAS 224, 41

Balona L.A., Stobie R.S., 1979, MNRAS 189, 649

Balona L.A., Dziembowski, W.A., Pamyatnykh, A.A., 1997, MNRAS 289, 25

Balona L.A., Evers E.A., 1999, MNRAS, in press

Brassard P., Fontaine G., Wesemael F., 1995, ApJS 96, 545

Breger M., Campos A.J., Roby S.W., 1978, PASP 90, 754

Breger, M., 1979, PASP 91, 5

Christensen-Dalsgaard, J., 1997, Lecture Notes on Stellar Oscillations[1]

Cox, J.P., 1980, Theory of Stellar Pulsation, Princeton University Press

Crawford D.L., Barnes J.V., 1970, AJ 75, 978

Crawford D.L., 1975, AJ 80, 955

Crawford D.L., 1979, AJ 84, 1858

Cugier H., Dziembowski W.A., Pamyatnykh A.A., 1994, A&A 291, 143

Dworetsky M.M., Moon T.T., 1986, MNRAS 220, 787

Dziembowski W.A., 1977, Acta Astr. 27, 203

Fontaine G., Brassard P., Bergeron P., Wesemael F., 1996, ApJ 469, 320

Garrido R., García-Lobo E., Rodríguez E., 1990, A&A 234, 262

Gupta, S.K., 1980, ApSS 71, 377

Helt B.E., 1984, A&AS 56, 457

Heynderickx D., 1994, A&A 283, 835

[1]Available on the World Wide Web at http://www.obs.aau.dk/ jcd/oscilnotes/

Heynderickx D., Waelkens C., Smeyers P., 1994, A&AS 105, 447

Hobart M.A., Pena J.H., Peniche R., 1989, Rev Mex Astron Astrof. 17, 103.

Joner M.D., 1986, PASP 98, 651

Joner M.D., Johnson S.B., 1985, PASP 97, 153

Jørgensen H.E., Nørgaard-Nielsen H.U., 1975, A&AS 19, 235

Kilambi G.C., DuPuy D.L., Koegler C.A., 1978, PASP 90, 194

Kippenhahn R., & Wiegert, A., 1990, Stellar Structure and Evolution, Springer-Verlag

Künzli M, North P., Kurucz R.L., Nicolet B., 1997, A&AS 122, 51

Kurtz D.W., 1980, MNRAS 193, 29

Kurucz R.L., 1979, ApJS 40, 1

Ledoux, P., Walraven, Th., 1958, Handbuch der Physik 51, ed S. Flügge (Springer-Verlag) p 353

McNamara D.H., 1997, PASP 109, 1221.

Mihalas, D., 1978, Stellar Atmospheres, 2nd Edition, W.H. Freeman and Company.

Moon T.T., Dworetsky M.M., 1985, MNRAS 217, 315

Morrison D., Wolff S., & Fraknoi A., 1995, Abell's Exploration of the Universe, 7th Edition, Saunders College Publishing.

Motz L., & Duveen A., 1977, Essentials of Astronomy, 2nd Edition, Columbia University Press

Novotny, E., 1973, Introduction to Stellar Atmospheres and Interiors, Oxford University Press

Petersen J.O., Christensen-Dalsgaard J.,1996, A&A 312, 463

Poretti E., 1989, A&A 220, 144

Poretti E., Mantegazza L., Bossi M., 1996, A&A 312, 912

Powell J.M., Joner,M.D., McNamara, D.H., 1990, PASP 102, 1131

Ribas I., Jordi C., Torra J., Giménez A., 1997, A&A 327, 207

Rodriguez E., Rolland A., López de Coca P., 1988a, Rev Mex Astron Astrof 16, 7

Rodriguez E., Rolland A., López de Coca P., 1988b, IAU file 259

Rodriguez E., López de Coca P., Rolland A., Garrido R., 1990, Rev Mex Astron Astrof 20, 37

Rodriguez E., Rolland A., López de Coca P., Garcia-Lobo E., Sedano J.L., 1992a, A&AS 93, 189

Rodriguez E., Rolland A., López de Coca P., Garrido R., González-Bedolla S.F., 1992b, A&AS 96, 429

Rodriguez E., Rolland A., López de Coca P., Garrido R., Mendoza E.E. , 1993, A&A 273, 473

Rodriguez E., López de Coca P., Rolland A., Garrido R., Costa V., 1994, A&AS 106, 21

Rodriguez E., Rolland A., Costa V., Martins S., 1995, MNRAS 277, 965

Rodriguez E., González-Bedolla S.F., Rolland A., Costa V., López-González M.J., López de Coca P., 1997, A&A 328, 235

Stamford P.A., Watson R.D., 1981, ApSS 77, 131

Unno W., Osaki Y., Ando H., Saio H., Shibahashi H., 1989, Nonradial Oscillations of stars, 2nd Edition, University of Tokyo Press.

Vander Linden D., Sterken C., 1986, A&A 168, 155

Wade, R.A., Rucinski, S.M., 1985, A&AS 60, 471

Watson R.D., 1988, ApSS 140, 255

Wegner G., 1981, AJ 247, 969

Summary

This thesis discusses mode identification in periodic pulsating stars from multicolour photometry. These stars pulsate in one or more modes, where each mode is described by a spherical harmonic degree ℓ, an azimuthal number m and the number of radial nodes n. The amplitudes and phases of the light curve vary with wavelength and also depend on the spherical harmonic degree ℓ, and thus allow the mode to be determined.

In stars where the light curves in different colours are essentially in phase the mode can be identified using graphical methods. In stars such as the δ Sct stars where the phase differences between the light curves in different wavebands are significant, there is extra information which can be used for the mode identification. The currently used two-colour diagrams do not always allow the mode to be identified unambiguously, and only use information from two wavebands. There is a need to develop a better method of mode identification for these stars. A new algorithm for mode identification is proposed which allows all the information from the light curves in two or more wavebands to be used simultaneously. If information from three or more wavebands is available, then a significance can also be assigned to each mode identification.

The number of free parameters in the mode identification procedure is reduced by using linear non-adiabatic models to calculate the parameters f and ψ. There is some uncertainty in these values due to the uncertainty in the treatment of convection. This is explored by using three sets of models corresponding to different mixing lengths, α for the mode identification.

The method is applied to some δ Sct stars with the required photometric observations. The expected radial mode is identified in most of the high amplitude stars, provided that the evolutionary status of the observed star is covered by the models. For the other stars, there is frequently little discrimination between the radial and $\ell = 1$ modes. The results are sensitive to the α, but there is no single value of α which gives the best results. It is recommended that

the wavelength coverage of these stars be extended to longer or shorter wavelengths to improve the discrimination between modes.

The main aim of mode identification is to enable the stellar parameters to be determined from the pulsation parameters. i.e. asteroseismology. The mode-identification algorithm discussed above does not yield reliable stellar parameters.

An algorithm to deduce the temperature and luminosity from the pulsation frequencies is formulated. This consists of relationships between pulsation frequency and the stellar parameters obtained from linear non-adiabatic models. The resulting equations depend on the mode and α, and are only valid for p-modes. They are not useful for many of the non-radial modes found in δ Sct stars, or for the low amplitude stars. Using these equations, a solution for the temperature and luminosity is in principle possible if two axisymmetric frequencies or three or more frequencies are available.

The method is applied to a small selection of δ Sct stars, assuming radial pulsation and an evolutionary status before ECHB. It is found that the resulting luminosity is sensitive to α, while the temperature is less sensitive.

If the algorithm is used without the mode-identification, and all modes are allowed for each of the frequencies present in a star, then a unique solution for the stellar parameters is not obtained. Mode identification is essential for a unique solution. At this stage, asteroseismology for the low amplitude stars seems to be less hopeful than for the high amplitude stars. There is still much work to be done on asteroseismology in δ Sct stars.

Opsomming

Hierdie verhandeling bespreek die identifikasie van die pulsasiemodusse van pulserende sterre met behulp van fotometriese data van verskeie kleurbande. Hierdie sterre pulseer in een of meer modusse, waar elke modus beskryf word deur 'n sferiese bolfunksie van graad ℓ en assimutale getal m, en 'n getal n wat die aantal nodusse van die staande golf in die ster weergee. Die verandering van die amplitude en fase van die ligkromme met golflengte en graad ℓ maak dit moontlik om die pulsasiemodusse te bepaal.

In sterre waar die ligkrommes van die verkillende kleurbande amper in fase is, kan die pulsasiemodusse met behulp van grafiese metodes bepaal word. In sterre soos die δ Sct sterre is daar egter 'n beduidende verskil tussen die fases van die ligkromme van die verskillende kleurbande. Daar is dus meer inligting beskikbaar wat gebruik kan word om die modusse te identifiseer. Die huidige metode van die twee-kleurdiagramme gebruik net twee kleurbande op 'n slag en maak dit nie altyd moontlik om die modus ondubbelsinning te bepaal nie. Dit is nodig om 'n nuwe tegniek te ontwikkel om die pulsasiemodusse van hierdie sterre te identifiseer. Die nuwe algoritme wat voorgestel word, gebruik al die inligting van die ligkromme in twee of meer kleurbande gelyktydig vir die identifikasie. As die amplitude en fase van drie of meer ligkrommes beskikbaar is, kan die betroubaarheid van die identifikasie ook bepaal word.

Die aantal vrye parameters is verminder deur f en ψ met behulp van liniêre nie-adiabatiese struktuurmodelle te bepaal. Daar is 'n onsekerheid in hierdie waardes omdat daar 'n onsekerheid in die mengskaal, α, van die modelle is. Dit is ondersoek deur drie verskillende stelle modelle te gebruik met drie verskillende mengskale.

Die metode is toegepas op sekere δ Sct sterre waarvan data in drie of meer kleurbande beskikbaar is. Die verwagte radiale pulsasies is geïdentifiseer in die meeste van die hoër amplitude sterre. Vir die ander sterre kon daar dikwels nie eenduidig onderskei word tussen radiale en die $\ell =$

1 modusse nie. Die resultate is sensitief vir die gekose mengskaal in die modelle, maar daar is geen enkele waarde vir die mengskaal wat die beste resultate lewer nie. Dit word aanbeveel dat hierdie sterre ook in hoër of laer golflengtes waargeneem word om makliker tussen die verskillende modusse te onderskei.

Die hoof rede vir die identifiseering van die pulsasiemodusse is om verskeie parameters met betrekking tot die struktuur van die ster met behulp van die pulsasie frekwensies te bepaal. Dit heet ster-seismologie. Die metode om die modusse te identifiseer wat hierbo verduidelik word, gee nie betroubare waardes vir die parameters nie.

Daar is gepoog om algoritmes af te lei om die ster temperatuur en helderheid met behulp van die pulsasie frekwensies te bepaal. Dit berus op die verband tussen die pulsasie frekwensies en sekere parameters wat met behulp van die liniêre nie-adiabatiese modelle bepaal word. Die vergelykings wat afgelei is, is afhanklik van die modus en die mengskaal van die ster, en is slegs geldig vir p-modusse. Die vergelykings is nie bruikbaar vir die meeste van die nie-radiale modusse en vir die lae-amplitude δ Sct sterre nie. As 'n ster in twee modusse met $m = 0$ of in drie modusse pulseer, is dit in beginsel moontlik om die temperatuur en heldereid van die ster te bepaal.

Die metode is toegepas op 'n beperkte keuse van 'n aantal δ Sct sterre. Die was aangeneem dat die sterre radiaal pulseer en op die hoofreeks lê. Daar is bepaal dat die helderheid van die ster senstitief afhang van die waarde van die mengskaal, terwyl die temperatuur minder sensitief daarvan afhang.

As die algoritme gebruik word sonder om die pulsasiemodusse in ag te neem, met ander woorde alle modusse word toegelaat vir elke frekwensie wat waargeneem is, dan is daar geen unieke oplossing vir die ster temperatuur en helderheid nie. Die identifisering van die modusse is nodig om 'n unieke oplossing te verkry. Op die stadium is ster-seismologie makliker vir die hoër amplitude sterre as vir die laer amplitude sterre. Daar is nog baie werk wat in die veld van ster-seismologie vir die δ Sct sterre gedoen moet word.